Universitat Autònoma de Barcelona

Desarrollo preclínico de una nueva técnica para la detección y caracterización de la cicatriz de infarto de miocardio basada en medidas de bioimpedancia

Gerard Amorós Figueras

Desarrollo preclínico de una nueva técnica para la detección y caracterización de la cicatriz de infarto de miocardio basada en medidas de bioimpedancia

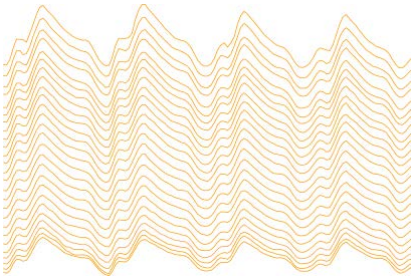

Tesis presentada por Gerard Amorós Figueras para la obtención del grado de Doctor

Director y tutor: Dr. Juan María Cinca Cuscullola

Año: 2018

Programa de doctorado en Medicina, Departamento de Medicina

Universidad Autónoma de Barcelona

D. Juan María Cinca Cuscullola, doctor en Medicina y catedrático del Departamento de Medicina de la Universidad Autónoma de Barcelona

certifica que la tesis titulada “Desarrollo preclínico de una nueva técnica para la detección y caracterización de la cicatriz de infarto de miocardio basada en medidas de bioimpedancia” ha sido realizada bajo su dirección en el Hospital de la Santa Creu i Sant Pau de Barcelona por D. Gerard Amorós Figueras, licenciado en Física y máster en Ingeniería Biomédica.

considera que esta tesis se encuentra terminada y reúne los requisitos necesarios para que el interesado pueda optar al título de Doctor por la Universidad Autónoma de Barcelona.

En Barcelona, febrero de 2018

Doctorando Director

Gerard Amorós Figueras Juan María Cinca Cuscullola

A la meva mare i la meva germana

Agradecimientos

Primer de tot vull agrair al Dr. Joan Cinca l'oportunitat de poder formar part del seu equip i de poder continuar treballant en una línia de recerca que fa molts anys que desenvolupa. També vull agrair-li ésser tan proper, totes les seves explicacions, consells, i sobretot, que m'hagi transmès la seva il·lusió i perseverança en tot el que fa.

Vull agrair també la feina de la Esther Jorge. Hem realitzat un munt d'experiments junts i hem passat llargues hores analitzant els "*phasic changes during the entire cardiac cycle*". Gràcies per tot el teu esforç i també per haver-me donat tants bons consells.

A en Xavier Rosell i en Ramón Bragós per tota la seva feina en aquest llarg camí i per estar a primera línia en tots els experiments.

A la Conchi Alonso, el Jose Guerra, el Davit Arzamendi i el Xavi Millan per la seva paciència i la seva ajuda a l'hora de realitzar els experiments, i a tot l'equip d'electrofisiologia i hemodinàmica per fer-ho possible.

A en Dani Traver i el Fran Alarcón, per involucrar-se a fons i per tota la seva ajuda desinteressada durant aquest projecte.

A la Laia Anglí, l'Andreu Ferrero, en Miquel Vives, el Jesús Álvarez i l'Eduard Solé per tota la vostra ajuda, consells, i pels ànims rebuts.

Als tots els amics pel seu suport moral, que és bàsic.

A tota la meva família, i en especial a la meva mare, el meu pare, i la meva germana, per fer-me sempre costat i animar-me a fer el que més m'agrada.

A la Yolanda, per animar-me sempre a continuar i per fer-me tan feliç.

Abreviaturas

ATP: Adenosina trifosfato.

BCP: Bypass cardio-pulmonar.

DAI: Desfibrilador automático implantable.

DA: Arteria coronaria descendente anterior.

DAI: Desfibrilador automático implantable.

DP: Arteria coronaria descendente posterior.

ECG: Electrocardiograma.

E_{max}: Elastancia telesistólica.

EPI: Epicardio.

ENDO: Endocardio.

FV: Fibrilación ventricular.

Hz: Hertz (ciclos/segundo).

j: Raíz cuadrada de -1.

MEI: Del inglés, Myocardial Electrical Impedance.

Φ: Ángulo de fase.

R: Resistencia.

ROC: Receiver operating characteristic.

V: Voltaje.

X: Reactancia.

Z: Impedancia.

Índice

Resumen

Antecedentes: Los pacientes que han sobrevivido a un infarto de miocardio tienen un riesgo elevado de sufrir muerte súbita por una arritmia ventricular. La ablación eléctrica puede eliminar el foco arrítmico, aunque el porcentaje de éxito de este procedimiento aumentaría con la introducción de mejoras en los sistemas de identificación del sustrato arritmogénico. Estos sistemas localizan la cicatriz post-infarto mediante el análisis de la amplitud de voltaje de los electrogramas locales, registrados mediante electrocatéteres intracavitarios. Sin embargo, esta técnica no permite discernir si en un punto determinado de la cicatriz la fibrosis es transmural, dato éste último importante para elegir los puntos de aplicación de la radiofrecuencia. Por otro lado, el voltaje de los electrogramas locales depende de la secuencia de activación cardíaca local con respecto al electrodo explorador y, por tanto, el mapeo de voltaje debe repetirse si el paciente sufre un episodio arrítmico.

La impedancia eléctrica es una propiedad pasiva del miocardio, y su magnitud guarda relación con la integridad estructural del mismo. Estudios previos han demostrado que su valor medio varía durante el ciclo cardíaco y que es capaz de identificar la cicatriz post-infarto. Sin embargo, su interrelación con otros parámetros fisiológicos o sus ventajas frente al mapeo de voltaje se desconocen.

Métodos: Esta tesis consta de diferentes series experimentales en cerdos en las que se analiza la impedancia eléctrica local en el tejido miocárdico sano, en el isquémico agudo y en la cicatriz post-infarto. En este estudio hemos utilizado un nuevo método de medida de la impedancia capaz de registrar hasta 1000 espectros de impedancia por segundo.

Resultados: El valor medio de la impedancia local del miocardio sano tiene una variación del 9% entre la sístole y la diástole ($p<0.001$). Por otro lado, hemos encontrado una alta correlación entre los valores locales de la impedancia registrados con una sonda desde el epicardio y los diferentes grados de fibrosis en la cicatriz (Magnitud a 1 kHz: $r=-0.86$; Ángulo de fase a 307 kHz: $r=0.83$, $p<0.001$). Además, hemos determinado que la medida endocárdica de la impedancia eléctrica a través de un electrocatéter permite identificar el tejido infartado ($p<0.001$) y que, a diferencia de la cartografía de voltaje, no se ve afectada por los cambios en la secuencia de activación cardíaca.

Conclusiones: La impedancia eléctrica local del miocardio tiene una variación periódica íntimamente ligada al ciclo cardíaco que se ve modificada durante la isquemia aguda miocárdica y en la cicatriz del infarto. La medida intracavitaria de la impedancia local del miocardio permite detectar el tejido infartado y además no se ve afectada por alteraciones en la secuencia de activación cardíaca. Por ello, podría ser una nueva herramienta clínica para la detección y caracterización de la cicatriz de infarto de miocardio en pacientes sometidos a ablación de arritmias ventriculares post-infarto.

Summary

Background: Patients who have suffered a myocardial infarction are at an increased risk of sudden cardiac death. Electrical ablation can eradicate the arrhythmogenic focus, although the success of this procedure could be increased by the introduction of improvements in the arrhythmogenic recording systems. In clinical practice, the delineation of the infarct scar zone is performed by mapping the voltage of local electrograms recorded with intracavitary electrocatheters. However, this technique does not allow to discern whether fibrosis is transmural at a certain point of the scar, which is important in order to choose the points of radiofrequency application. On the other hand, the voltage of the local electrograms depends on the sequence of local cardiac activation with respect to the exploring electrode and, therefore, the voltage mapping must be repeated if the patient suffers an arrhythmic episode.

The electrical impedance is a passive property of the myocardium related to their structural integrity. Previous studies have shown that their mean value varies during the cardiac cycle and that it is able to identify the post-infarct scar. However, their interrelation with other physiological parameters or their advantages over voltage mapping are unknown.

Methods: This thesis consists of different experimental series using pigs. We have analyzed the characteristics of local electrical impedance in healthy myocardial tissue, acute ischemic myocardium and 1-month old post-infarction scar. To perform the impedance measurements, a new impedance system capable of recording up to 1000 impedance spectra per second has been developed.

Results: The mean value of the local impedance of the healthy myocardium has a variation of 9% between systole and diastole ($p < 0.001$). We have found a high correlation between the local impedance values and the different degrees of local fibrosis in the post-infarction scar (Magnitude at 1 kHz: $r = -0.86$; Phase angle at 307 kHz: $r = 0.83$, $p<0.001$). In addition, we have shown that the endocardial measurement of myocardial impedance using a conventional electrocatheter is capable of identifying the infarcted tissue ($p < 0.001$) and that, unlike voltage mapping, it is not affected by changes in the cardiac activation sequence.

Conclusions: Local electrical impedance of the myocardium has a biphasic pattern closely linked to the cardiac cycle that is modified by both acute and chronic ischemia. The local values of myocardial impedance and phase angle are related to the percentage of fibrosis and are not affected by changes in the cardiac activation pattern. Myocardial impedance is a new preclinical tool able to recognize and characterize the myocardial infarct scar.

Introducción

Las arritmias ventriculares conllevan un riesgo seis veces mayor de muerte súbita en pacientes que han sufrido un infarto de miocardio (1). La inserción de un desfibrilador automático implantable (DAI) es actualmente el tratamiento más eficaz para prevenir la muerte súbita (2). Sin embargo, aunque el DAI puede revertir el episodio arrítmico en un alto porcentaje de casos, este dispositivo no está diseñado para intervenir o modificar directamente el sustrato estructural responsable de la arritmia.

La ablación eléctrica mediante radiofrecuencia puede eliminar el foco arritmogénico en un 50% de los pacientes con arritmias ventriculares post-infarto (3). Este porcentaje de éxito puede incrementarse con la introducción de mejoras en los sistemas de identificación y localización del foco arritmogénico durante el procedimiento en el laboratorio de electrofisiología. Los sistemas de navegación cardiaca (CARTO, NavX, Rhythmia) localizan la cicatriz post-infarto mediante el análisis de la amplitud de voltaje de los electrogramas locales registrados mediante electrocatéteres intracavitarios. La zona de la cicatriz se reconoce por el reducido voltaje de los electrogramas locales en comparación con los registrados en el miocardio normal circundante (4). Por otro lado, el voltaje de los electrogramas locales depende de la orientación del frente de activación con respecto al electrodo explorador y, por tanto, la localización de la cicatriz de infarto mediante esta técnica puede variar si el paciente sufre un episodio arrítmico durante el procedimiento (5), lo que obliga a repetir la cartografía y ocasiona un alargamiento del estudio.

La impedancia eléctrica del miocardio es una propiedad pasiva del corazón cuya magnitud guarda relación con la integridad estructural del mismo (6). Estudios previos han demostrado que la cicatriz de infarto tiene una impedancia menor que la del miocardio normal y gracias a esta circunstancia es posible identificar zonas de infarto cicatricial mediante un electrocatéter en modelos experimentales (7,8). Las medidas experimentales en esta tesis se han realizado con un nuevo sistema que analiza de forma continua los valores de la impedancia a múltiples frecuencias a lo largo de todo el ciclo cardiaco (9). La aplicación de esta nueva técnica al tratamiento de las arritmias ventriculares conllevaría dos grandes ventajas sobre el procedimiento actual guiado por criterios de voltaje: 1) permitiría diferenciar las zonas de la cicatriz de infarto en las que la fibrosis es transmural (valores de impedancia muy bajos) de las zonas en las que subyacen islotes de miocardio viable (valores de impedancia intermedios respecto al miocardio normal) y 2) la cartografía basada en criterios de impedancia tisular no variaría ante un cambio en el patrón de activación generado por un ritmo ectópico ventricular, a diferencia de lo que sucede con la cartografía de voltaje.

Esta tesis se ha llevado a cabo dentro del proyecto FIS-PI13/00765 del Instituto de Salud Carlos III.

1. Impedancia eléctrica

1.1. Conceptos básicos

La impedancia eléctrica es la oposición que presenta un circuito conductor al paso de una corriente eléctrica (I) cuando se aplica un voltaje (V). Físicamente está oposición es debida a la interacción de la corriente con el tipo de material que atraviesa y a las características estructurales del mismo. Si la corriente utilizada es una corriente continua, se puede definir por una componente, la resistencia (R). Si la corriente aplicada es alterna, se define por dos componentes: 1) el componente capacitivo (X_C), que tiene en cuenta las pérdidas de corriente debidas al almacenamiento de carga de la membrana y las estructuras celulares y 2) el componente inductivo (X_L) que tiene en cuenta las pérdidas de corriente por el campo magnético creado por la propia corriente, aunque es despreciable en el caso de los tejidos biológicos. La suma de ambos componentes se engloba en el término "reactancia" (X). Matemáticamente la impedancia eléctrica (Z) se puede representar por la ecuación 1 (ec.1).

$$Z = R + j \cdot X \qquad \text{(ec.1)}$$

donde R es la resistencia, X la reactancia y j=√-1. Otra forma de caracterizarla es a través de su magnitud, que representa la relación entre las amplitudes del voltaje y corriente (ec.2), y de su ángulo de fase, que representa el desfase temporal de la onda de corriente respecto a la onda de voltaje (ec.3) (Figura 1).

$$|Z| = \sqrt{R^2 + X^2} \qquad \text{(ec.2)}$$

$$\theta = \tan^{-1}\left(\frac{X}{R}\right) \qquad \text{(ec.3)}$$

Este desfase es debido a las características estructurales intrínsecas de los tejidos biológicos explorados.

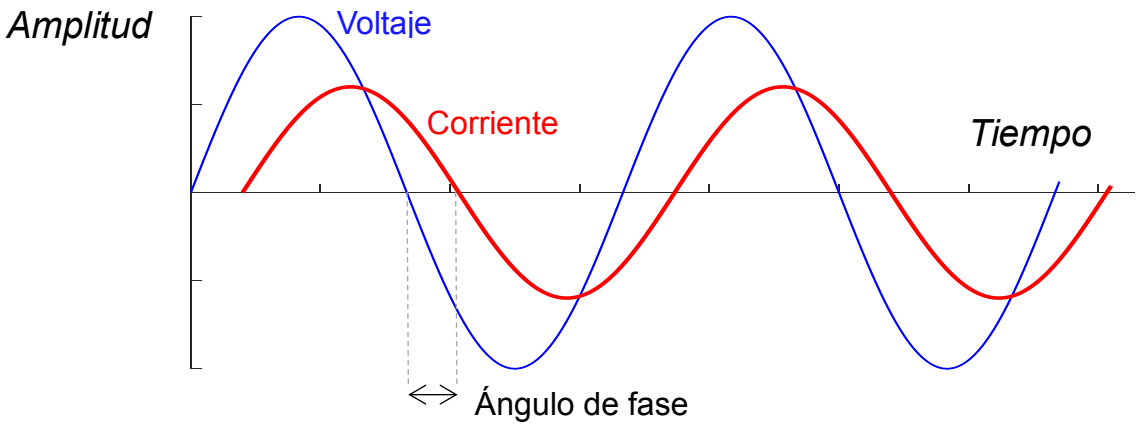

Figura 1. Diagrama que ilustra el desfase temporal de la onda de corriente respecto a la onda de voltaje aplicada a un tejido biológico.

La unidad de medida de la impedancia es el ohm (Ω), y el ángulo de fase se expresa en grados (º). La resistividad (ρ) es una propiedad intrínseca de cada material que cuantifica su oposición al paso de una corriente independientemente de su geometría, y se expresa en ohm·metro (Ω·m). La conductividad eléctrica (σ) se define como la inversa de la resistividad y se expresa como siemens por metro (S/m).

1.2. Propiedades eléctricas de los medios biológicos

La unidad básica de los tejidos biológicos es la célula. Las propiedades eléctricas pasivas de los tejidos biológicos dependen de las conductividades de los medios intra- y extracelulares y de las características eléctricas de las membranas celulares. La conductividad de ambos medios está en gran medida determinada por su

composición iónica. Así, el medio intracelular es rico en iones de potasio (K^+), y tiene en menor medida iones de cloro (Cl^-) y sodio (Na^+). En cambio, el medio extracelular contiene mayores concentraciones de Na^+ y Cl^-, y menores niveles de K^+ (10). Ambos medios están separados por membranas celulares, que se componen de una doble capa lipídica que actúa como un material dieléctrico y que tiene la capacidad de almacenar energía eléctrica. Esta propiedad se cuantifica a través del término "permitividad" (ε), y en general su valor se expresa en relación a la permitividad del vacío (ec.4).

$$\varepsilon = \varepsilon_{relativa} \cdot \varepsilon_{vacío} \qquad \text{(ec.4)}$$

La conductividad y la permitividad de los tejidos biológicos varía con la frecuencia de la corriente aplicada (Figura 2). En la figura 2 se puede observar el aumento de la conductividad de un tejido biológico con la frecuencia, y al mismo tiempo, la disminución de la permitividad en tres dispersiones, denominadas alfa, beta y gamma.

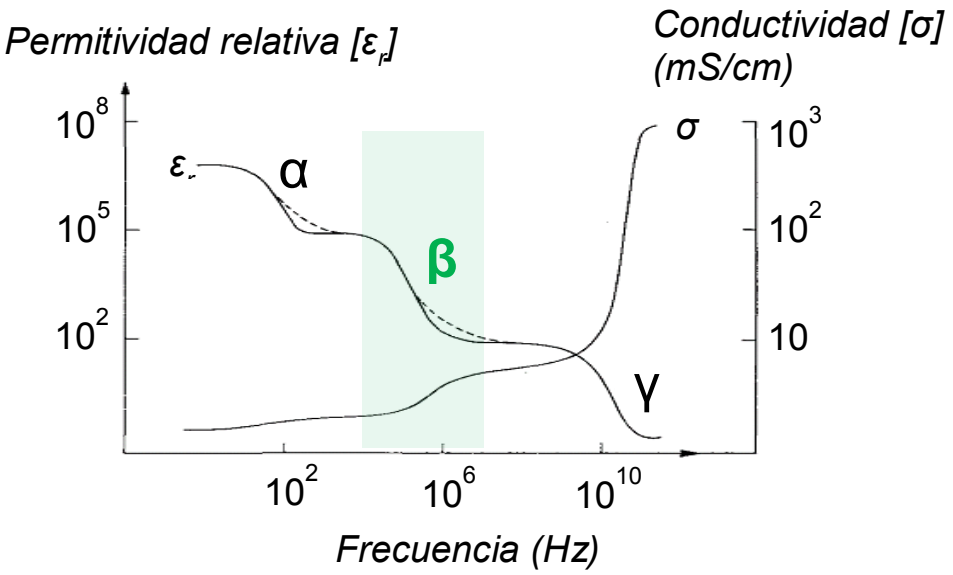

Figura 2. Variación de la conductividad y la permitividad relativa con la frecuencia de corriente en un músculo. Figura modificada de Schwan H.P. 1988.

Las dispersiones (o relajaciones) de los tejidos biológicos son zonas del espectro de frecuencias donde varía la conductividad de forma substancial. En este trabajo nos centraremos en el rango de frecuencias de la dispersión beta (1-1000 kHz), ya que esta relajación está asociada a las propiedades eléctricas de las membranas celulares y a sus interacciones con los medios intra- y extracelulares (11–13). En este rango, una corriente de baja frecuencia fluirá preferencialmente a través del medio extracelular. Por el contrario, una corriente de alta frecuencia lo hará tanto a través del medio extracelular como del intracelular ya que tiene la capacidad de travesar las membranas celulares (Figura 3). Gracias a estas características diferenciales, la medida de la impedancia usando múltiples frecuencias (espectro) nos aportará información sobre el estado del medio extracelular y sobre el estado de integridad del medio celular.

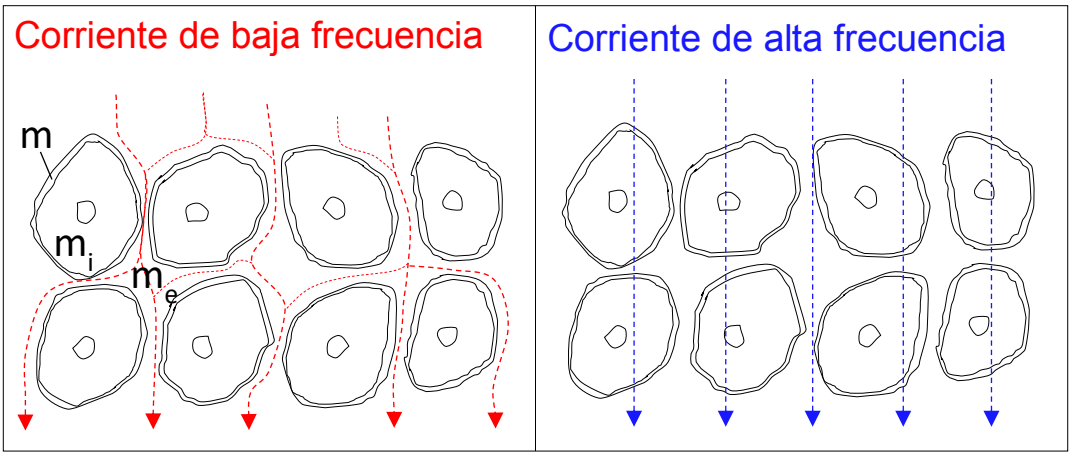

Figura 3. Representación del camino recorrido por una corriente de baja frecuencia (izquierda) y una corriente de alta frecuencia (derecha) a través de un tejido biológico. m =membrana celular; m_i=medio interno; m_i =medio externo.

Para caracterizar de forma teórica el comportamiento de las propiedades eléctricas pasivas en tejidos biológicos se suelen usar modelos de circuitos

equivalentes. Así, la impedancia de un tejido biológico se puede modelar como una resistencia que representa el medio extracelular, conectada en paralelo con una resistencia y una capacitancia que representan respectivamente el medio intracelular y las membranas celulares (Figura 4).

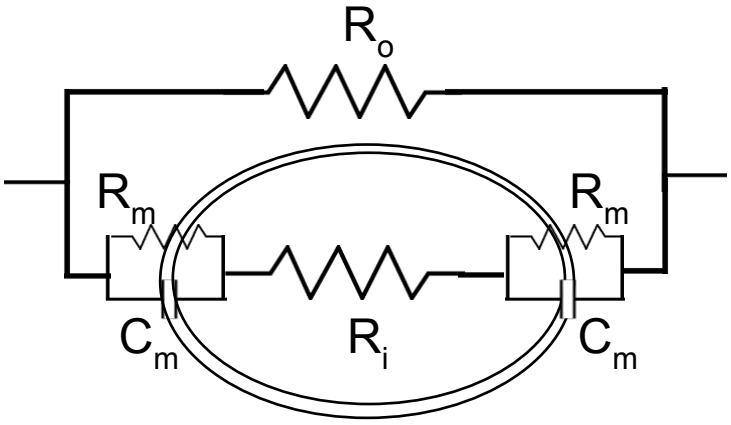

Figura 4. Circuito equivalente de las propiedades eléctricas pasivas en un tejido biológico. R_o, R_i, R_m, representan respectivamente las resistencias de los medios extracelulares, intracelulares y de las membranas celulares y C_m representa la capacitancia de las membranas celulares.

El modelo matemático más usado para caracterizar las medidas de impedancia a varias frecuencias es el propuesto por Cole ya en el año 1941 (14). Este modelo teórico se sigue usando para caracterizar las medias experimentales de bioimpedancia.

Finalmente, es importante enfatizar que la impedancia de los tejidos biológicos depende también de otros factores como la temperatura, el contenido de agua del tejido, etc., por lo que estas variables deben ser consideradas en los estudios de bioimpedancia.

1.3. Medida experimental de la bioimpedancia

Para determinar experimentalmente la impedancia de un tejido biológico es necesario aplicar una corriente a través de unos electrodos en contacto con el tejido y al mismo tiempo medir el voltaje inducido. Para medidas *in vivo,* la corriente aplicada directamente en el miocardio ha de cumplir unas normas de seguridad que establecen límites a su amplitud, frecuencia, y duración. Estos límites son importantes al objeto de evitar "microshocks" que pudieran inducir una arritmia, un reflejo neural o daño estructural (15,16). Además, el uso de densidades de corriente bajas implica que las propiedades eléctricas de los tejidos explorados se puedan considerar en el rango lineal y por tanto que cumplen la ley de Ohm (17). En esta circunstancia, la magnitud de la impedancia se obtendrá dividiendo el valor del voltaje y la corriente (ec. 5) y el ángulo de fase restando sus fases (ec. 6).

$$|Z| = \frac{|\mathrm{V}|}{|\mathrm{I}|} \qquad \text{(ec. 5)}$$

$$\angle \mathrm{Z} = \angle \mathrm{V} - \angle \mathrm{I} \qquad \text{(ec.6)}$$

En esta tesis hemos usado una nueva técnica de medida rápida con la que es posible obtener hasta 1000 muestras del espectro de la impedancia por segundo a diferentes frecuencias (9). De esta forma se pueden registrar sus cambios durante la sístole y la diástole del ciclo cardíaco y correlacionarlos con la actividad mecánica del corazón.

Para realizar la medida experimental hay varias configuraciones de electrodos. Las tres más usadas son:

Medida a cuatro electrodos

Este es el método usado en la mayoría de publicaciones ya que con esta disposición de electrodos la impedancia de la interfaz electrodo-tejido afecta en menor grado la medida (18–23). En esta configuración la corriente se inyecta al tejido a través del par de electrodos exteriores y se mide el voltaje a través del par de electrodos internos (Figura 5A). Cuanto más alejados estén los electrodos que inyectan la corriente de los electrodos que miden el voltaje, la distribución de corriente es más uniforme y por tanto la relación entre corriente y voltaje es más lineal (24). Las medidas a tórax abierto de esta tesis se han realizado usando esta configuración.

Medida a tres electrodos

Esta configuración es la que se ha usado tradicionalmente para registrar la impedancia a través de un electrocatéter endocavitario y un parche superficial de referencia (7,25). Esta medida consiste en aplicar la corriente a través de dos electrodos y medir el voltaje a través de un tercer electrodo y uno de los electrodos usado para inyectar la corriente (Figura 5B). Aunque en menor orden que en la medida a 2 electrodos, hay que tener en cuenta que este método es sensible a la impedancia del electrodo de referencia y, por tanto, se debe realizar una calibración previa para sustraer su valor. También lo hemos usado en esta tesis para medir la impedancia del miocardio a tórax cerrado a través de un electrocatéter convencional.

Medida a dos electrodos

En este tipo de disposición, se inyecta la corriente por el mismo par de electrodos que se usan para medir el voltaje. Es la configuración de electrodos más simple y la que presenta un tamaño de la sonda de registro más reducido. Existen diferentes

trabajos experimentales en los que se han aprovechado unos electrodos temporales para hacer *pacing* desde el picárdio para realizar las medidas (26,27). Esta configuración se puede usar siempre que la impedancia del tejido sea mucho más grande que la impedancia del electrodo para minimizar la influencia de la impedancia del electrodo (12,28).

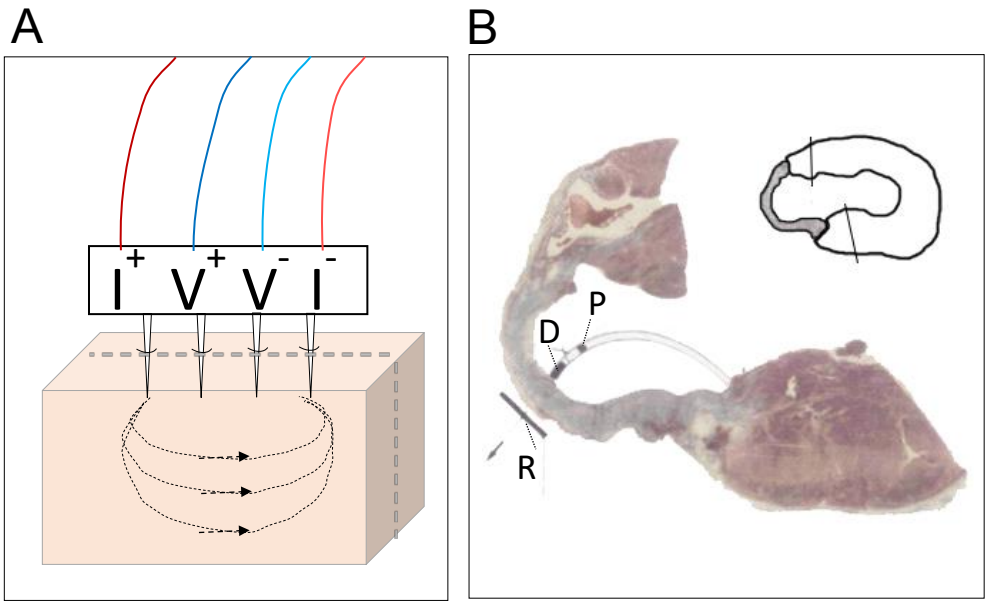

Figura 5. A: Esquema de la medida de impedancia mediante un electrodo tetrapolar. B: Esquema de la medida de la impedancia a 3 electrodos. La corriente se inyecta entre el electrodo distal (D) de un electrocatéter y un parche de referencia (R) y el voltaje se mide entre el electrodo proximal (P) y el mismo parche de referencia. Figura modificada de Warren et al. 2000.

Para expresar los valores registrados de impedancia en valores de resistividad es necesario conocer el factor de celda, que depende de la geometría y la disposición del electrodo con que hayamos realizado la medida. En esta tesis hemos calculado el factor de celda midiendo la resistencia de una solución de NaCl al 0.9% y 25°C, que ofrece una resistividad de 70 Ω·cm.

2. Caracterización de la impedancia eléctrica del miocardio

2.1. Miocardio sano

El estudio de la impedancia eléctrica del miocardio es de interés ya que permite conocer mejor su estructura y las propiedades eléctricas pasivas que gobiernan la propagación electrotónica de la corriente a través del miocardio (20). Su valor depende principalmente de las resistencias extra e intracelulares, de la capacitancia de la membrana celular y de la impedancia de las gap junctions, que son zonas de baja resistencia dentro de la membrana que conectan los miocitos y que permiten el paso de iones y pequeñas moléculas de forma intracelular (29,30) (Figura 6). Además, al ser el miocardio anisótropo, si realizamos las medidas con electrodos superficiales hay que tener en cuenta la dirección de las fibras miocárdicas (20). Por último, otro factor de variación son los cambios que se producen en la curva de la impedancia durante el ciclo cardíaco (29,31).

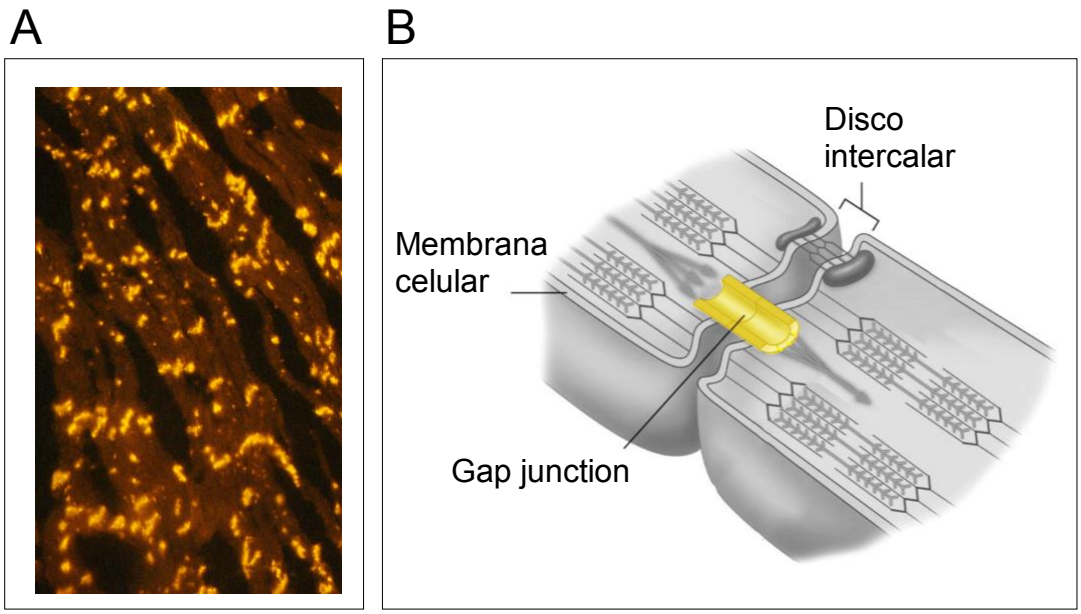

Figura 6. A: Microfotografía de la distribución de las gap junctions en el miocardio de una rata (regiones de amarillo intenso). B: Esquema de la unión de dos miocitos.

2.2. Miocardio inflamado (rechazo cardíaco agudo)

El rechazo agudo y las infecciones son la principal causa de muerte a partir del mes y hasta el primer año del trasplante cardíaco (32). En la práctica clínica el *gold standard* para diagnosticar el rechazo agudo es el análisis histológico de biopsias endomiocárdicas, aunque es un método invasivo con riesgos asociados (33). Si bien existen diversas técnicas no invasivas para detectar de forma temprana el rechazo agudo, como las alteraciones del biomarcador SERCA2a o el alargamiento del tiempo de relajación T2 en la cardio-resonancia magnética, sigue habiendo una escasez de evidencia para su uso en la clínica (34,35).

La medida de la impedancia eléctrica es capaz de detectar el rechazo cardíaco agudo. Varios estudios tanto en modelos animales como en pacientes han descrito cambios en su valor medio ligados al grado de rechazo, que retrogradan al iniciar el tratamiento con corticoesteroides (25,36,37). Concretamente, la impedancia en pacientes sometidos a un trasplante cardíaco fue menor que la de los pacientes control, y una reducción mayor en su valor a 10 kHz se correlacionó con un grado más pronunciado de rechazo (Figura 7). Estos cambios se han atribuido al proceso inflamatorio (edema), tal y como se ha observado en preparaciones in vitro (38).

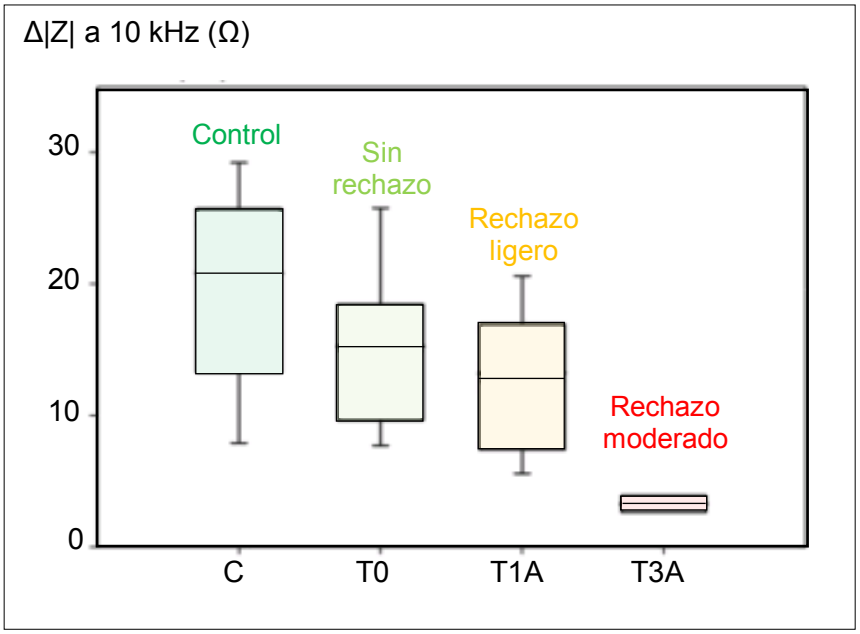

Figura 7. Valores de la impedancia intracardiaca a 10 kHz del ventrículo derecho en pacientes control (C) y en pacientes trasplantados sin rechazo cardíaco (T0), con rechazo ligero (T1A) y con rechazo moderado (T3A). Figura extraída de Cinca J, *et al.* 2008.

2.3. Miocardio con isquéma aguda

La isquemia miocárdica conlleva una reducción del aporte de oxígeno y nutrientes metabólicos a las células no irrigadas y una acumulación de metabolitos deshecho en el espacio intra- y extracelular. Los cambios fisiológicos producidos por la isquemia miocárdica se ven reflejados en la impedancia en tres fases diferenciadas (Figura 8):

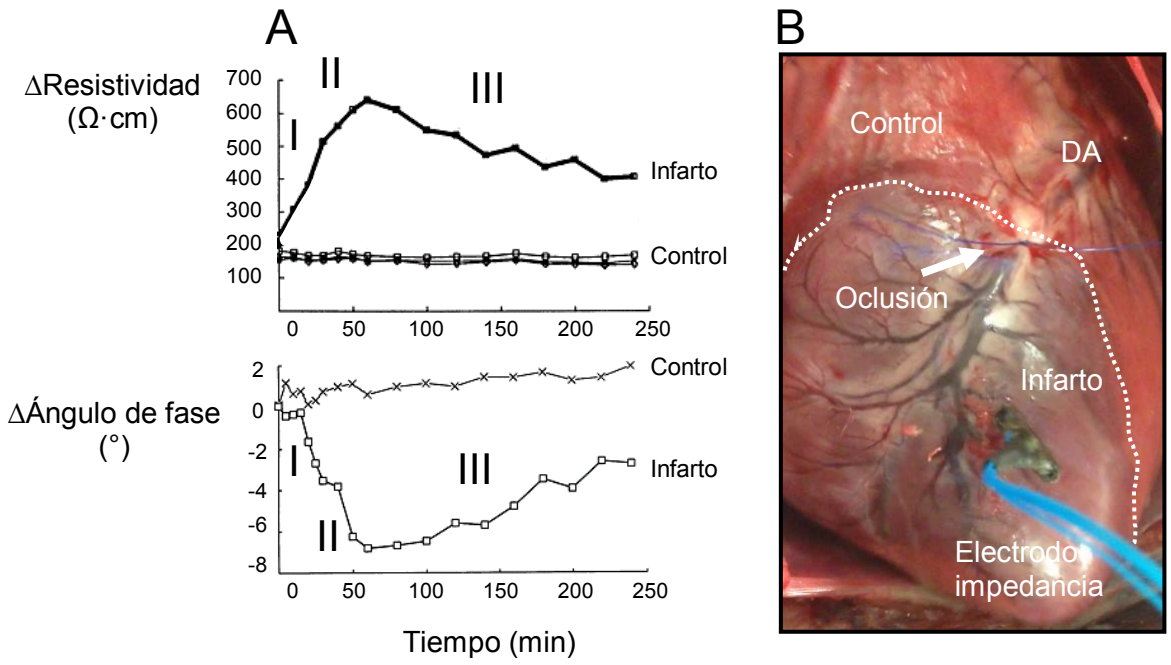

Figura 8. A: Evolución de los cambios de resistividad y ángulo de fase en una región del miocardio sana (Control) y una región isquémica (Infarto) durante 4 horas de oclusión coronaria (Fase I, II y II) en ovejas anestesiadas. Figura modificada de Fallert, et al. 1993; B: Fotografía del ventrículo izquierdo de un cerdo anestesiado sometido a oclusión de la descendente anterior (DA).

- *Fase I*: Al inicio de la isquemia las zonas afectadas presentan un aumento de la magnitud de la impedancia de entre un 50 y un 200% y una disminución similar del ángulo de fase, mientras que en las zonas no isquémicas la impedancia permanece inalterada (19,21,30,39). Estudios in vitro muestran que las resistencias extracelulares aumentan al inicio de la isquemia debido a la reducción del espacio extracelular provocado por el aumento de volumen de las células, mientras que las resistencias intracelulares permanecen inalteradas durante los primeros 10-15 minutos. Transcurrido este tiempo, las resistencias intracelulares aumentan debido a la acumulación intracelular de Ca^{2+} y Na^{2+} y al cierre de las gap junctions (6,40). Además, la fase de arritmias 1A coincide con el primer aumento leve de la resistividad y la fase de arritmias 1B con el aumento brusco de la resistividad y la

disminución del ángulo de fase. Durante esta fase, se ha demostrado que un periodo breve de isquemia (precondicionamiento) retrasa la aparición de arritmias 1B y de los cambios bruscos en la impedancia (21).

- *Fase II*: Transcurridos entre 20 y 150 minutos la magnitud y el ángulo de fase de la zona isquémica alcanzan sus valores máximos de forma sostenida entre unos 30 y 100 minutos (21,41). Durante las fases I y II de isquemia el miocardio podría recuperarse si se realiza una reperfusión, sin embargo transcurridas estas dos fases las posibilidades disminuyen rápidamente (30,42).

- *Fase III*: En esta fase hay una disminución de la resistencia y un aumento del ángulo de fase. En el mismo intervalo temporal hay una disminución en la concentración de ATP y un aumento en la concentración de lactato tisular. Los cambios en los valores de la impedancia se han asociado al inicio de la destrucción de las membranas celulares y la formación de una necrosis irreversible (18,41).

Otros estudios experimentales han descrito que la medida de la impedancia puede ser útil para monitorizar el estado de perfusión durante el trasplante cardíaco (43,44) y la cirugía de bypass coronario (26,27,45,46).

2.4. Miocardio con infarto crónico

Transcurridas 6-8 semanas de la oclusión coronaria, la zona infartada ha sido reemplazada por fibroblastos y posteriormente por depósitos de colágeno y por tanto es una zona carente de contracción activa (47). Las propiedades eléctricas del tejido infartado reflejan los cambios estructurales durante este periodo: al cabo de 2 días de sufrir un infarto, la impedancia de la zonas cicatriciales se reduce de forma permanente, entre un 50% y un 70% respecto al tejido sano (19,48,49). Aunque

menos estudiado, el ángulo de fase de la cicatriz de infarto también decrece en valor absoluto y pasa a tener unos valores cercanos a cero (7,50,51) (Figura 9).

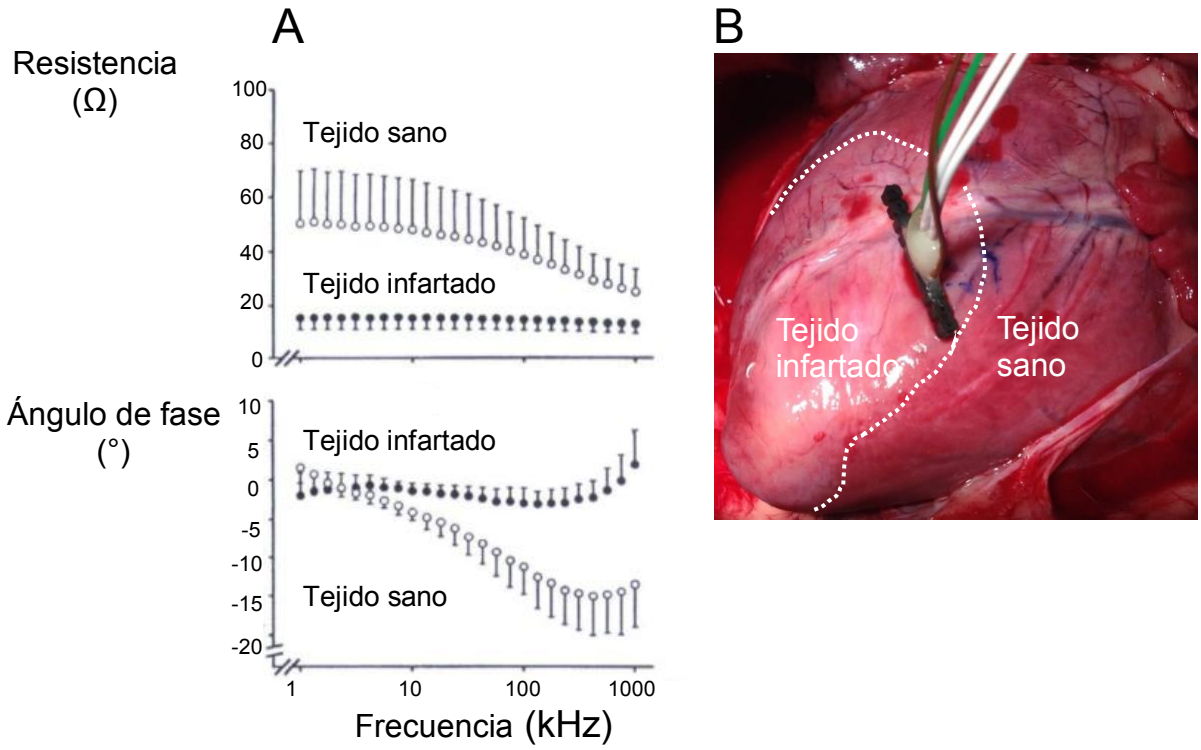

Figura 9. A: Variación de la resistencia y el ángulo de fase con la frecuencia de la corriente en tejido sano e infartado. Figura modificada de Warren, M., et al. 2000. B: Fotografía del ventrículo izquierdo de un cerdo anestesiado con un infarto anterior de 1 mes de evolución.

El descenso de la magnitud de la impedancia y del ángulo de fase en la cicatriz de infarto se ha atribuido a los cambios en la composición bioquímica de la misma y al aumento de la ratio entre volumen extracelular e intracelular. La cicatriz de infarto es un tejido pobre en miocitos y posee una matriz extracelular aumentada. (52). Esta matriz extracelular está formada por proteínas inmersas en agua y glicoproteínas que facilitan una alta conductividad iónica y por tanto una baja resistencia. Al existir un menor número de membranas celulares se reduce el efecto capacitivo, y por tanto el ángulo de fase. Además, algunos autores apuntan que los valores de impedancia elevados en las zonas de miocardio sanas remotas al infarto serían

debidas a un mal remodelado post-infarto, y que este hecho aumentaría el riesgo de arritmias (48).

En los bordes de la cicatriz de infarto existen miocitos sanos y tejido fibrótico y, debido a esto, la resistividad tiene valores intermedios (49). La medida de la impedancia se ha propuesto como posible método diagnóstico y se han realizado estudios que demuestran que es posible delimitar la cicatriz a través de un electrocatéter endocavitario (7,8).

2.5. Miocardio con patología infiltrativa

La presencia de hipertrofia del ventrículo izquierdo está asociada a un incremento del riesgo en el desarrollo de insuficiencia cardiaca, cardiopatía isquémica, muerte súbita, fibrilación auricular e ictus (53). Según la teoría del cable, el aumento del diámetro de los miocitos que ocurre durante la hipertrofia debería aumentar la velocidad de conducción del potencial de acción. Sin embargo, los estudios muestran que la velocidad de conducción está disminuida (54,55). Diversos autores han demostrado que los miocitos de corazones hipertróficos porcinos tienen una resistencia más elevada que las de los miocitos control debido al aumento de la impedancia de las gap junctions (56,57). Este hecho apoya la hipótesis que el aumento de la resistencia intracelular en los corazones hipertróficos crea una discontinuidad en la propagación del potencial de acción que podría ser el precursor de arritmias por mecanismos de reentrada.

Los estudios descritos en esta introducción demuestran que la medida de la impedancia eléctrica en el miocardio puede caracterizar su estructura y ser de utilidad para diagnosticar la isquemia aguda, crónica o episodios el rechazo post-trasplante. Sin embargo, en la literatura no hemos encontrado ningún trabajo que haya relacionado los cambios de la curva de impedancia eléctrica local del miocardio para caracterizar su estado y así, mejorar el guiado de la ablación de arritmias. Por este motivo planteamos este trabajo, con la siguiente hipótesis.

Hipótesis

La medida continua de la impedancia local del miocardio permite caracterizar el infarto cicatricial y no se ve afectada por cambios en la secuencia de activación cardíaca.

Objetivos

Objetivo general

- Desarrollar una nueva técnica para la detección y caracterización de la cicatriz de infarto de miocardio basada en medidas de bioimpedancia.

Objetivos específicos

- Cuantificar los cambios de la impedancia eléctrica durante el ciclo cardiaco en el tejido miocárdico sano, así como su interrelación con la actividad mecánica ventricular y con el gasto cardíaco.
- Detallar las alteraciones en el patrón de la impedancia eléctrica local del miocardio con isquemia aguda y crónica.
- Correlacionar los valores de la impedancia eléctrica medidos en diferentes puntos de la cicatriz post-infarto con el grado de afectación transmural determinado por análisis anatomopatológico.
- Validar la detección endocárdica de la cicatriz post-infarto mediante la impedancia eléctrica utilizando sistemas de navegación cardiaca idénticos a los usados en la clínica y evaluar su variación ante cambios en la secuencia de activación cardíaca.

Resultados

Artículo 1: *Early detection of acute transmural myocardial ischemia by the phasic systolic- diastolic changes of local tissue electrical impedance*.

Esther Jorge, Gerard Amorós-Figueras, Tomás García-Sánchez, Ramon Bragós, Javier Rosell-Ferrer y Juan Cinca J. *American Journal of Physiology. Heart and Circulatory Physiology* 2015; 310: H436-43.

https://doi.org/10.1152/ajpheart.00754.2015

Am J Physiol Heart Circ Physiol 310: H436–H443, 2016.
First published November 25, 2015; doi:10.1152/ajpheart.00754.2015.

Early detection of acute transmural myocardial ischemia by the phasic systolic-diastolic changes of local tissue electrical impedance

Esther Jorge,[1]* Gerard Amorós-Figueras,[1]* Tomás García-Sánchez,[2] Ramón Bragós,[2] Javier Rosell-Ferrer,[2] and Juan Cinca[1]

[1]*Department of Cardiology, Hospital de la Santa Creu i Sant Pau, Institute of Biomedical Research Sant Pau, Universitat Autonoma de Barcelona, Barcelona, Spain; and* [2]*Electronic and Biomedical Instrumentation Group, Department of Electronics Engineering, Universitat Politecnica de Catalunya, Barcelona, Spain*

Submitted 28 September 2015; accepted in final form 19 November 2015

Jorge E, Amorós-Figueras G, García-Sánchez T, Bragós R, Rosell-Ferrer J, Cinca J. Early detection of acute transmural myocardial ischemia by the phasic systolic-diastolic changes of local tissue electrical impedance. *Am J Physiol Heart Circ Physiol* 310: H436–H443, 2016. First published November 25, 2015; doi:10.1152/ajpheart.00754.2015.—Myocardial electrical impedance is influenced by the mechanical activity of the heart. Therefore, the ischemia-induced mechanical dysfunction may cause specific changes in the systolic-diastolic pattern of myocardial impedance, but this is not known. This study aimed to analyze the phasic changes of myocardial resistivity in normal and ischemic conditions. Myocardial resistivity was measured continuously during the cardiac cycle using 26 different simultaneous excitation frequencies (1 kHz–1 MHz) in 7 anesthetized open-chest pigs. Animals were submitted to 30 min regional ischemia by acute left anterior descending coronary artery occlusion. The electrocardiogram, left ventricular (LV) pressure, LV dP/d*t*, and aortic blood flow were recorded simultaneously. Baseline myocardial resistivity depicted a phasic pattern during the cardiac cycle with higher values at the preejection period (4.19 ± 1.09% increase above the mean, $P < 0.001$) and lower values during relaxation phase (5.01 ± 0.85% below the mean, $P < 0.001$). Acute coronary occlusion induced two effects on the phasic resistivity curve: *1*) a prompt (5 min ischemia) holosystolic resistivity rise leading to a bell-shaped waveform and to a reduction of the area under the LV pressure-impedance curve (1,427 ± 335 vs. 757 ± 266 Ω·cm·mmHg, $P < 0.01$, 41 kHz) and *2*) a subsequent (5–10 min ischemia) progressive mean resistivity rise (325 ± 23 vs. 438 ± 37 Ω·cm at 30 min, $P < 0.01$, 1 kHz). The structural and mechanical myocardial dysfunction induced by acute coronary occlusion can be recognized by specific changes in the systolic-diastolic myocardial resistivity curve. Therefore these changes may become a new indicator (surrogate) of evolving acute myocardial ischemia.

animal model; bioelectrical impedance; hemodynamics; myocardial ischemia.

NEW & NOTEWORTHY

This study affords a new method to promptly recognize the presence of acute myocardial ischemia based on the measurement of the local changes in myocardial resistivity elicited during heart contraction and relaxation.

MYOCARDIAL ELECTRICAL resistivity is a passive biophysical property of the heart that is influenced by geometrical cell characteristics and by the structural integrity of the myocardium (16). Classical measurements of myocardium electrical resistivity have usually been performed at a single current frequency, in the 1–15 kHz range (6) or using the frequency-sweep electrical impedance spectroscopy (EIS) technique, in the 0.1 kHz to 10 MHz range (8) or in the 1 kHz to 1 MHz range (12). With these techniques, stationary characterization of myocardial resistivity in normal and ischemic myocardium was possible (20), but due to the time required for the whole impedance spectrum acquisition, only a few measurements could be drawn during the cardiac cycle. Therefore, the phasic changes in myocardial resistivity that are closely linked to the mechanical activity of the beating heart were not well defined.

Recently, with the use of the fast broadband EIS, it is feasible to obtain up to 1,000 spectrums/s and therefore a more refined information about the time behavior of myocardial impedance during the mechanical cardiac activity. It is predictable that in the presence of acute myocardial ischemia the resultant structural and mechanical derangements will exert specific changes in the phasic systolic-diastolic resistivity curve, but this is not known.

This study aimed to characterize the phasic (systolic-diastolic) changes of myocardial resistivity in normal and ischemic conditions in the in situ pig heart by using fast broadband EIS.

MATERIALS AND METHODS

Study Population

Seven female domestic swine (Landrace-Large White cross) weighing 40 kg were premedicated with a combination of midazolam (0.6 mg/kg) and ketamine (12 mg/kg), both injected intramuscularly. Anesthesia was induced with intravenous propofol (2–4 mg/kg). After endotracheal intubation, general anesthesia was maintained with sevofluorane inhalation (2.5–3.5% with oxygen) and the animals were mechanically ventilated. Ventilatory parameters were adjusted to maintain blood gases within physiological ranges. Remifentanyl (0.2 $\mu g \cdot kg^{-1} \cdot min^{-1}$) was administered during the procedure for analgesia.

The study protocol was approved by the Institutional Animal Care and Use Committee (IACUC) of our institution, and conformed to the regulation for the treatment of animals established by the *Guide for the Care and Use of Laboratory Animals*, 8th ed. (National Research Council, Washington, DC: the National Academies Press, 2010).

Experimental Preparation

A femoral arterial access was established by using the Seldinger technique and a 6-F introducer sheath (Cordis; Miami, FL) was introduced percutaneously into the femoral artery. Under fluoroscopic guidance, a 5-F Millar micromanometer catheter (Millar Instruments,

* E. Jorge and G. Amorós-Figueras contributed equally to this work.
Address for reprint requests and other correspondence: E. Jorge, Dept. of Cardiology, Hospital de la Santa Creu i Sant Pau, Sant Antoni MªClaret, 167, 08025, Barcelona, Spain (e-mail: ejorge@santpau.cat).

Houston, TX) was advanced to the left ventricle (LV) to continuously monitor the LV pressure. The peripheral electrocardiogram (ECG) was recorded (Nihon Kohden; Tokyo, Japan). The thorax was opened through a midline sternotomy, and the heart was suspended in a pericardial cradle. An ultrasonic flow probe (Transonic Systems, Ithaca, NY) was carefully deployed around the aortic root to monitor the aortic blood flow (ABF). The left anterior descending (LAD) coronary artery was dissected after the first diagonal and was looped with a Prolene 3/0 snare (Ethicon).

Electrocardiographic and Hemodynamic Parameters

In all cases, we recorded the following signals: *1*) the conventional ECG lead II, *2*) the LV pressure with an intracavitary Millar micromanometer catheter, and *3*) ABF. An amplifier system (Nihon Kohden) was used to record the LV pressure and ECG and a Transonic Systems to construct the ABF curve. All signals were digitized at 1 kHz (PowerLab with LabChart, ADInstruments) and stored for subsequent offline analysis. The first derivative of LV pressure was also calculated.

Myocardial Electrical Impedance

Theoretical background. The whole myocardial electrical impedance is an overall estimation of the intra- and extracellular resistances and the cell membrane capacitance (7). Impedance (Z) is defined as the voltage (V) divided by the sinusoidal current (I) of a given frequency (f) applied through a region [$Z(f) = V/I$]. Since biological tissues are not purely resistive, there will be a time delay (Δt) between the voltage and current waves which is measured as a phase angle shift ($\Theta = 360 \cdot \Delta t \cdot f$). Therefore, myocardial impedance has two components: tissue resistivity (ρ) and phase angle (Θ). Tissue resistivity was calculated from the relation $R = k\rho$, where R is the in-phase component of V with respect to I, and k is the cell constant of the electrode determined by measuring the electrical resistance of a 0.9% NaCl solution at 25°C, which affords a resistivity of 70 Ω·cm.

Tissue impedance spectroscopy. Tissue impedance was measured with a four-electrode probe to minimize the electrode-tissue interface impedance (17). The probe consisted of a linear array of four platinum-iridium needle electrodes (5 mm long, 0.4 mm diameter, with a constant interelectrode distance of 1.27 mm). The outer pair of electrodes was used to apply the test currents to the myocardium, while the inner two electrodes were employed to measure the resulting potential difference. The electrode probe was inserted into the LV myocardial wall, perpendicular to the trajectory of the LAD coronary artery (Fig. 1). An analog front-end was used to interconnect the electrode array with the signal generation and acquisition system. The impedance measurements were performed using a current excitation consisting of a multisine signal (1-ms duration, 1-mA peak amplitude) of 26 frequencies logarithmically spaced in the range from 1 kHz to 1 MHz, obtaining 1,000 spectra/s. Both current generation and acquisition were synchronized using a custom setup based on a PXI system from National Instruments. The acquired signals were low-pass filtered and then digitized at 5 MHz sampling rate. The physiological signals (LV pressure, ABF, ECG) were acquired synchronously with the impedance measurements, using an additional 8-channel digitizer card included in the PXI system. To compensate for the potential error effects elicited by the cables and the amplifier response, the electrical impedance setup was calibrated at the beginning of each study by measuring the impedance spectrum of a test saline solution of known resistivity.

We have analyzed the time course of the resistivity patterns during three phases of the cardiac cycle: *1*) preejection, *2*) ejection, and *3*) relaxation. The preejection phase was defined as the interval between the peak of the R wave of the ECG to the start of the steep increase of the ABF (aortic valve opening); the ejection phase was delimited between the last point of the previous phase and the moment where ABF dropped rapidly towards 0 l/min (aortic valve closure); and the relaxation phase was defined as the rest of the cycle until the next R wave peak. We measured the maximum value of the resistivity during the preejection phase, the mean value of the resistivity during the ejection phase, and the minimum value of the resistivity during the relaxation phase at baseline and after coronary occlusion. These measures were performed in three consecutive cardiac cycles, and data were averaged for statistical analysis. The resistivity values were normalized to their relative change from the total resistivity mean: $\Delta Z = 100 \times [Z(ph) - Z(mean)]/Z(mean)$, where Z is tissue resistivity, Z(ph) is resistivity in a given cardiac phase, and Z(mean) is the mean resistivity value during the entire cardiac cycle. Further analyses of resistivity

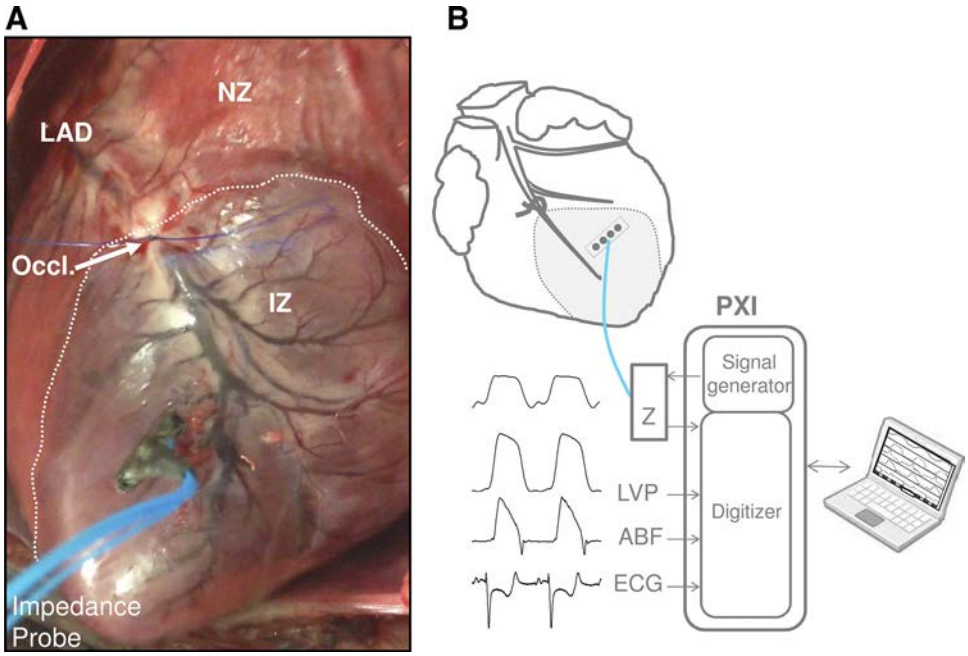

Fig. 1. Schematic representation of the experimental model. *A*: a photograph of the left ventricular anterior wall in an open-chest pig heart preparation submitted to occlusion (occl.) of the left anterior descending (LAD) coronary artery. The dotted white line delineates the border between the cyanotic ischemic region (IZ) and the nonischemic myocardium (NZ). The impedance probe is inserted inside the cyanotic region. *B*: a schematic representation of the system used to record simultaneously the phasic changes of myocardial electrical impedance (Z), left ventricular (LV) pressure, aortic blood flow (ABF), and surface ECG.

Table 1. *Hemodynamic parameters in seven anesthetized pigs submitted to 30 min of left anterior descending (LAD) coronary artery occlusion*

	Basal (n = 7)	30′ LAD occl (n = 7)	P
RR interval, ms	842 ± 63	804 ± 74	NS
LVSP, mmHg	83 ± 4	76 ± 4	<0.01
LVEDP, mmHg	10.0 ± 2	12 ± 2	NS
dP/dt_{max}, mmHg/s	1,410 ± 94	1,246 ± 63	NS
dP/dt_{min}, mmHg/s	−1,274 ± 131	−1,091 ± 128	<0.01
ABF, l/min	3.0 ± 0.3	2.3 ± 0.2	<0.05

Values are means ± SE; n = 7. LVSP, left ventricular systolic pressure; LVEDP, left ventricular end-diastolic pressure; dP/dt, first derivative of the left ventricular pressure; ABF, aortic blood flow.

changes in relation to the LV pressure (pressure-impedance curves) were also performed.

Study Protocol

The study began after stabilization of the anesthesia level and hemodynamic parameters. Then the hemodynamic and electrical signals were recorded at baseline and sequentially during 30 min of acute transmural myocardial ischemia in the territory of the implanted impedance electrode by occluding the LAD coronary artery. At the end of the study the animals were euthanized and the heart was removed to verify the appropriate location of the impedance electrode in the ischemic region.

Statistical Analysis

Data were expressed as means ± standard error of the mean (SE). Differences in the study variables were assessed using repeated-measures t-test, and analysis of variance (ANOVA) with Bonferroni correction for post hoc comparisons, as appropriate. A P value of <0.05 was considered statistically significant. Statistical analyses were performed using the software SPSS v.22.0 (IBM SPSS, Chicago, IL).

RESULTS

ECG and Hemodynamic Parameters

As shown in Fig. 1, LAD occlusion induced a visible area of cyanosis in the subtended myocardial region, which was associated with reciprocal ST segment depression in lead II, and a decrease of the LV systolic pressure, negative LV dP/dt, and aortic blood flow (Table 1 and Fig. 2). The positive LV dP/dt also followed a decreasing tendency, but this was not statistically significant.

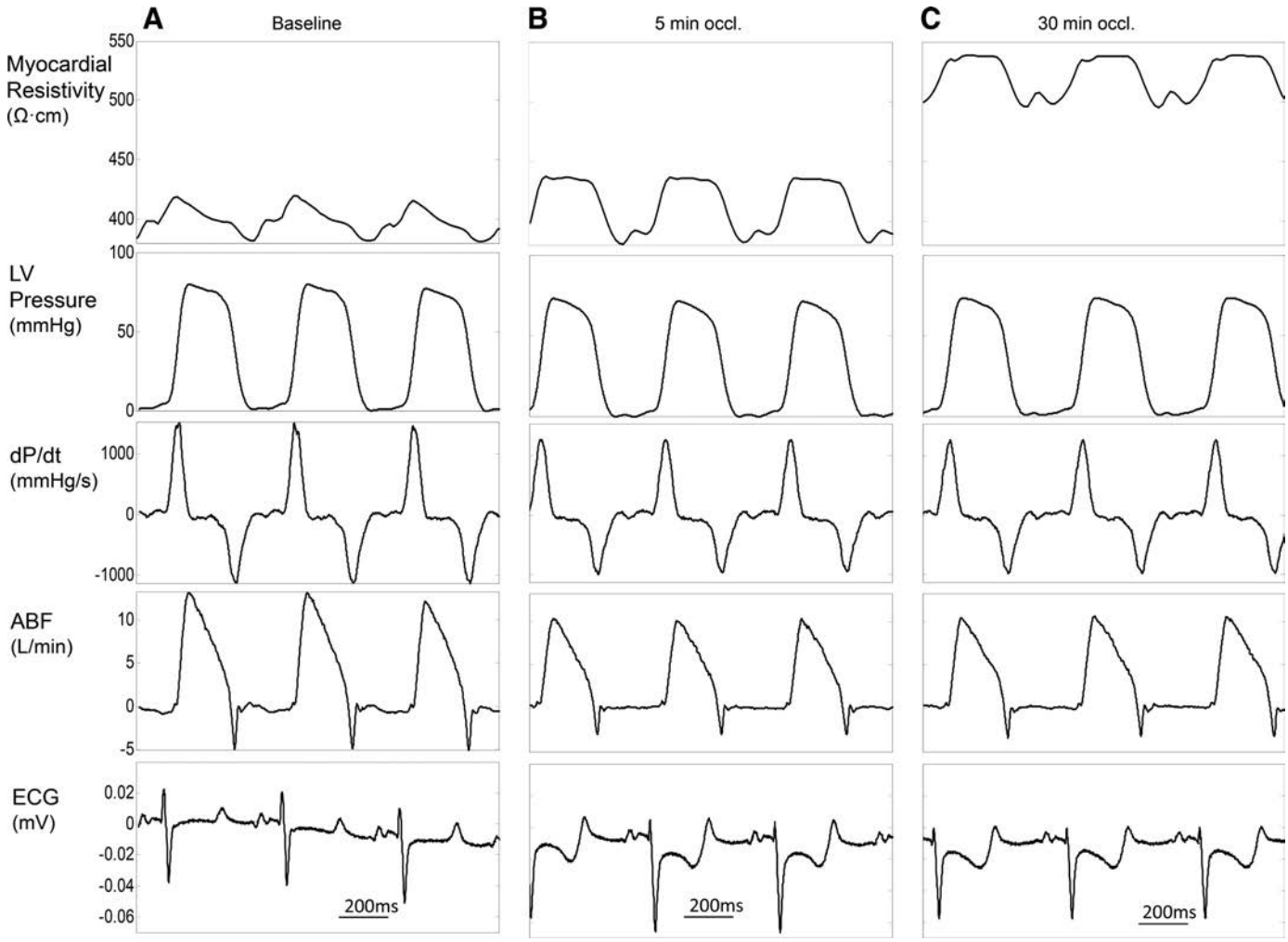

Fig. 2. Simultaneous recording of myocardial resistivity at 1 kHz, LV pressure, LV dP/dt, ABF, and lead II of the ECG at baseline (*A*), and after 5 min (*B*) and 30 min of LAD coronary occlusion (*C*).

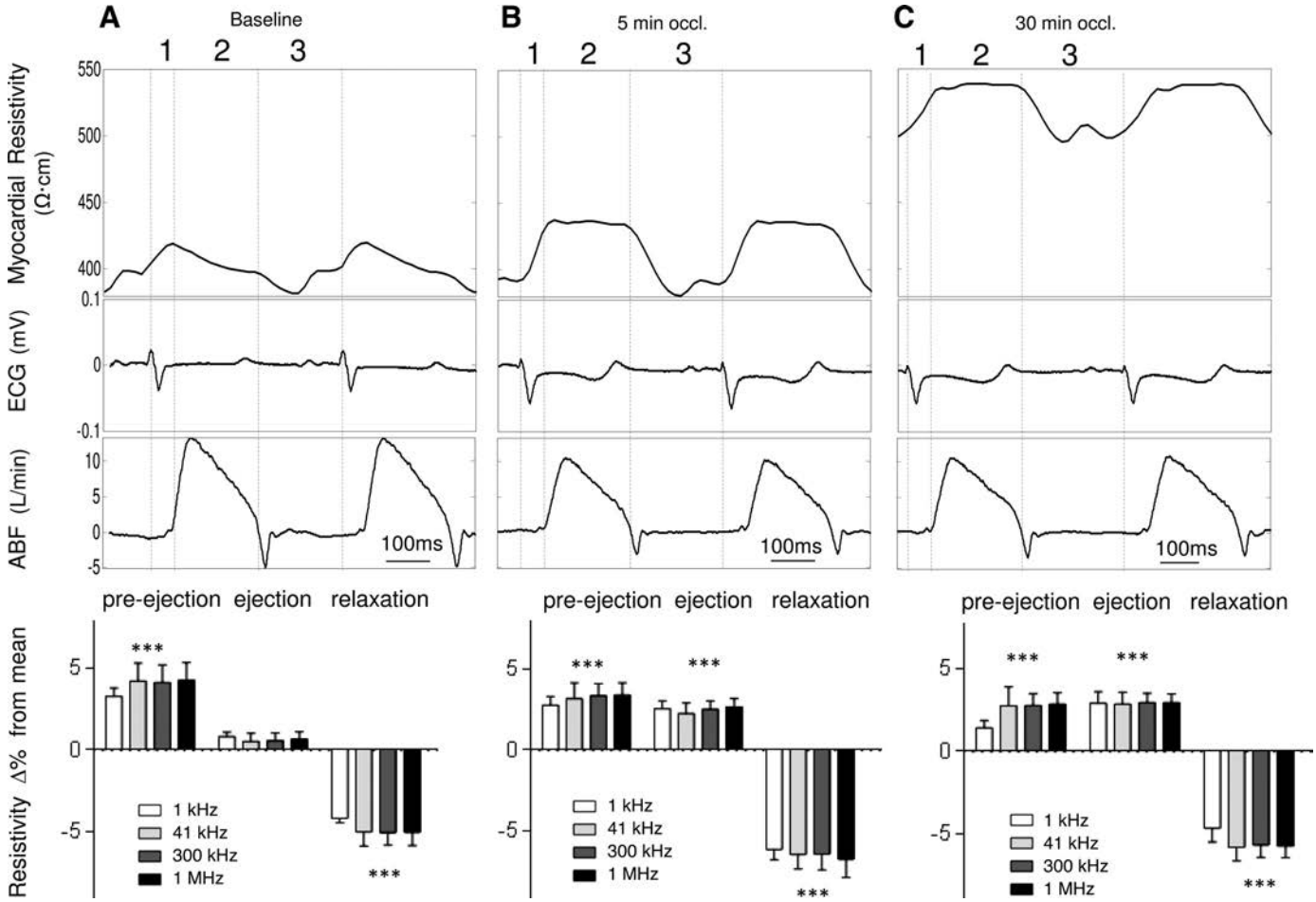

Fig. 3. Time course of the changes in myocardial resistivity during 30 min of LAD occlusion at different current frequencies. *A* (top): the simultaneous recording of baseline resistivity at 1 kHz, ECG, and aortic blood flow during the 3 different phases of the cardiac cycle: preejection (*1*), ejection (*2*), and relaxation (*3*), in one anesthetized pig. The bottom panel shows the percentage change from the mean resistivity value at different frequencies in the group of 7 pigs. Five minutes after LAD occlusion (*B*) there was a plateau increase of resistivity during the ejection period which was statistically significant in the group of 7 pigs (bottom panel). *C* shows an increase in the myocardial resistivity (upward shift) maintaining the bell-shaped contour seen at 5 min occlusion. ***$P < 0.001$ vs. mean.

Phasic Changes in Myocardial Impedance

As illustrated in Fig. 3*A*, electrical resistivity of the normal myocardium depicted phasic changes during the cardiac cycle: a maximal value was attained during the preejection period and a minimal value during the relaxation phase. The bottom panel in Fig. 3*A* shows the phasic changes in resistivity at various frequencies expressed as %variation from the mean value in the 7 studied pigs. This analysis indicated that during the preejection period the resistivity at 41 kHz increased by 4.19 ± 1.09% ($P < 0.001$) over the mean, whereas a decrease of about 5.01 ± 0.85% ($P < 0.001$) occurred during the relaxation phase. The phasic pattern of resistivity changes was valid for all test current frequencies analyzed.

Acute LAD occlusion induced remarkable changes in both the shape of the phasic pattern and magnitude of local tissue resistivity (Fig. 3, *B* and *C*). As shown in Fig. 3*B*, soon after coronary occlusion the resistivity curve recorded in the ischemic region evolved to a bell-shaped contour as a result of a sustained resistivity rise that persisted throughout the whole ejection phase. The bottom panel of Fig. 3 illustrates the phasic changes at various frequencies in the whole experimental series. Thus at 5 min of LAD occlusion the % change over the mean resistivity at 41 kHz was 3.14 ± 0.97% at preejection ($P < 0.001$); 2.24 ± 0.64% during ejection ($P < 0.001$); and −6.42 ± 0.89% during the relaxation phase ($P < 0.001$). Thereafter, the changes in the resistivity pattern were accompanied by a progressive increase in the magnitude of the whole tissue resistivity as illustrated in Fig. 3*C*. At 30 min of LAD occlusion the mean resistivity increased significantly at 1 kHz and 41 kHz (from 325 ± 23 to 438 ± 37 Ω·cm, $P < 0.001$, at 1 kHz and from 276 ± 21 to 339 ± 27 Ω·cm, $P < 0.01$, at 41 kHz).

Myocardial Impedance Spectroscopy

Figure 4 illustrates the dependence of myocardial resistivity and its phase angle on the frequency of the injected alternating current. In normal conditions (Fig. 4*A*), the magnitude of myocardial resistivity (solid line represents the mean values and dashed lines the maximum and minimum values of the whole phasic changes) decreased as the frequency increased (from 325 ± 23 Ω·cm at 1 kHz to 213 ± 17 Ω·cm at 1 MHz, $P < 0.001$). Under ischemic conditions, myocardial resistivity

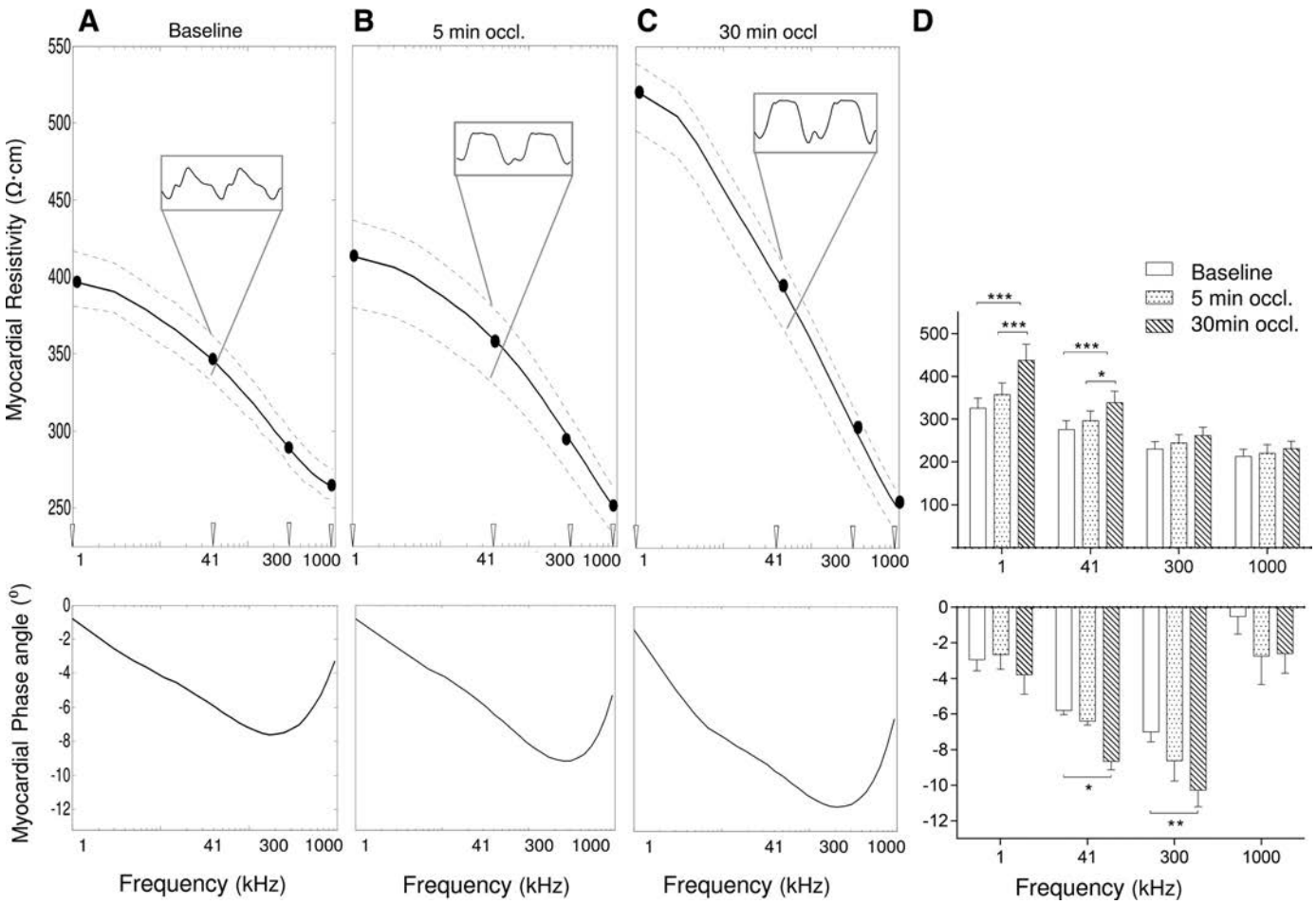

Fig. 4. Myocardial resistivity (top) and phase angle (bottom) at different frequencies (1 kHz–1 MHz) during baseline (*A*), and after 5 min (*B*) and 30 min of LAD occlusion (*C*) in one anesthetized pig. The solid line represents the mean values of the phasic resistivity changes and the dashed lines their maximum and minimum values. Signals in the inset boxes represent the phasic patterns of myocardial electrical resistivity at 41 kHz. *D* shows the mean value of resistivity and phase angle for the whole group of 7 pigs at four specified excitation frequencies in baseline conditions and after 5 and 30 min of LAD occlusion. ***$P < 0.001$; **$P < 0.01$; *$P < 0.05$.

followed a similar trend of changes (from 438 ± 37 Ω·cm at 1 kHz to 231 ± 18 Ω·cm at 1 MHz, $P < 0.001$) although with a greater mean value (mean resistivity rise of about 23% at 41 kHz, $P < 0.01$).

The bottom panels in Fig. 4 illustrate the frequency dependence of the phase angle of myocardial impedance. In the nonischemic myocardium the phase angle followed a progressive decline to more negative values as the frequency of the injected current was increased from 1 kHz to 300 kHz. At frequencies higher than 300 kHz, the phase angle depicted less negative values. In the presence of acute myocardial ischemia the phase angle evolved to more negative values than baseline at all current frequencies. Moreover, Fig. 4 shows a deepest deviation at 300 kHz and a new relaxation at 5–10 kHz. The current frequencies that better differentiate the resistivity of the healthy and acute ischemic myocardium were those comprised between 1 and 41 kHz. By contrast, the phase angle changes are better differentiated at frequencies ranging from 41 kHz to 300 kHz.

LV Pressure-Impedance Curves

The temporal relationship between the whole cardiac mechanical activity and the concurrent changes in regional myocardial impedance can be better analyzed by constructing the LV pressure-impedance loop (Fig. 5*B*). This shows that during the preejection phase (*segment 1* in Fig. 5) both the LV pressure and myocardial resistivity increased progressively. However, during the ejection phase (*segment 2*) resistivity dropped rapidly while the LV pressure remained rather stationary. At the beginning of the relaxation phase (*segment 3*) both the LV pressure and resistivity decreased progressively but at the end of this period, when the LV pressure dropped to nearly 0 mmHg, the resistivity increased rapidly to the preejection value.

The LV pressure-impedance loop suffered marked changes during acute LAD occlusion. As illustrated in Fig. 6, the area under the LV pressure-impedance curve (AUC) decreased dramatically 5 min after LAD occlusion (from 1,427 ± 335 to 733 ± 157 Ω·cm·mmHg at 41 kHz, $P < 0.01$). Figure 6 reveals that the AUC reduction is likely caused by the lack of changes in resistivity during the plateau rise at the ejection phase. Likewise, the progressive increase in the magnitude of resistivity that was detected in the ensuing stages of ischemia shifted the LV pressure-resistivity loop upwards to higher resistivity values. Figure 6 illustrates the shift of the depressed loop at

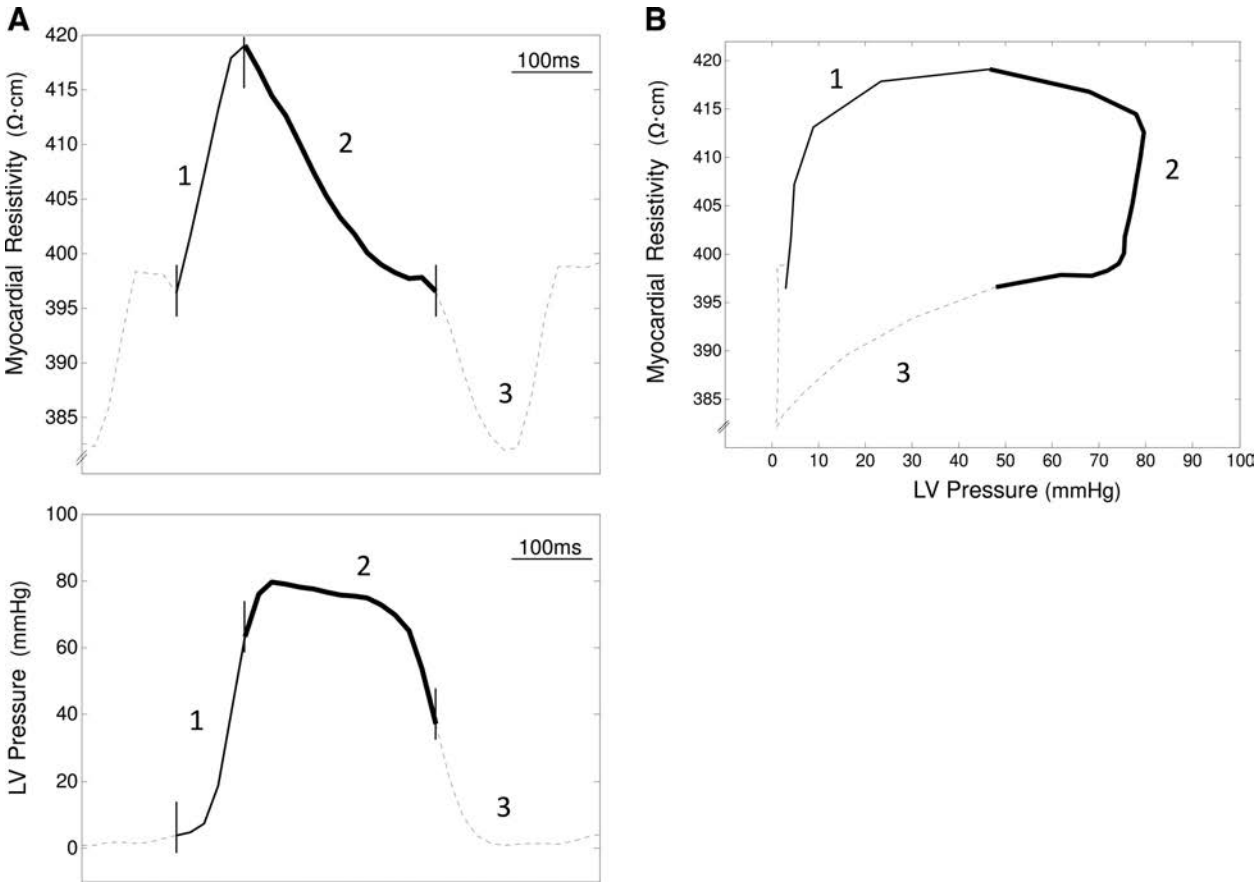

Fig. 5. Time relationship between the changes in myocardial impedance and LV pressure (*A*) expressed graphically by the LV pressure-impedance curves (*B*) during the preejection (*1*), ejection (*2*), and relaxation (*3*) phases of the cardiac cycle in one anesthetized pig.

30 min of LAD occlusion (AUC: 1,427 ± 335 vs. 757 ± 266 Ω·cm·mmHg at 41 kHz $P < 0.01$). The shape of the LV pressure-impedance loops was comparable among the different current frequencies analyzed in this study.

DISCUSSION

Main Findings

This study shows that acute transmural myocardial ischemia exerts two well-defined effects on local tissue electrical impedance. One effect was already known and consisted of a myocardial resistivity rise that became significant after 5–10 min of ischemia (5, 11, 20). The second effect, which has not been previously reported, was characterized by a fast change in the contour of the local systolic-diastolic resistivity curve. Specifically, within the first 5 min of ischemia the resistivity curve evolved from a biphasic pattern—with higher values at preejection phase and lower values during relaxation—to a bell-shaped contour caused by a sustained resistivity rise during systole. This local holosystolic sustained resistivity rise shared a close time-relationship with the local mechanical systolic bulging that develops during the first min of interruption of the LAD coronary flow in the ischemic region, also in the pig heart model (3). Therefore, this study suggests a close relationship between the morphology of the phasic myocardial resistivity curve obtained by continuous measurement of the tissue resistivity during the cardiac cycle and the local mechanical cardiac activity.

Mechanism of the Phasic Changes in Myocardial Impedance

The phasic changes in myocardial resistivity are likely related to the cyclic variations of myocardial cell geometry that occur during cardiac contraction and relaxation. This assumption is based on the fact that myocardial impedance is modulated by changes in cell dimension and structural integrity (16) and, on the other hand, on the observation that cardiac contraction and relaxation induce cyclic changes in myocardial thickness (19) and cell length (2).

Recording of the phasic resistivity curve was not feasible until recently. The inability to detect specific impedance differences between systole and diastole was alluded by previous investigators (6, 10) and was mainly due to the low sampling rate imposed by the impedance measuring system. Recently, we (13, 14) reported a novel methodological procedure allowing detection of the evolving temporal changes of bioimpedance during the cardiac cycle by using fast broadband electrical impedance spectroscopy (EIS). Thus we were able to acquire up to 1,000 spectra/s in healthy porcine myocardium although in that study we could not fully characterize the phasic resistivity curve due to the lack of synchronized physiological parameters. Using the frequency-sweep EIS technique in healthy tissue other authors (17) reported impedance changes during the cardiac cycle in relation to the myocardial fiber orientation: higher longitudinal resistivity values during the ejection phase and higher transverse resistivity values during late diastole. In our study myocardial resistivity was higher in

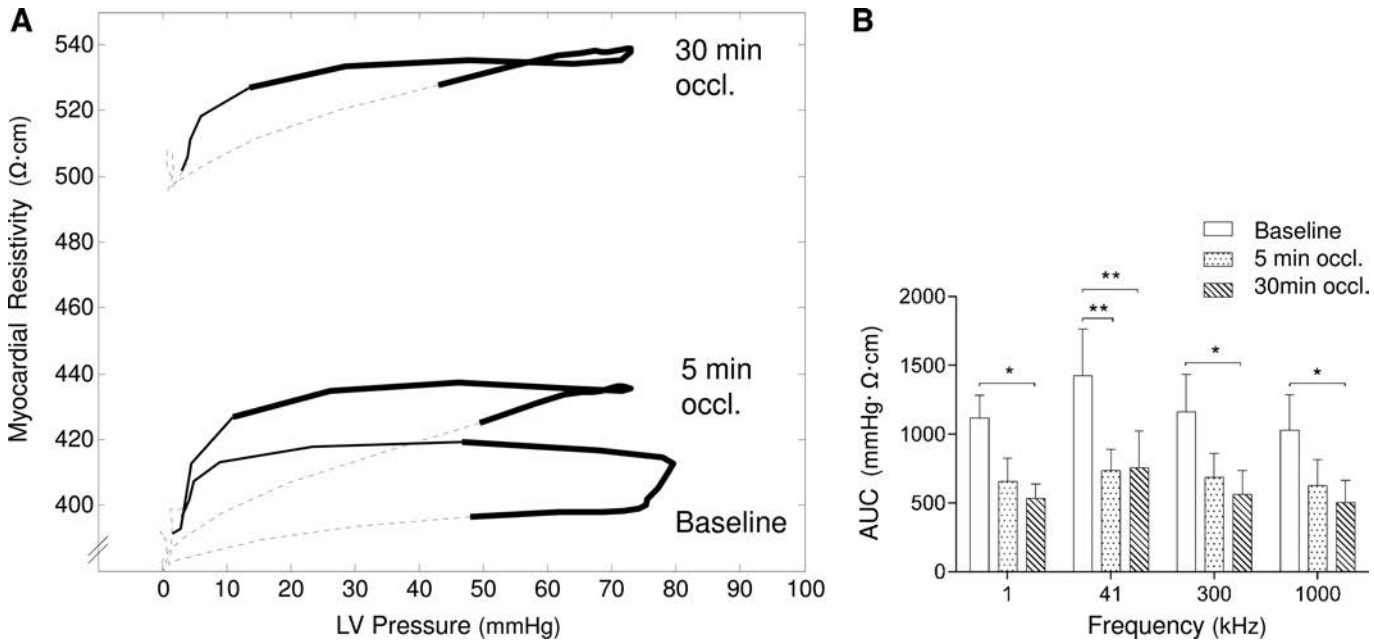

Fig. 6. Changes in the LV pressure-impedance curve during 30 min of LAD occlusion. *A* shows a drop of the area under the LV pressure-impedance curve (AUC) soon after LAD occlusion (5 min) that was followed by an upright deviation towards higher myocardial resistivity values at 1 kHz after 30 min LAD occlusion in one anesthetized pig. *B* shows the LV pressure-impedance curve AUC of the whole group of animals at different excitation frequencies at baseline and after 5 and 30 min of ischemia. Loops are divided in three periods: preejection (slim line), ejection (bold line), and relaxation (dashed line). $^{**}P < 0.01$; $^{*}P < 0.05$.

the preejection phase and lower during diastole. These two studies used distinct measurement techniques: a contact epicardial probe in the first study and a four needle electrode inserted 5 mm deep into the myocardium in ours. The intramural electrode encompasses the different myocardial layers of the ventricular wall and would be expected to average the effects of layer fiber orientation. In addition, in the study by Steendijk et al. (17) the impedance spectrum (8 current frequencies) was measured stepwise during 30 s and as a consequence of the large measuring time required, the temporal variation of the bioimpedance spectrum during the cardiac cycle might be underestimated.

The myocardial structure consists of two electrically conducting compartments (the intra- and extracellular spaces) separated by insulating membranes. The conductance of the electric current flowing through this structure is highly dependent on the current frequency (8, 12, 20). The present study shows that the average specific myocardial impedance is frequency dependent in the 1 kHz–1 MHz range, but the phasic changes of resistance during the cardiac cycle are not. These observations suggest that the impedance is mainly modulated by the structural and/or morphological changes, whereas the impedance waveform is highly synchronized with changes in wall thickness as reported by Sasaki et al. (15).

Myocardial ischemia causes intracellular edema and this results in cellular enlargement and extracellular space volume reduction (18, 21). Under these conditions the average impedance increases at all studied frequencies as reported previously by us and others (4, 6, 12). In addition, our results showed that the frequencies that better differentiate normal from ischemic tissue are 1 and 41 kHz for the resistance and 41 and 300 kHz for the phase angle.

LV Pressure-Impedance Curves

We analyzed the temporal relationship between the cyclic changes in myocardial resistivity and the concurrent level of LV pressure by constructing the LV pressure-impedance loop. Establishing a parallelism with the well-known pressure-volume curve that reflects the whole work performed by the corresponding ventricle (1) then, the LV pressure-impedance loop would indicate the LV resistance strength referred to a particular explored area. As a novel contribution our study shows that early after coronary occlusion the area under the LV pressure-impedance began to decrease dramatically and therefore this parameter will further contribute to recognize acute myocardial ischemia. The virtual abolition of the area under the LV pressure-impedance curve during the first 5 min of ischemia was due to the lack of resistivity decrease during the ejection period. Lyseggen et al. (9) studied the relationship between LV pressure and local segment length (SL), and observed that regions with depressed motility, characterized by regional work close to 0, showed reduced LV pressure-SL area.

Thus our findings suggest that the LV pressure-impedance loop would allow differentiating the segments that generate active force (healthy tissue) from those ischemic dyskinetic segments that are entirely passive. In fact, active myocardial regions with cell contraction contribute to the pressure changes, whereas passive regions with ischemia-induced local dyskinesis are not contributing to pressure generation and instead, they suffer tissue deformation as a consequence of the whole intraventricular pressure changes generated by the cardiac beat.

Considerations on the Model

The systolic-diastolic impedance patterns described in this study were recorded with intramural needle electrodes in the

open-chest swine model. Although the direct intramyocardial measurements are the most appropriate for a refined detection of the local tissue resistivity changes, this is an invasive approach which on the other hand required a thoracotomy. An intracavitary approach based on an endocardial contact electrocatheter probe is theoretically feasible and would overcome these limitations. Indeed, we have previously reported in the same experimental model, that the myocardial resistivity changes induced by coronary occlusion can be successfully detected with an electrocatheter-based approach in the closed chest (20).

Conclusions

Acute transmural myocardial ischemia can be promptly recognized by specific changes in the systolic-diastolic pattern of local electrical myocardial resistivity.

GRANTS

This work was supported by grants from Spanish Ministerio de Economía y Competitividad, Instituto de Salud Carlos III and Fondo Europeo de Desarollo Regional (FEDER): FIS-PI13/00765 and RIC-RD12/0042/0002, Red de Investigación Cardiovascular (Redes Temáticas de Investigación Cooperativa en Salud-RETICS).

DISCLOSURES

No conflicts of interest, financial or otherwise, are declared by the author(s).

AUTHOR CONTRIBUTIONS

Author contributions: E.J., G.A.-F., T.G.-S., R.B., J.R.-F., and J.C. performed experiments; E.J., G.A.-F., and J.C. analyzed data; E.J., G.A.-F., and J.C. interpreted results of experiments; E.J., G.A.-F., and J.C. prepared figures; E.J., G.A.-F., and J.C. drafted manuscript; E.J., G.A.-F., T.G.-S., R.B., J.R.-F., and J.C. edited and revised manuscript; E.J., G.A.-F., T.G.-S., R.B., J.R.-F., and J.C. approved final version of manuscript; R.B., J.R.-F., and J.C. conception and design of research.

REFERENCES

1. **Baan J, van der Velde ET, de Bruin HG, Smeenk GJ, Koops J, van Dijk AD, Temmerman D, Senden J, Buis B.** Continuous measurement of left ventricular volume in animals and humans by conductance catheter. *Circulation* 70: 812–823, 1984.
2. **Bramlage P, Joss G, Staudt A, Jarrin A, Podlowski S, Baumann G, Stangl K, Felix SB, Stangl V.** Computer-aided measurement of cell shortening and calcium transients in adult cardiac myocytes. *Biotechnol Prog* 17: 929–934, 2001.
3. **Cinca J, Carreño A, Mont L, Blanch P, Soler-Soler J.** Neurally mediated negative inotropic effect impairs myocardial function during cholinergic coronary vasoconstriction in pigs. *Circulation* 94: 1101–1108, 1996.
4. **Cinca J, Warren M, Carreño A, Tresànchez M, Armadans L, Gómez P, Soler-Soler J.** Changes in myocardial electrical impedance induced by coronary artery occlusion in pigs with and without preconditioning: correlation with local ST-segment potential and ventricular arrhythmias. *Circulation* 96: 3079–3086, 1997.
5. **Cinca J, Warren M, Rodríguez-Sinovas A, Tresànchez M, Carreño A, Bragós R, Casas O, Domingo A, Soler-Soler J.** Passive transmission of ischemic ST segment changes in low electrical resistance myocardial infarct scar in the pig. *Cardiovasc Res* 40: 103–112, 1998.
6. **Fallert MA, Mirotznik MS, Downing SW, Savage EB, Foster KR, Josephson ME, Bogen DK.** Myocardial electrical impedance mapping of ischemic sheep hearts and healing aneurysms. *Circulation* 87: 199–207, 1993.
7. **Gebhard MM, Gersing E, Brockhoff CJ, Schnabel PA, Bretschneider HJ.** Impedance spectroscopy: a method for surveillance of ischemia tolerance of the heart. *Thorac Cardiovasc Surg* 35: 26–32, 1987.
8. **Gersing E.** Impedance spectroscopy on living tissue for determination of the state of organs. *Bioelectrochem Bioenerg* 45: 145–149, 1998.
9. **Lyseggen E, Skulstad H, Helle-Valle T, Vartdal T, Urheim S, Rabben SI, Opdahl A, Ihlen H, Smiseth OA.** Myocardial strain analysis in acute coronary occlusion: A tool to assess myocardial viability and reperfusion. *Circulation* 112: 3901–3910, 2005.
10. **Van Oosterom A, de Boer RW, van Dam RT.** Intramural resistivity of cardiac tissue. *Med Biol Eng Comput* 17: 337–43, 1979.
11. **Padilla F, Garcia-Dorado D, Rodríguez-Sinovas A, Ruiz-Meana M, Inserte J, Soler-Soler J.** Protection afforded by ischemic preconditioning is not mediated by effects on cell-to-cell electrical coupling during myocardial ischemia-reperfusion. *Am J Physiol Heart Circ Physiol* 285: H1909–H1916, 2003.
12. **Salazar Y, Bragos R, Casas O, Cinca J, Rosell J.** Transmural versus nontransmural in situ electrical impedance spectrum for healthy, ischemic, and healed myocardium. *IEEE Trans Biomed Eng* 51: 1421–1427, 2004.
13. **Sanchez B, Louarroudi E, Jorge E, Cinca J, Bragos R, Pintelon R.** A new measuring and identification approach for time-varying bioimpedance using multisine electrical impedance spectroscopy. *Physiol Meas* 34: 339–357, 2013.
14. **Sanchez B, Schoukens J, Bragos R, Vandersteen G.** Novel estimation of the electrical bioimpedance using the local polynomial method. Application to in vivo real-time myocardium tissue impedance characterization during the cardiac cycle. *IEEE Trans Biomed Eng* 58: 3376–3385, 2011.
15. **Sasaki E, Conger JL, Kadipasaoglu KA, Pehlivanoglu S, Frazier OH.** Simultaneous evaluation of cardiac wall motion and myocardial ischemic injury by measurement of electrical impedance. *ASAIO J* 40: M826–M829, 1994.
16. **Sperelakis N, Hoshiko T.** Electrical impedance of cardiac muscle. *Circ Res* 9: 1280–1283, 1961.
17. **Steendijk P, Van der Velde ET, Baan J.** Dependence of anisotropic myocardial electrical resistivity on cardiac phase and excitation frequency. *Basic Res Cardiol* 89: 411–426, 1994.
18. **Tranum-Jensen J, Janse MJ, Fiolet WT, Krieger WJ, D'Alnoncourt CN, Durrer D.** Tissue osmolality, cell swelling, and reperfusion in acute regional myocardial ischemia in the isolated porcine heart. *Circ Res* 49: 364–381, 1981.
19. **Troy BL, Pombo J, Rackley CE.** Measurement of left ventricular wall thickness and mass by echocardiography. *Circulation* 45: 602–611, 1972.
20. **Warren M, Bragós R, Casas O, Rodríguez-Sinovas A, Rosell J, Anivarro I, Cinca J.** Percutaneous electrocatheter technique for on-line detection of healed transmural myocardial infarction. *Pacing Clin Electrophysiol* 23: 1283–1287, 2000.
21. **Whalen DA, Hamilton DG, Ganote CE, Jennings RB.** Effect of a transient period of ischemia on myocardial cells. I. Effects on cell volume regulation. *Am J Pathol* 74: 381–397, 1974.

Artículo 2: *Recognition of Fibrotic Infarct Density by the Pattern of Local Systolic-Diastolic Myocardial Electrical Impedance*.

Gerard Amorós-Figueras, Esther Jorge, Tomás García-Sánchez, Ramon Bragós, Javier Rosell-Ferrer, Juan Cinca. *Frontiers in Physiology.* 2016; 7: 389.

https://doi.org/10.3389/fphys.2016.00389

frontiers in Physiology

ORIGINAL RESEARCH
published: 31 August 2016
doi: 10.3389/fphys.2016.00389

Recognition of Fibrotic Infarct Density by the Pattern of Local Systolic-Diastolic Myocardial Electrical Impedance

Gerard Amorós-Figueras[1†], Esther Jorge[1†], Tomás García-Sánchez[2], Ramón Bragós[2], Javier Rosell-Ferrer[2] and Juan Cinca[1]*

[1] Department of Cardiology, Hospital de la Santa Creu i Sant Pau, Institut d'Investigació Biomèdica - Sant Pau, Universitat Autònoma de Barcelona, Barcelona, Spain, [2] Electronic and Biomedical Instrumentation Group, Department of Electronics Engineering, Universitat Politècnica de Catalunya, Barcelona, Spain

Myocardial electrical impedance is a biophysical property of the heart that is influenced by the intrinsic structural characteristics of the tissue. Therefore, the structural derangements elicited in a chronic myocardial infarction should cause specific changes in the local systolic-diastolic myocardial impedance, but this is not known. This study aimed to characterize the local changes of systolic-diastolic myocardial impedance in a healed myocardial infarction model. Six pigs were successfully submitted to 150 min of left anterior descending (LAD) coronary artery occlusion followed by reperfusion. 4 weeks later, myocardial impedance spectroscopy (1–1000 kHz) was measured at different infarction sites. The electrocardiogram, left ventricular (LV) pressure, LV dP/dt, and aortic blood flow (ABF) were also recorded. A total of 59 LV tissue samples were obtained and histopathological studies were performed to quantify the percentage of fibrosis. Samples were categorized as normal myocardium (<10% fibrosis), heterogeneous scar (10–50%) and dense scar (>50%). Resistivity of normal myocardium depicted phasic changes during the cardiac cycle and its amplitude markedly decreased in dense scar (18 ± 2 Ω·cm vs. 10 ± 1 Ω·cm, at 41 kHz; $P < 0.001$, respectively). The mean phasic resistivity decreased progressively from normal to heterogeneous and dense scar regions (285 ± 10 Ω·cm, 225 ± 25 Ω·cm, and 162 ± 6 Ω·cm, at 41 kHz; $P < 0.001$ respectively). Moreover, myocardial resistivity and phase angle correlated significantly with the degree of local fibrosis (resistivity: $r = 0.86$ at 1 kHz, $P < 0.001$; phase angle: $r = 0.84$ at 41 kHz, $P < 0.001$). Myocardial infarcted regions with greater fibrotic content show lower mean impedance values and more depressed systolic-diastolic dynamic impedance changes. In conclusion, this study reveals that differences in the degree of myocardial fibrosis can be detected *in vivo* by local measurement of phasic systolic-diastolic bioimpedance spectrum. Once this new bioimpedance method could be used via a catheter-based device, it would be of potential clinical applicability for the recognition of fibrotic tissue to guide the ablation of atrial or ventricular arrhythmias.

Keywords: healed myocardial infarction, myocardial electrical impedance, hemodynamics, novel bioimpedance device, swine

OPEN ACCESS

Edited by:
Gaetano Santulli, Columbia University, USA

Reviewed by:
Sang-Bing Ong, Universiti Teknologi Malaysia, Malaysia
Veronica Crisostomo, Centro de Cirugía de Mínima Invasión Jesús Usón, Spain

****Correspondence:***
Gerard Amorós-Figueras
gamorosf@santpau.cat

† These authors have contributed equally to this work.

Specialty section:
This article was submitted to Clinical and Translational Physiology, a section of the journal Frontiers in Physiology

Received: *18 July 2016*
Accepted: *22 August 2016*
Published: *31 August 2016*

Citation:
Amorós-Figueras G, Jorge E, García-Sánchez T, Bragós R, Rosell-Ferrer J and Cinca J (2016) Recognition of Fibrotic Infarct Density by the Pattern of Local Systolic-Diastolic Myocardial Electrical Impedance. Front. Physiol. 7:389. doi: 10.3389/fphys.2016.00389

INTRODUCTION

Myocardial electrical impedance is a biophysical marker of the state of integrity of the myocardial tissue (Sperelakis and Hoshiko, 1961). Early studies conducted in experimental animal models have consistently shown that acute myocardial ischemia induced by coronary artery ligation increased dramatically the myocardial impedance (Cinca et al., 1998; Padilla et al., 2003; Rodriguez-Sinovas et al., 2005). In contrast, during the healing over process the necrotic scar turns to lower than normal impedance values (Fallert et al., 1993; Wolf et al., 2001; Salazar et al., 2004). In these studies, the technique of measuring the changes in myocardial impedance did not allow to delineate the sequential impedance variations elicited during the systole and diastole phases of the cardiac cycle because of the long time required for the whole impedance spectrum acquisition (Gersing, 1998; Casas et al., 1999; Warren et al., 2000; Cinca et al., 2008). Quite recently, the use of refined fast broadband electrical impedance spectroscopy (EIS; Sanchez et al., 2011) allowed to describe the cyclic pattern of systolic-diastolic impedance changes in a swine model of acute myocardial ischemia (Jorge et al., 2015). As compared with the classical technique, the new EIS-based method permitted a prompt detection of local myocardial ischemia based on the occurrence of specific changes in the phasic systolic-diastolic impedance curve. These were characterized by an holosystolic resistivity rise leading to a bell-shaped impedance waveform and a reduction of the area under the left ventricular (LV) pressure-impedance curve. In that study, the holosystolic impedance rise maintained a temporal relationship with the local mechanical dyskinesis induced in the ischemic region, thus it may emerge as a new indicator (surrogate) of early acute myocardial ischemia. During the healing-over process the acute ischemic myocardium suffers a profound structural and functional remodeling, with collagen deposition and fibroblasts proliferation. These structural alterations will affect the pattern of systolic-diastolic impedance of the infarct scar region, but this has not yet been investigated.

This study aimed to characterize the phasic (systolic-diastolic) changes of myocardial resistivity in the *in situ* swine heart with 1 month old healed myocardial infarction by using fast broadband EIS. Specifically, we assessed how myocardial resistivity is influenced by the amount of fibrotic content of the infarct scar.

MATERIALS AND METHODS

The study protocol was approved by the Animal Care and Use Committee of our institution and conformed to the *Guide for the Care and Use of Laboratory Animals*: Eighth Edition (National Research Council. Washington, DC: The National Academies Press, 2010).

Study Protocol

The study began after stabilization of the level of anesthesia and the hemodynamic parameters. Then, the ECG, LVP, ABF and impedance signals were recorded during 4 s at each site. In each pig, we explored 8–11 myocardial impedance sites spaced 10 mm apart, beginning at the healthy region and extending toward the infarcted area. At the end of the study the animals were euthanized by administration of an intravenous KCl overdose and the heart was removed.

Experimental Preparation

Eight female domestic swine (Landrace-Large White cross) weighing 33 ± 2 kg were submitted to two interventions spaced 30 days. The first intervention aimed at inducing an acute myocardial infarction. Animals received 400 mg oral amiodarone and 500 mg aspirin from 2 days before to 7 days after infarct induction. They were premedicated (midazolam 0.6 mg/kg and ketamine 12 mg/kg), anesthesized (propofol 2–4 mg/kg), and maintained with sevoflurane inhalation (2.5–3.5%). After endotracheal intubation animals were mechanically ventilated. Analgesia was maintained with a perfusion of remifentanil (0.2 $\mu g \cdot kg^{-1} \cdot min^{-1}$). Continuous infusion of lidocaine at a rate of 1 mg/kg/h (Lidocaina Braun. B. Braun Medical, Barcelona, Spain) was used through the procedure. Systemic sodium heparin was injected IV (150 UI/kg) 5 min prior to percutaneous sheath placement.

Under aseptic conditions, a femoral arterial access was established using the Seldinger technique and a 7F introducer sheath (Cordis; Miami, FL) was placed percutaneously into the femoral artery. To better mimic the clinical human scenario of a reperfused infarction, a coronary artery occlusion-reperfusion was performed. The infarction created with this models is characterized histologically by surviving strands of myocardium interwoven with fibrotic scar. A small modification of the Sasano model was used (Sasano et al., 2006). Briefly, a 6F hockey stick guiding catheter (Cordis) was introduced and placed at the origin of the left coronary artery under fluoroscopic guidance, and a 3 mm diameter over-the-wire coronary catheter balloon (Cordis) was placed at the mid segment of the left anterior descending (LAD) below the origin of the first diagonal. The position of the catheter was verified by coronary angiography. An additional lidocaine bolus was also administered immediately before balloon inflation and deflation. The coronary artery was checked for patency by repeating the coronary angiography.

The second intervention was performed 30 ± 2 days later, when the pigs had developed a healed myocardial infarction. The animals were again sedated, anesthetized, and mechanically ventilated as in the first intervention. The femoral artery was catheterized and a 5F Millar micromanometer catheter (Millar Instruments) was advanced into the left ventricle (LV) to measure the LV pressure. A conventional ECG lead was continuously recorded. The thorax was opened through a midsternotomy and the heart was suspended in a pericardial cradle. An ultrasonic flow probe was carefully deployed around the aortic root to monitor the aortic blood flow (ABF).

Electrocardiographic and Hemodynamic Parameters

In all cases we recorded the conventional ECG lead II (Nihon Kohden; Tokyo, Japan), the LV pressure (Nihon Kohden) and the ABF (Transonic Systems Inc., Ithaca, NY, US). All signals were digitized at 1 kHz (PowerLab with LabChart, ADInstruments) and stored for subsequent offline analysis. The first derivative of the LV pressure was also calculated.

Myocardial Electrical Impedance

Theoretical Background

The electrical impedance of the myocardium reflects an overall estimation of the intra- and extra-cellular resistances and the cell membrane capacitance (Gebhard et al., 1987; Kléber et al., 1987). Myocardial impedance has two components: tissue resistivity (ρ) and phase angle. Tissue resistivity quantifies the drop of voltage (V) amplitude for a given applied current (I). It was calculated from the relation $R = k \cdot \rho$, where R is the in phase component of V with respect to I, and k is the cell constant of the electrode determined by measuring the electrical resistance of a 0.9% NaCl solution at 25°C, which affords a resistivity of 70 Ω·cm. Phase angle shift is related to the time delay between the voltage and current waves caused by the fact that biological tissues are not purely resistive.

Myocardial Electrical Impedance Spectroscopy

Tissue impedance spectroscopy was measured as reported previously (Jorge et al., 2015). Briefly, a 4-needle electrode probe connected to a signal generation and acquisition system (PXI system, National Instruments) was inserted into the LV wall. The electrode was placed sequentially at different sites following a parallel linear array perpendicular to the trajectory of the LAD (**Figure 1**). Myocardial impedance spectroscopy was measured using current excitations consisting of a multisine signal (1 ms duration, 1 mA peak amplitude) of 26 frequencies logarithmically spaced in the range from 1 to 1000 kHz, leading up to 1000 spectra/s. The LV pressure, ABF and ECG signals were acquired simultaneously with the impedance signals using an additional digitizer card.

Systolic-diastolic Myocardial Electrical Impedance

The impedance changes occurring throughout the cardiac cycle were analyzed. In each recording we measured the mean resistivity value, the amplitude of the phasic resistivity (maximum–minimum value) and the mean value of phase angle during the entire cardiac cycle. Thereafter, an analysis of the resistivity changes in relation to the LV pressure (LV pressure-impedance curves) was also performed. In addition, to determine the time relationship between the ECG and the systolic-diastolic myocardial resistivity, we measured the time interval between

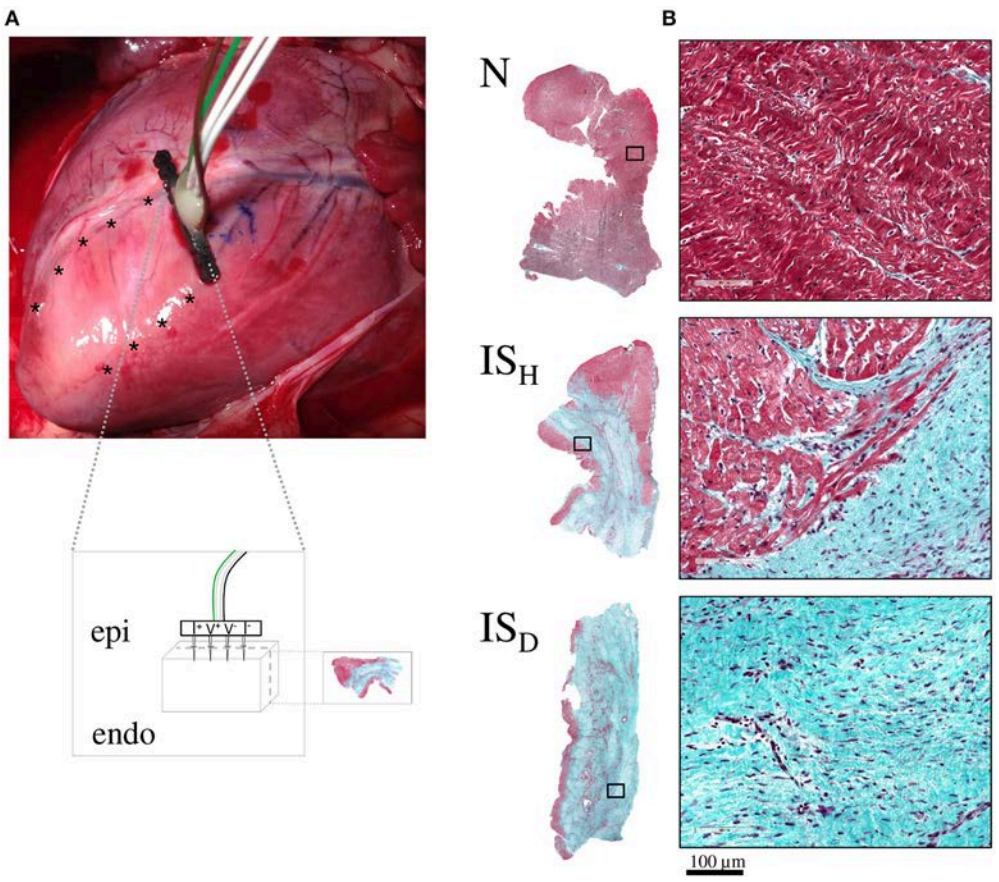

FIGURE 1 | Schematic representation of the experimental model. (A) Photograph of a swine heart illustrating the location of the infarcted region in the anterior wall of the left ventricle and the sites where the impedance electrode was sequentially inserted (asterisks). The inset box depicts a schematic representation of the 4-needle impedance electrode (5 mm length spaced 1.27 mm, 0.4 mm diameter). **(B)** Representative microphotographs (at 1x and 20x magnification) of myocardial samples from normal zones (N) and from heterogeneous and dense infarct scar regions (IS_H and IS_D, respectively) stained with Masson's trichrome.

the R wave peak and the moment at which resistivity reached its maximum value.

Anatomopathological Examination

To assess the correlation between the degree of fibrosis in the infarcted region and the magnitude of local tissue impedance, we obtained myocardial samples in the same sites of impedance measurements. These sampling sites were marked with black ink after each myocardial impedance measurement to ensure an appropriate identification of the biopsies during tissue processing. The specimens were fixed in 10% buffered formalin, embedded in paraffin and sliced (4-μm thickness) perpendicularly to the epicardial surface up to the half of the sample block (**Figure 1**). After this, samples were stained with Masson's trichrome. All slides were digitized using an Aperio ScanScope Scanner (Aperio; CA) and the extent of the infarct scar was assessed by semi-automatic image quantification. Thus, the percentage of fibrosis was measured at 1.25X magnification using a custom-made Matlab algorithm (MathWorks; MA) which was based on color segmentation by K-means clustering (Wu et al., 2015). The percentage of fibrosis in each slide was calculated using the formula: 100 × (Area of fibrosis / Total slide area). According to the percentage of fibrosis the samples were categorized as proposed by Sivagangabalan et al. (2008); (1) healthy myocardium (N) (<10% of fibrosis); (2) heterogeneous infarct scar (IS_H; 10–50% of fibrosis) and (3) dense infarct scar (IS_D; >50% of fibrosis).

Statistical Analysis

Data were expressed as mean ± standard error of the mean (SEM). Differences in the study variables were assessed by the analysis of variance (ANOVA) with Bonferroni correction for *post-hoc* comparisons. Pearson's correlation between tissue fibrosis and impedance (resistivity and phase angle parameters) were calculated. A P-value <0.05 was considered statistically significant. Statistical analyses were performed using the software SPSS v.22.0 (IBM SPSS Inc., Chicago, IL, USA).

RESULTS

Two animal died during acute coronary occlusion due to irreversible ventricular fibrillation. The remaining animals ($n = 6$) completed their allotted follow up and were used for the study. As shown in **Figure 1**, 1 month after LAD occlusion there was a visible scar area in the anterior wall of the left ventricle in all animals. Local intramural myocardial impedance was recorded simultaneously with the physiological signals in a total number of 59 sites (**Figure 2**).

Impedance Spectroscopy

Figure 3A shows the behavior of the mean values of resistivity and phase angle of normal and infarcted myocardium measured during the entire cardiac cycle at the 26 excitation frequencies studied in six pigs. Resistivity in normal myocardium decreased

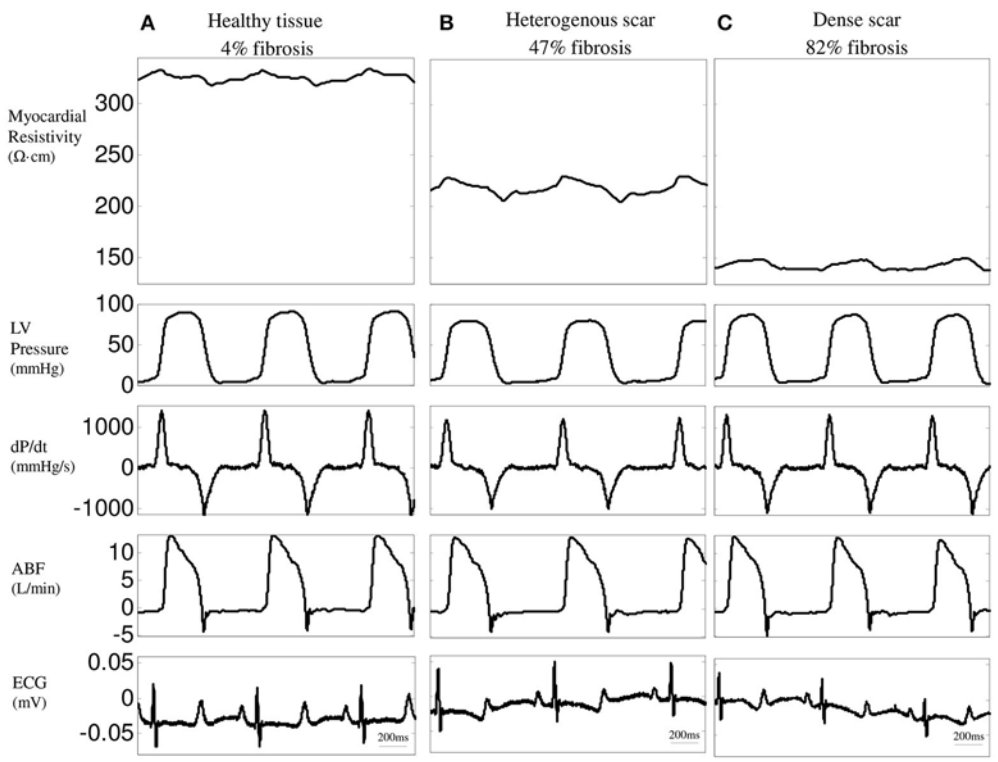

FIGURE 2 | Time-relationship between resistivity at 1 kHz, left ventricular (LV) pressure, LV dP/dt, aortic blood flow (ABF), and ECG in three representative LV regions: healthy tissue (A), heterogeneous (B) and dense infarct scar (C).

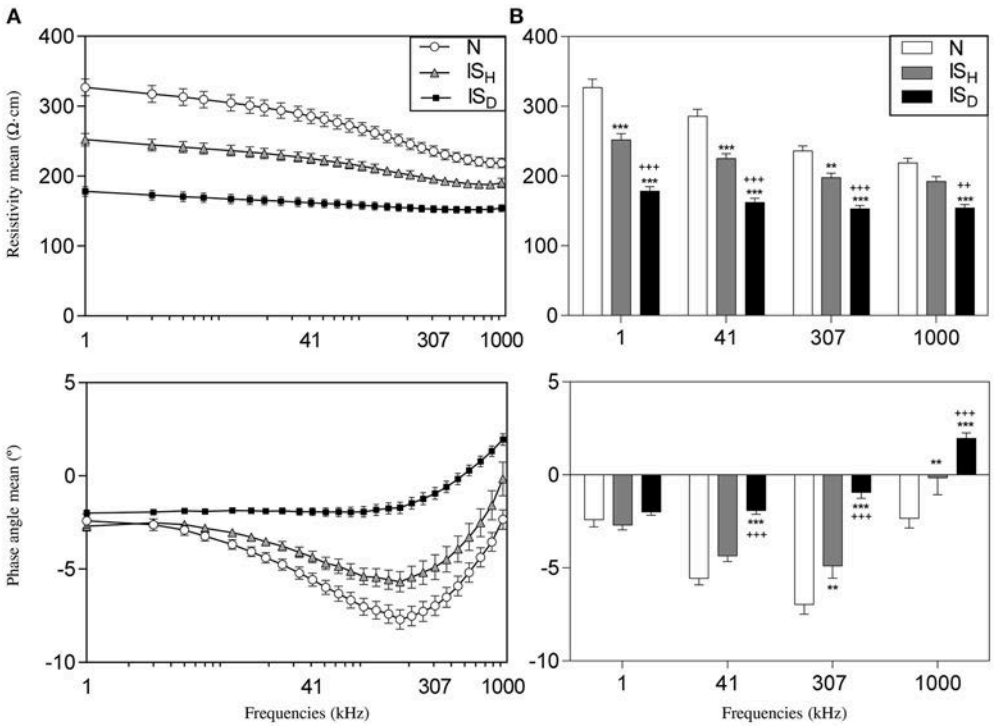

FIGURE 3 | Impedance spectroscopy of 1 month old myocardial infarction in the six studied pigs. (A) Mean values of resistivity (top) and phase angle (bottom) of myocardial impedance at different excitation frequencies in normal (N), heterogeneous (IS_H), and dense infarcted myocardial regions (IS_D). **(B)** Mean resistivity (top) and phase angle (bottom) at 4 selected frequencies (1 kHz, 41 kHz, 307 kHz, and 1000 kHz). *Significantly different from N (** <0.01, *** <0.001). $^{+}$Significantly different from IS_H ($^{++}$ <0.01, $^{+++}$ <0.001).

progressively at increasing excitation frequencies (from 327 ± 12 Ω·cm at 1 kHz to 218 ± 7 Ω·cm at 1000 kHz, $P < 0.001$). Moreover, phase angle spectrum showed a negative relaxation which was maximal at about 307 kHz. Regions with heterogeneous scar tissue (10–50% of fibrosis) showed a similar trend of changes (from 252 ± 9 Ω·cm at 1 kHz to 192 ± 7 Ω·cm at 1000 kHz, $P < 0.001$) although with a lower mean value (23% decrease at 1 kHz, $P < 0.001$) and a less marked phase angle relaxation. In contrast, sites with dense fibrosis presented an almost flat resistivity spectrum (178 ± 7 Ω·cm at 1 kHz and 154 ± 5 Ω·cm at 1000 kHz, P = ns) with lower mean resistivity values (46% reduction at 1 kHz, $P < 0.001$). Likewise, the phase angle relaxation vanished in the dense infarct scar.

Figure 3B illustrates the differences in the mean values of resistivity and phase angle at 4 selected frequencies (1, 41, 307, and 1000 kHz) in the different myocardial regions in six pigs. The excitation frequencies that better differentiated healthy myocardium, heterogeneous scar tissue and dense infarct scar were 1, 41, and 307 kHz for the resistivity and 307 and 1000 kHz for the phase angle.

Correlation between Local Myocardial Impedance and Infarct Fibrosis

As illustrated in **Figure 4**, higher degrees of fibrotic deposition in the infarcted region were associated with gradually lower mean values of local myocardial resistivity ($r = -0.86$ at 1 kHz, $P < 0.001$) and with a less negative phase angle deviation ($r = 0.84$ at 41 kHz, $P < 0.001$). **Table 1** summarizes the values of the linear correlation coefficients at the four selected excitation frequencies of the studied spectrum (1, 41, 307, and 1000 kHz). Although a significant linear correlation existed between local tissue fibrosis and local bioimpedance parameters at most frequencies, the best discriminative frequencies were 1 kHz for myocardial resistivity and 41 kHz for phase angle.

Systolic-Diastolic Phasic Changes in Myocardial Electrical Resistivity

As shown in **Figure 5**, electrical resistivity of the normal myocardium depicted phasic changes during the cardiac cycle: a maximal value was attained during systole and a minimal value during diastole, leading to a mean amplitude of 18.1 ± 1.9 Ω·cm at 41 kHz. By contrast, infarct regions with dense fibrotic content showed a reduced systolic-diastolic impedance amplitude of 9.7 ± 0.9 Ω·cm, with only a small holosystolic displacement. Areas with less marked fibrotic density showed an intermediate pattern of systolic-diastolic impedance with an amplitude of 17.7 ± 1.9 Ω·cm.

Analysis of the temporal relationship between the myocardial impedance and the ECG showed that the systolic-diastolic resistivity curve of healthy myocardial regions presented its maximal peak shortly after the R wave. By contrast, **Figure 5** illustrates that areas with densely infarcted myocardium were characterized by having its maximal resistivity peak beyond the R wave peak (188 ± 27 ms vs. 67 ± 16, $P < 0.05$) with

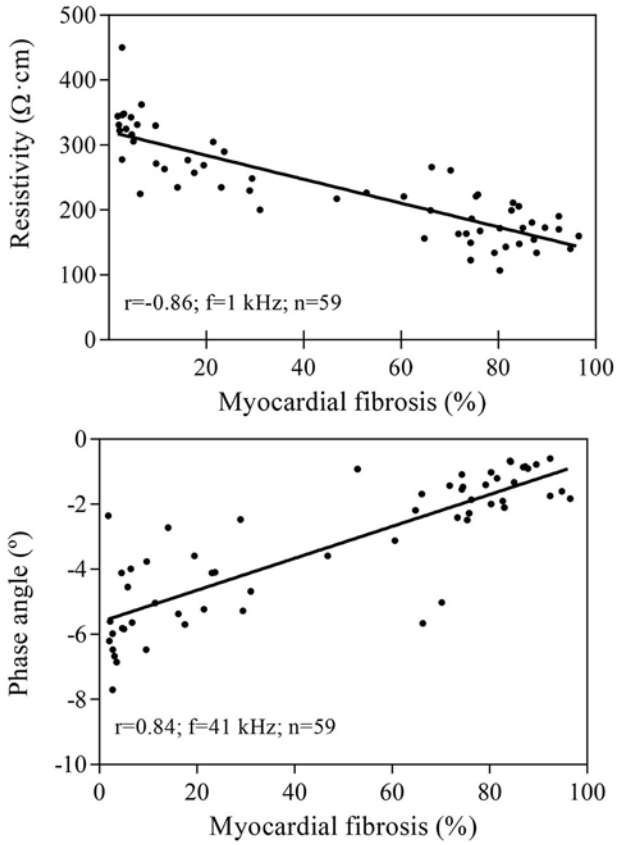

FIGURE 4 | Linear correlation between the local degree of myocardial fibrosis and myocardial resistivity (upper panel) or phase angle (lower panel) in 59 samples from six pigs. Resistivity values are measured at 1 kHz and phase angle at 41 kHz.

an holosystolic plateau. The heterogeneous infarct scar zones attained their maximal resistivity peak at a delay similar to healthy myocardium.

LV Pressure-Impedance Curves during the Cardiac Cycle

The temporal relationship between the whole cardiac mechanical activity and the concurrent changes in regional myocardial impedance can be better analyzed by constructing the LV pressure-impedance (LVPI) curves. As illustrated in **Figure 6**, dense infarcted zones showed an area under the LVPI curves (AUC) smaller than the heterogeneous scar tissue or the healthy myocardium (IS_D: 214.7 ± 44.2 mmHg·Ω·cm, IS_H: 655.4 ± 160.7 mmHg·Ω·cm, N: 665.5 ± 137.8 mmHg·Ω·cm; $p < 0.05$ IS_D vs. IS_H and $p < 0.01$ IS_D vs. N). These changes were comparable among the different studied frequencies.

DISCUSSION

Main Findings

This study reveals that the degree of fibrotic deposition in the infarcted myocardium is a direct determinant of both the local decrease in tissue impedance and the attenuation of systolic-diastolic impedance oscillations.

TABLE 1 | Correlation coefficients (*r*) between electrical impedance and percentage of infarct fibrosis in 59 tissue samples from six pigs.

	Excitation frequency (kHz)	*r*	*P*
Myocardial resistivity	1	−0.86	<0.001
	41	−0.85	<0.001
	307	−0.82	<0.001
	1000	−0.76	<0.001
Phase angle	1	0.19	=0.15
	41	0.84	<0.001
	307	0.83	<0.001
	1000	0.67	<0.001

Electrical Impedance of Normal and Infarcted Myocardium

Previous experimental studies in models of transmural healed myocardial infarction induced by permanent coronary occlusion have consistently found low electrical resistivity values in the necrotic scar (Fallert et al., 1993; Warren et al., 2000; Wolf et al., 2001; Salazar et al., 2004). However, the prolonged time required for measuring the impedance spectrum in these studies prevented knowing the time course of myocardial impedance during the whole cardiac cycle. A recent refinement of the bioimpedance method based on fast broadband EIS permitted to characterize the changes in myocardial impedance induced during the cardiac cycle under normal and acute ischemic conditions in the *in situ* porcine heart (Sanchez et al., 2011; Jorge et al., 2015). In that model the normal myocardium depicted a biphasic resistivity pattern that turned to a bell-shaped morphology with an increased mean value following coronary occlusion.

The moment at which the high-resistivity, biphasic bioimpedance pattern observed in the acute phase of ischemia evolves to a low-resistivity and flat systolic-diastolic pattern in the healed infarcted tissue is not well defined. Previous studies in sheep showed the 200% increase in myocardial impedance after 4 h of permanent coronary occlusion that turned to a 60% decrease 1 week later, and this was maintained 6 weeks after (Fallert et al., 1993). The mechanisms implicated in the progressive reduction of tissue resistivity during infarct healing are likely related to the sequential occurrence of interstitial edema, loss of myocyte content, and collagen and fat deposition in the ischemic region (Fallert et al., 1993; Schwartzman et al., 1999; Del Rio et al., 2008; Farraha et al., 2014). These structural derangements will be less marked in infarction areas with surviving myocardial cells and therefore could be detected by bioimpedance techniques. In 4 sheep with 60-days old anterior myocardial infarction induced by permanent ligature of the LAD coronary artery, epicardial impedance measured with the 4-electrode technique at 1 kHz was lower in the visually defined dense infarction than in the border zone or in the healthy myocardium (Schwartzman et al., 1999). Using a 3 h LAD

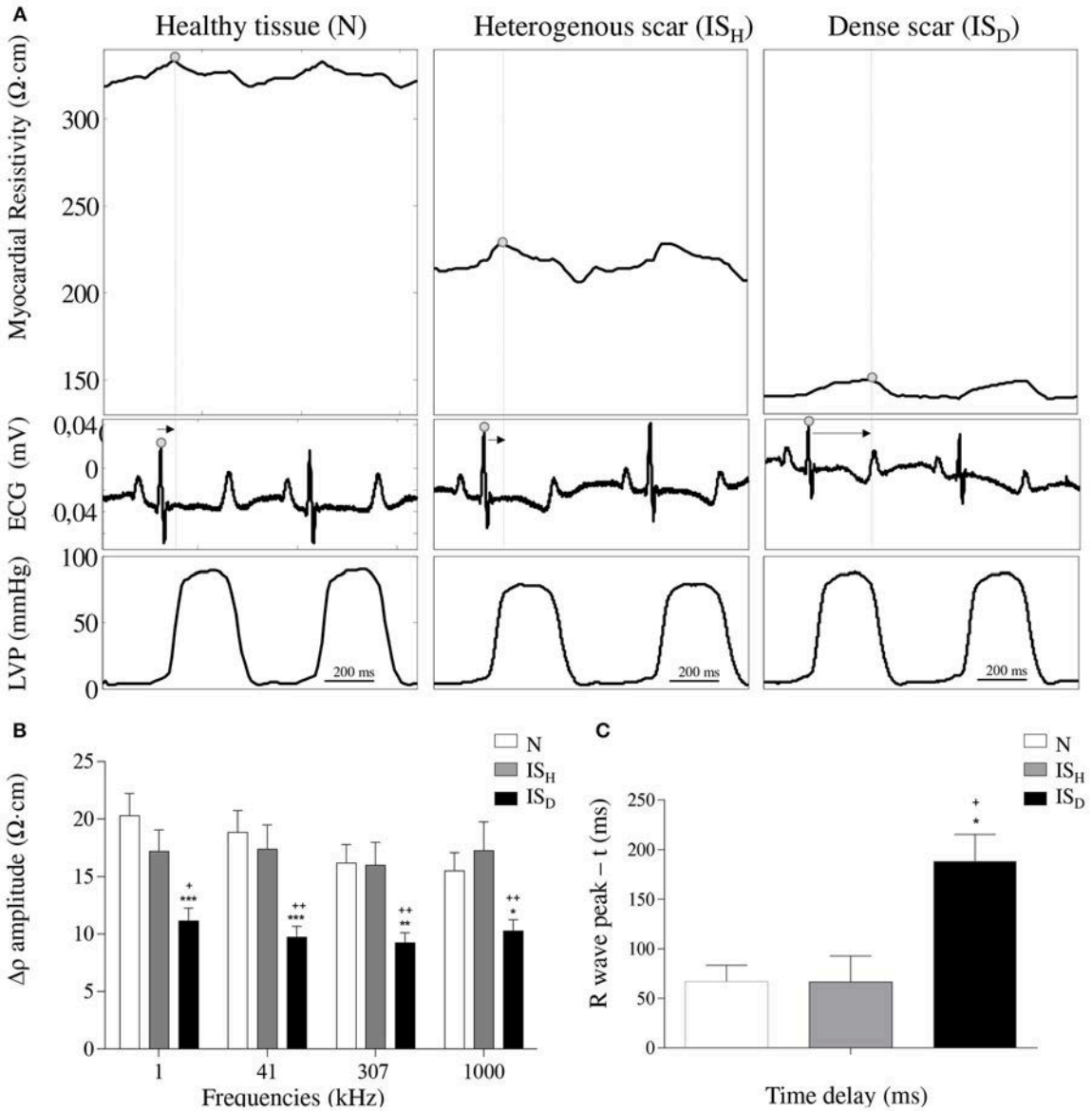

FIGURE 5 | Effects of infarct fibrotic content on myocardial resistivity curve. (A) Systolic-diastolic myocardial resistivity waveform in healthy myocardial tissue (left), heterogeneous scar (middle) and dense scar tissue (right). Arrows indicate the time interval between the R wave peak and the max peak of the resistivity curve. **(B)** Mean values of the systolic-diastolic resistivity curve amplitude -$\Delta\rho$- at 4 selected frequencies (1 kHz, 41 kHz, 307 kHz, 1000 kHz). **(C)** Mean temporal delays between the peak of the systolic-diastolic resistivity curve and its corresponding R wave peak of the ECG. Resistivity waveforms and delays are shown at 41 kHz. * Significantly different from N (* <0.05, ** <0.01, *** <0.001). $^{+}$Significantly different from IS$_H$ ($^{+}$ <0.05, $^{++}$ <0.01).

occlusion-reperfusion model in three sheep it has been reported that areas with greater myocardial injury (<50% viability), assessed by histologic examination, had greatest attenuation of impedance magnitude compared with areas with >50% viability in a 5 weeks-myocardial infarction (Farraha et al., 2014).

As a novelty, our data show a robust correlation between the local degree of fibrosis and the values of resistivity and phase angle, based on a quantitative site-by-site analysis. Indeed, dense scar areas exhibited the lowest resistivity values and the sites with intermediate degree of fibrosis showed transitional values. Moreover, we found that tissue viability can also be assessed by changes in the amplitude of systolic-diastolic resistivity and by the analysis of the temporal delay between phasic myocardial resistivity and the ECG. We recently proposed that the amplitude of the impedance curve is modulated by the mechanical cardiac activity thus the flat resistivity curve of the dense scar could be in part due to the local severe dyskinesis (Helle-Valle et al., 2009; Garcia-Sanchez et al., 2015). In addition, the drop of the AUC supports the hypothesis that the LVPI curves would allow differentiating the segments able to generate active force

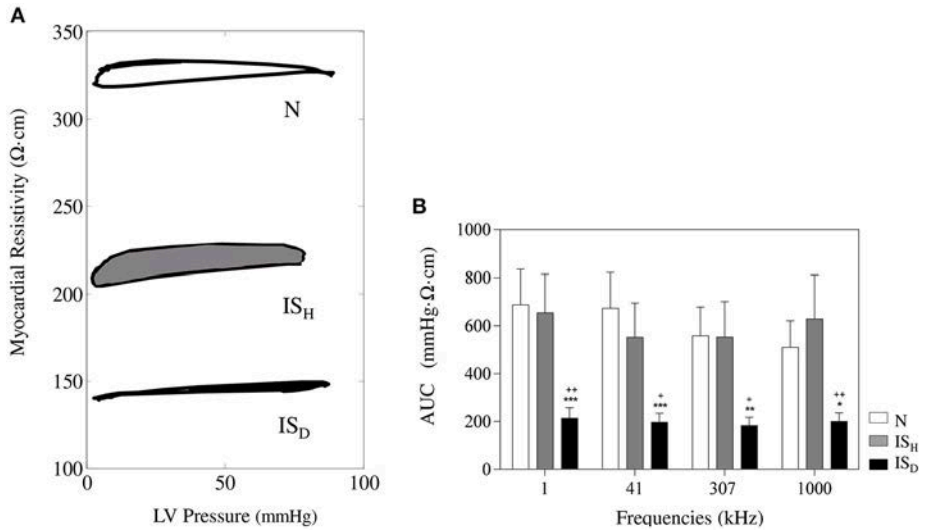

FIGURE 6 | Time relationship between the systolic-diastolic changes in myocardial impedance and left ventricular pressure. (A) Representative LV pressure-impedance curves at sites with <10% of fibrosis (white), 10–50% of fibrosis (gray) and >50% of fibrosis (black). **(B)** Mean values of the area under the curve at different current frequencies. *Significantly different from set N (* <0.05, ** <0.01, *** <0.001). $^{+}$Significantly different from set IS_H ($^{+}$ <0.05, $^{++}$ <0.01).

(healthy tissue) from those that are dyskinetic (necrotic tissue) and therefore mechanically passive (Jorge et al., 2015). The AUC reduction is caused by two main factors: (1) the low-amplitude of the impedance phasic changes and (2) the delayed occurrence of the resistivity peaks. In fact, the significant delay between the peaks of systolic-diastolic resistivity of the infarct scar and the physiological signals could also be a consequence of the passive movement of this tissue, reinforcing the hypothesis that the analysis of the systolic-diastolic myocardial impedance curves may be useful to recognize the infarct scar.

Impedance Spectroscopy

The resistivity and phase angle values are highly dependent on the frequency of the applied current: the low frequency currents flow preferentially through the extracellular space, whereas the high frequency currents can pass through the cell membrane capacitance and therefore could flow through both the intracellular and extracellular compartments. Since the infarcted tissue is characterized by loss of myocardial cell structures and replacement of extracellular space by collagen deposition, the applied current frequency will have a negligible influence on the values of resistivity and phase angle. This concept was confirmed in previous studies (Cinca et al., 1998; Warren et al., 2000; Salazar et al., 2004) and also in the present investigation. However, as a novel finding our data revealed that heterogeneous areas of infarction containing viable myocytes do show different frequency related patterns (Foster and Schwan, 1989). Interestingly, we found that the amplitude of systolic-diastolic resistivity either in normal or infarcted tissues does not change with the applied current frequency. Thus, suggesting that the amplitude variations in local resistivity in normal and infarcted tissue are more dependent on the strength of local mechanical activity.

Clinical Implications

Our data represent the proof-of-concept that myocardial impedance can identify the degree of fibrosis, and therefore the extent of the infarct scar. Theoretically, fibrotic myocardial infiltration other than that of ischemic origin (i.e., infiltrative diseases, myocarditis, hypertension) could also be detected by means of bioimpedance methods in atrial or ventricular level. Thus, recognition of local fibrosis by endocardial catheter mapping would improve the yielding of radiofrequency catheter ablation of either atrial or ventricular arrhythmias.

Study Limitations

The impedance measurements described in this study were obtained with an intramural 4-needle electrode probe in the open-chest swine model in order to achieve optimal recording sensitivity and accessibility to tissue samples. Due to the thinning of the left ventricle in the sites of infarction we cannot entirely exclude that the impedance spectrum at those site could be more flat due to the short distance between the blood volume in the ventricle and the tip of the 4-needle electrode. Theoretically, this could affect the decrease in the systolic-diastolic impedance values. However, *in vitro* calibration measurements using the 4-needle electrode probe in contact with blood showed much lower impedance values with completely flat impedance spectrum.

On the other hand, this method is an invasive approach precluding direct clinical use until an intracavitary approach based on endocardial contact electrocatheter probe is developed. We have previously reported in the swine model, that the changes in myocardial resistivity induced by coronary occlusion can be successfully detected with an electrocatheter based approach in the closed chest

(Warren et al., 2000). In the canine model, other authors have been able to delineate the borders of infarct scar using endocardial catheter impedance mapping (Wolf et al., 2001).

CONCLUSIONS

As compared with the normal myocardium, the local impedance of healed myocardial infarction tissue shows lower mean values and depressed systolic-diastolic oscillations. These changes have their maximal expression in infarcted regions with greater fibrotic content. Once this new bioimpedance method can be implemented in a catheter-based device it might have potential clinical applicability in the detection of fibrotic tissue to guide the ablation of atrial or ventricular arrhythmias.

AUTHOR CONTRIBUTIONS

JC, RB, and JR conception and design of research; GA, EJ, TG, RB, JR, and JC performed experiments; GA and EJ analyzed data; GA, EJ, and JC interpreted results of experiments; GA and EJ prepared figures; GA, EJ, and JC drafted manuscript; GA, EJ, TG, RB, JR, and JC edited and revised manuscript. GA, EJ, TG, RB, JR, and JC approved final version of manuscript.

ACKNOWLEDGMENTS

This work was supported by grants from Fundació "La Marató" of TV3 [20150830]; and from the Spanish Ministerio de Economía y Competitividad, Instituto de Salud Carlos III [FIS-PI13/00765, DTS-15/00099 and RIC-RD12/0042/0002] and Fondo Europeo de Desarrollo Regional (FEDER).

REFERENCES

Casas, O., Bragós, R., Riu, P. J., Rosell, J., Tresànchez, M., Warren, M., et al. (1999). *In vivo* and *in situ* ischemic tissue characterization using electrical impedance spectroscopy. *Ann. N.Y. Acad. Sci.* 873, 51–58. doi: 10.1111/j.1749-6632.1999.tb09448.x

Cinca, J., Ramos, J., Garcia, M. A., Bragos, R., Bayés-Genís, A., Salazar, Y., et al. (2008). Changes in myocardial electrical impedance in human heart graft rejection. *Eur. J. Heart Fail.* 10, 594–600. doi: 10.1016/j.ejheart.2008.04.013

Cinca, J., Warren, M., Rodríguez-Sinovas, A., Tresànchez, M., Carreño, A., Bragós, R., et al. (1998). Passive transmission of ischemic ST segment changes in low electrical resistance myocardial infarct scar in the pig. *Cardiovasc. Res.* 40, 103–112.

Del Rio, C. L., McConnell, P. I., Kukielka, M., Dzwonczyk, R., Clymer, B. D., Howie, M. B., et al. (2008). Electrotonic remodeling following myocardial infarction in dogs susceptible and resistant to sudden cardiac death. *J. Appl. Physiol.* 104, 386–393. doi: 10.1152/japplphysiol.01106.2007

Fallert, M. A., Mirotznik, M. S., Downing, S. W., Savage, E. B., Foster, K. R., Josephson, M. E., et al. (1993). Myocardial electrical impedance mapping of ischemic sheep hearts and healing aneurysms. *Circulation* 87, 199–207. doi: 10.1161/01.CIR.87.1.199

Farraha, M., Nguyen, D. T., Barry, M. A., Lu, J., McEwan, A. L., and Pouliopoulos, J. (2014). Investigating the utility of *in vivo* bio-impedance spectroscopy for the assessment of post-ischemic myocardial tissue. *Conf. Proc. IEEE Eng. Biol. Soc.* 2014, 1111–1114. doi: 10.1109/embc.2014.6943789

Foster, K. R., and Schwan, H. P. (1989). Dielectric properties of tissues and biological materials: a critical review. *Crit. Rev. Biomed. Eng.* 17, 25–104.

Garcia-Sanchez, T., Jorge, E., Amoros-Figueras, G., Bragos, R., Cinca, J., and Rosell-Ferrer, J. (2015). Myocardial contractility assessed by dynamic electrical impedance measurements during dobutamine stress. *Conf. Proc. IEEE Eng. Biol. Soc.* 2015, 6548–6551. doi: 10.1109/embc.2015.7319893

Gebhard, M. M., Gersing, E., Brockhoff, C. J., Schnabel, P. A., and Bretschneider, H. J. (1987). Impedance spectroscopy: a method for surveillance of ischemia tolerance of the heart. *Thorac. Cardiovasc. Surg.* 35, 26–32. doi: 10.1055/s-2007-1020192

Gersing, E. (1998). Impedance spectroscopy on living tissue for determination of the state of organs. *Bioelectrochem. Bioenerg.* 45, 145–149. doi: 10.1016/S0302-4598(98)00079-8

Helle-Valle, T., Remme, E. W., Lyseggen, E., Pettersen, E., Vartdal, T., Opdahl, A., et al. (2009). Clinical assessment of left ventricular rotation and strain: a novel approach for quantification of function in infarcted myocardium and its border zones. *Am. J. Physiol. Heart Circ. Physiol.* 297, H257–H267. doi: 10.1152/ajpheart.01116.2008

Jorge, E., Amorós-Figueras, G., García-Sánchez, T., Bragós, R., Rosell-Ferrer, J., and Cinca, J. (2015). Early detection of acute transmural myocardial ischemia by the phasic systolic- diastolic changes of local tissue electrical impedance. *Am. J. Physiol. Heart Circ. Physiol.* 310, H436–H443. doi: 10.1152/ajpheart.00754.2015

Kléber, A. G., Riegger, C. B., and Janse, M. J. (1987). Electrical uncoupling and increase of extracellular resistance after induction of ischemia in isolated, arterially perfused rabbit papillary muscle. *Circ. Res.* 61, 271–279. doi: 10.1161/01.RES.61.2.271

Padilla, F., Garcia-Dorado, D., Rodríguez-Sinovas, A., Ruiz-Meana, M., Inserte, J., and Soler-Soler, J. (2003). Protection afforded by ischemic preconditioning is not mediated by effects on cell-to-cell electrical coupling during myocardial ischemia-reperfusion. *Am. J. Physiol. Heart Circ. Physiol.* 285, H1909–H1916. doi: 10.1152/ajpheart.00438.2003

Rodriguez-Sinovas, A., García-Dorado, D., Pina, P., Ruiz-Meana, M., and Soler-Soler, J. (2005). Effect of sarcolemmal rupture on myocardial electrical impedance during oxygen deprivation. *Am. J. Physiol. Heart Circ. Physiol.* 288, H1396–H1403. doi: 10.1152/ajpheart.00754.2015

Salazar, Y., Bragos, R., Casas, O., Cinca, J., and Rosell, J. (2004). Transmural versus nontransmural *in situ* electrical impedance spectrum for healthy, ischemic, and healed myocardium. *IEEE Trans. Biomed. Eng.* 51, 1421–1427. doi: 10.1109/TBME.2004.828030

Sanchez, B., Schoukens, J., Bragos, R., and Vandersteen, G. (2011). Novel estimation of the electrical bioimpedance using the local polynomial method. Application to *in vivo* real-time myocardium tissue impedance characterization during the cardiac cycle. *IEEE Trans. Biomed. Eng.* 58, 3376–3385. doi: 10.1109/TBME.2011.2166116

Sasano, T., McDonald, A. D., Kikuchi, K., and Donahue, J. K. (2006). Molecular ablation of ventricular tachycardia after myocardial infarction. *Nat. Med.* 12, 1256–1258. doi: 10.1038/nm1503

Schwartzman, D., Chang, I., Michele, J. J., Mirotznik, M. S., and Foster, K. R. (1999). Electrical impedance properties of normal and chronically infarcted left ventricular myocardium. *J. Interv. Card. Electrophysiol.* 3, 213–224. doi: 10.1023/A:1009887306055

Sivagangabalan, G., Pouliopoulos, J., Huang, K., Lu, J., Barry, M. A., Thiagalingam, A., et al. (2008). Comparison of electroanatomic contact and noncontact mapping of ventricular scar in a postinfarct ovine model with intramural needle electrode recording and histological validation. *Circ. Arrhythm. Electrophysiol.* 1, 363–369. doi: 10.1161/CIRCEP.108.799619

Sperelakis, N., and Hoshiko, T. (1961). Electrical impedance of cardiac muscle. *Circ. Res.* 9, 1280–1283. doi: 10.1161/01.RES.9.6.1280

Warren, M., Bragós, R., Casas, O., Rodríguez-Sinovas, A., Rosell, J., Anivarro, I., et al. (2000). Percutaneous electrocatheter technique for on-line detection of healed transmural myocardial infarction. *Pacing Clin. Electrophysiol.* 23, 1283–1287. doi: 10.1111/j.1540-8159.2000.tb00945.x

Wolf, T., Gepstein, L., Hayam, G., Zaretzky, A., Shofty, R., Kirshenbaum, D., et al. (2001). Three-dimensional endocardial impedance mapping : a new approach for myocardial infarction assessment. *Am. J. Physiol. Heart Circ. Physiol.* 280, H179–H188.

Wu, G., Zhao, X., Luo, S., and Shi, H. (2015). Histological image segmentation using fast mean shift clustering method. *Biomed. Eng. Online* 14, 24. doi: 10.1186/s12938-015-0020-x

Conflict of Interest Statement: The authors declare that the research was conducted in the absence of any commercial or financial relationships that could be construed as a potential conflict of interest.

Artículo 3: *Endocardial infarct scar recognition by myocardial electrical impedance is not influenced by changes in cardiac activation sequence*.

Gerard Amorós-Figueras, Esther Jorge, Concepción Alonso-Martin, Daniel Traver, Maria Ballesta, Ramon Bragós, Javier Rosell-Ferrer, Juan Cinca. *Heart Rhythm.* 2017. In Press.

https://doi.org/10.1016/j.hrthm.2017.11.031

Endocardial infarct scar recognition by myocardial electrical impedance is not influenced by changes in cardiac activation sequence

Gerard Amorós-Figueras, MSc,[*] Esther Jorge, DVM, PhD,[*†] Concepción Alonso-Martin, MD, PhD,[*] Daniel Traver, MSc,[‡] Maria Ballesta, BSc,[§] Ramon Bragós, PhD,[§] Javier Rosell-Ferrer, PhD,[†§] Juan Cinca, MD, PhD[*†]

From the [*]Department of Cardiology, Hospital de la Santa Creu i Sant Pau, IIB-Sant Pau, Universitat Autònoma de Barcelona, Barcelona, Spain, [†]CIBERCV, Barcelona, Spain, [‡]Biosense Webster, Barcelona, Spain, and [§]Electronic and Biomedical Instrumentation Group, Department of Electronic Engineering, Universitat Politècnica de Catalunya, Barcelona, Spain.

BACKGROUND Measurement of myocardial electrical impedance can allow recognition of infarct scar and is theoretically not influenced by changes in cardiac activation sequence, but this is not known.

OBJECTIVES The objectives of this study were to evaluate the ability of endocardial electrical impedance measurements to recognize areas of infarct scar and to assess the stability of the impedance data under changes in cardiac activation sequence.

METHODS One-month-old myocardial infarction confirmed by cardiac magnetic resonance imaging was induced in 5 pigs submitted to coronary artery catheter balloon occlusion. Electroanatomic data and local electrical impedance (magnitude, phase angle, and amplitude of the systolic-diastolic impedance curve) were recorded at multiple endocardial sites in sinus rhythm and during right ventricular pacing. By merging the cardiac magnetic resonance and electroanatomic data, we classified each impedance measurement site either as healthy (bipolar amplitude $\geq$1.5 mV and maximum pixel intensity $<$40%) or scar (bipolar amplitude $<$1.5 mV and maximum pixel intensity $\geq$40%).

RESULTS A total of 137 endocardial sites were studied. Compared to healthy tissue, areas of infarct scar showed 37.4% reduction in impedance magnitude ($P < .001$) and 21.5% decrease in phase angle ($P < .001$). The best predictive ability to detect infarct scar was achieved by the combination of the 4 impedance parameters (area under the receiver operating characteristic curve 0.96; 95% confidence interval 0.92–1.00). In contrast to voltage mapping, right ventricular pacing did not significantly modify the impedance data.

CONCLUSION Endocardial catheter measurement of electrical impedance can identify infarct scar regions, and in contrast to voltage mapping, the impedance data are not affected by changes in cardiac activation sequence.

KEYWORDS Electroanatomic mapping; Healed myocardial infarction; Myocardial electrical impedance; Pig; Ventricular pacing

(Heart Rhythm 2017;■:1–8)

Introduction

The clinical outcomes of catheter ablation in patients with infarct-related ventricular arrhythmias are largely dependent on the accurate delineation of the infarct scar during the procedure. Identification of the infarcted region is currently guided by 3-dimensional (3D) electroanatomic mapping, which use the voltage magnitude of local electrograms as a reference criterion.[1] Location of the dense infarcted region by bipolar voltage mapping has been correlated with anatomopathological and cardiac magnetic resonance (CMR) studies; thus, a low voltage threshold of $<$1.5 mV is currently accepted to delimit the borders of the infarct scar.[2,3]

A potential limitation of voltage mapping is that the amplitude of local electrograms may vary depending on the direction of the activation wavefront. Therefore, the collected data can change according to the type of the instantaneous cardiac rhythm. Indeed, significant differences in the amplitude of bipolar and unipolar local electrograms have been observed when the intrinsic rhythm is replaced by ventricular pacing in patients undergoing ablation of scar-related arrhythmias.[4,5]

Myocardial electrical impedance is a biophysical property of the heart that is influenced by the intrinsic structural

The first 2 authors contributed equally to this work. This work was supported by Fundació "La Marató de TV3" (grant no. 20150830), Spanish Ministerio de Economía y Competitividad, Instituto de Salud Carlos III (grant nos. FIS-PI13/00765 and DTS-15/00099), and Fondo Europeo de Desarrollo Regional (FEDER). Mr Traver is an employee of Biosense Webster. **Address reprint requests and correspondence:** Dr Esther Jorge, Department of Cardiology, Hospital de la Santa Creu i Sant Pau, c/Sant Antoni Mª Claret, 167, 08025 Barcelona, Spain. E-mail address: ejorge@santpau.cat.

1547-5271/

https://doi.org/10.1016/j.hrthm.2017.11.031

characteristics of the tissue.[6] Previous studies revealed that electrical impedance is lower in the infarct scar than in the normal myocardium, and this allows the recognition of the necrotic region.[7–9] Since electrical impedance is a passive property of the myocardium, it is predictable that impedance measures will not be affected by abrupt changes in cardiac activation sequence.

This study aimed to assess the ability of local electrical impedance to recognize infarcted tissue using an endocardial catheter and, secondly, to analyze comparatively the effects of abrupt changes in cardiac activation sequence on local voltage and impedance measurements using a closed-chest swine model.

Methods

Study population

Female domestic swine (Landrace and Large White cross) weighing 36 ± 1 kg were submitted to 2 interventions.

The first intervention aimed to induce acute myocardial infarction by occluding the left anterior descending coronary artery during 150 minutes with a catheter balloon, followed by reperfusion, as previously described.[10] Animals were premedicated with midazolam 0.6 mg/kg and ketamine 12 mg/kg, and then they were submitted to general anesthesia with propofol 2–4 mg/kg and maintained with sevoflurane inhalation (2.5%–3.5%). Fentanyl (5 μg/kg) was administered for analgesia. A femoral artery was catheterized and a 7-F introducer was used to insert a 6-F hockey stick guiding catheter (Cordis, Miami, FL). Under fluoroscopic control, the catheter was advanced to the left anterior descending coronary artery and a catheter balloon (Cordis) was placed at the mid segment below the origin of the first diagonal branch.

One month after the first intervention, a CMR study was performed in all animals under general anesthesia and mechanical ventilation to confirm and characterize the infarct scar. The day after the CMR study, the animals were sedated and anesthetized as in the first intervention. A femoral vein and femoral artery were catheterized, and a pacing electrocatheter (Blazer, Boston Scientific Corporation, Natick, MA) and a mapping electrocatheter (NAVISTAR, Biosense Webster, Inc., Diamond Bar, CA) were advanced into the right ventricle (RV) and left ventricle (LV), respectively. The RV electrocatheter was connected to a temporary external pacemaker (Medtronic Inc., Minneapolis, MN). The LV catheter was connected to a CARTO XP system (Biosense Webster) to generate an electroanatomic map as well as to a custom-designed impedance recording system to measure myocardial electrical impedance.[11] A conventional electrocardiographic (ECG) lead signal was continuously recorded throughout the procedure.

Study variables

CMR

We used a 3T scanner (Achieva, Philips Medical Systems, Amsterdam, The Netherlands), and all images were obtained with ECG gating and ventilation holding. The CMR study permitted to assess LV wall motion, cardiac function, and infarct characterization by late gadolinium enhancement (LGE). LGE images were obtained 10 minutes after an intravenous injection of 0.1 mmol/kg gadolinium-based contrast agent (Gadopentetate dimeglumine, Magnevist, Berlex Laboratories Inc., Wayne, NJ) with a pixel resolution of 1.18 × 1.18 mm in-plane and a slice thickness of 5 mm, giving rise to ~20 slices covering the LV. Processing of the LGE-CMR data was performed using the 3D Slicer software.[12] Briefly, an experienced operator manually segmented the LV wall in all sequential short-axis slices from the LGE-CMR images to create a 3D volume model of the LV (Figure 1). Then, normal and infarcted tissues were visualized and classified according to a maximum pixel intensity (MPI) cutoff of 0.40 × MPI (normal <0.40 and infarcted >0.40).

LV electroanatomic mapping

Local unipolar and bipolar electrograms were recorded at multiple endocardial sites, and the voltage amplitude of the signals was used to create a 3D representation of the LV chamber, as in current clinical electrophysiological procedures (Figure 1).

LV myocardial electrical impedance

Tissue impedance is a passive property of the myocardium that encompasses the intra- and extracellular resistances and cell membrane capacitance. Tissue impedance has 2 components: the impedance magnitude and the phase angle. The magnitude quantifies the drop in voltage of a test current passing through the tissue, and the phase angle reflects the time shift of the exploring current wave caused by the intrinsic structural characteristics of the tissue.

We measured the tissue impedance by injecting alternating currents (1-ms duration and 1-mA peak amplitude) of 26 frequencies (ranging from 1 to 1000 kHz) between the distal catheter electrode and a precordial skin reference electrode (Dispersive pad, 3M Healthcare Ltd, Saint Paul, MN) placed in the anterior precordial region. The voltage induced by the injected current was measured between the same distal catheter electrode and a second skin reference electrode (ECG pad, 3M) placed in the left lateral precordial region. This electrode configuration aimed to reduce the potential influence of both the individual body anatomy and the skin electrode impedance on the measurements. Moreover, to overcome the effect of the electrocatheter design (ie, electrode size and irrigated vs nonirrigated), we measured the intrinsic impedance of the electrocatheter before the study and this value was thereafter subtracted from the impedance measurement recorded during the study. All impedance measurements were recorded continuously during the cardiac cycle and stored at intervals of 2 seconds. Although we analyzed the entire impedance spectra in all sites, we preferentially reported the data at 1, 41, 307, and 1000 kHz because we previously verified that these frequencies were highly discriminative.[10,13]

To characterize the curve of phasic impedance changes elicited during the cardiac cycle, we measured the amplitude

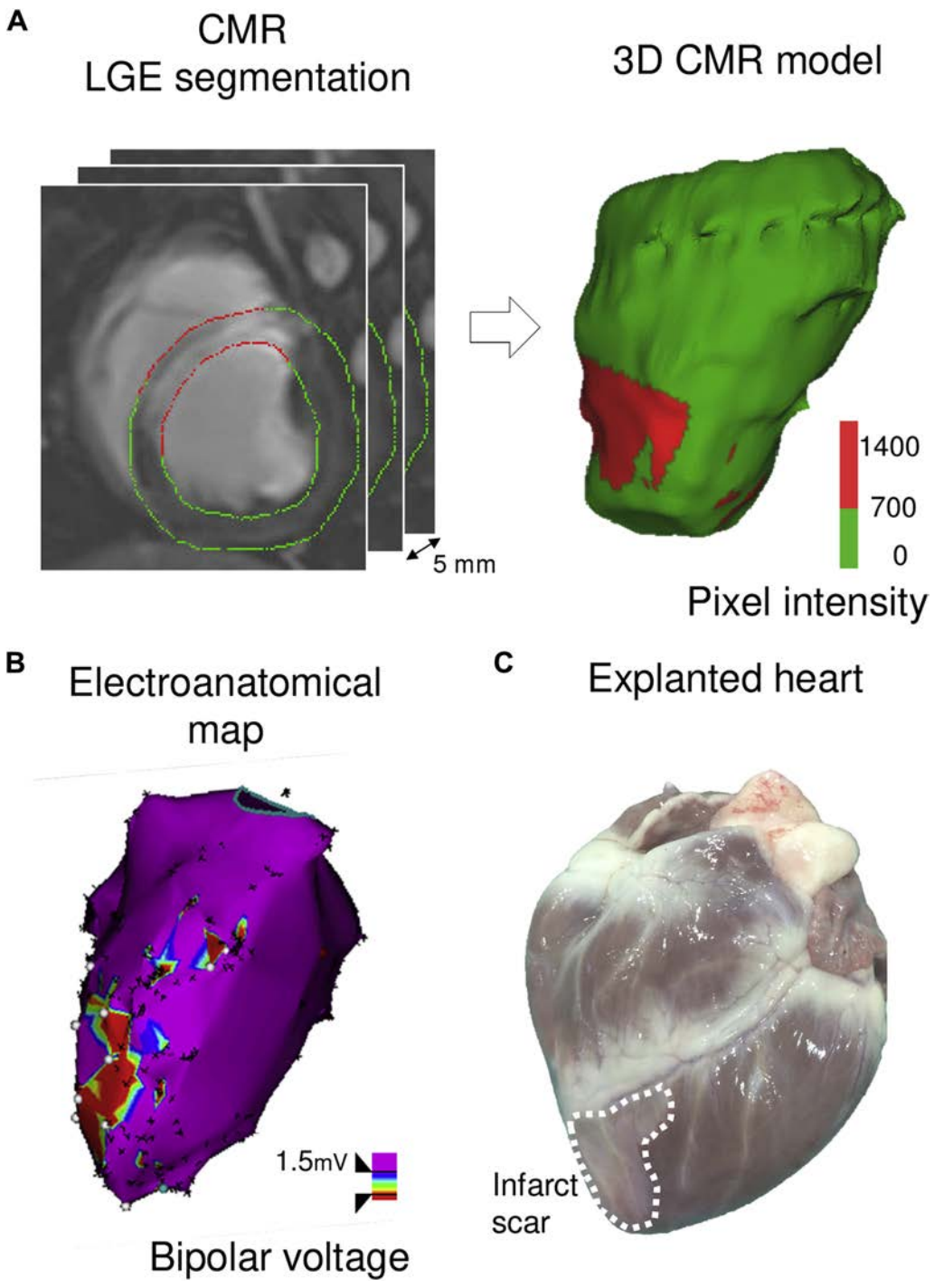

Figure 1 Illustration of the different imaging and electrophysiological techniques used in the study. **A:** Left: Myocardial wall segmentation in late gadolinium–enhanced cardiac magnetic resonance (LGE-CMR) imaging of a swine with a 1-month-old infarct scar. Right: Construction of a CMR model of the segmented slices. **B:** Electroanatomic map of the same case. **C**: Explanted heart of the same swine with the infarct scar borders delimited by a white dashed line.

of the curve and the time interval elapsed from the peak of the electrocardiographic R wave to the moment of maximum impedance magnitude (R wave impedance peak time).

CMR and electrical data merging

The electroanatomic data were automatically merged with the 3D CMR model using a fiducial registration guided by landmarks obtained in both techniques (LV apex and aortic and mitral annulus), as previously reported.[14] The areas of interest were defined on the basis of both the amplitude of bipolar electrograms and the extent of LGE on CMR imaging. Specifically, the measured sites were classified as healthy myocardium if they had a bipolar amplitude of $\geq$1.5 mV and an MPI of $<$40% or as infarct scar if they depicted a bipolar amplitude of $<$1.5 mV and an MPI of $\geq$40%. The sites not fulfilling this categorization were excluded.

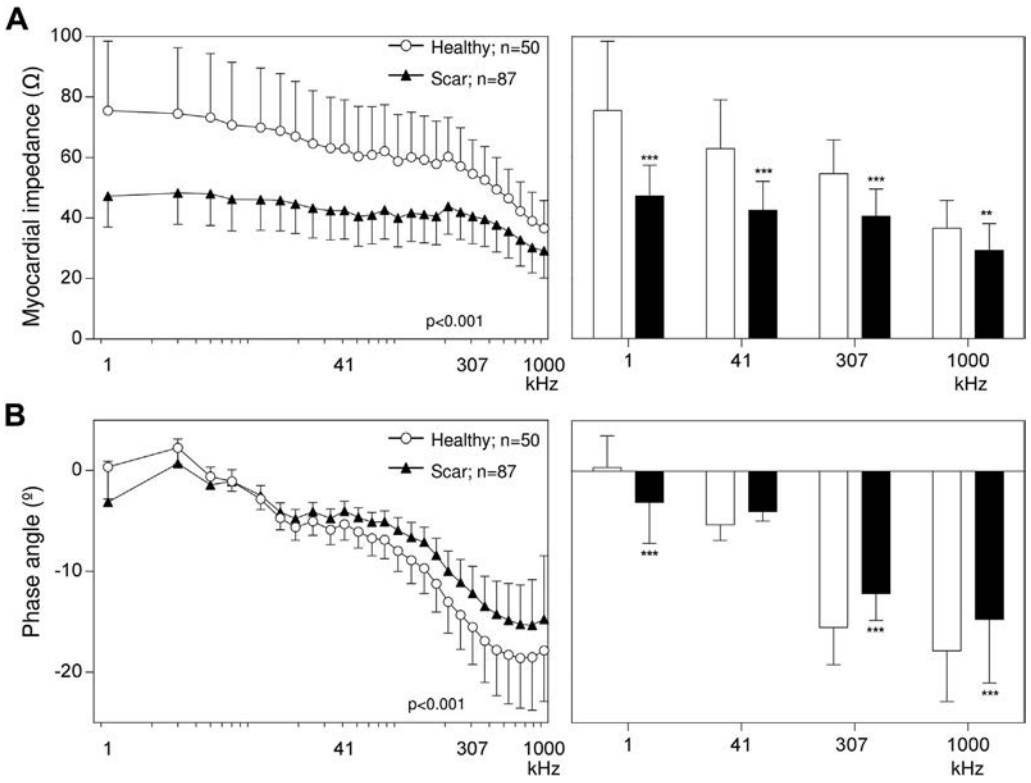

Figure 2 Mean values of the impedance magnitude and phase angle recorded in 137 endocardial sites (n = 50 healthy and n = 87 infarct scar) in 5 pigs. **A:** The left panel shows the mean of the impedance magnitude spectrum recorded in healthy and infarct scar sites. The right panel shows the mean of the impedance magnitude at 4 selected frequencies. **B:** The left panel shows the mean of the phase angle spectrum of healthy and infarct scar sites. The right panel shows the mean of the phase angle at 4 selected frequencies. ***$P < .001$; **$P < .01$.

Changes in the cardiac activation sequence

To compare the stability of the electroanatomic data and the tissue impedance data under abrupt changes in the cardiac activation wavefront, these parameters were analyzed in the same sites during sinus rhythm and during electrical RV stimulation in a subset of measures. The resultant changes were expressed as percentages using the following formula: $100 \times [(X_{RVP} - X_{SR})/X_{SR}]$, where X_{RVP} are the values of voltage or impedance during RV pacing and X_{SR} are the values of voltage or impedance in sinus rhythm.

Experimental protocol

After stabilization of the level of anesthesia and hemodynamic parameters, an endocardial high-density 3D electroanatomic bipolar voltage map of the LV was constructed during stable sinus rhythm using the mapping catheter and the CARTO XP system. Thereafter, the mapping catheter was moved to different endocardial sites, and the local voltage and myocardial electrical impedance were measured at the same sites. In a subgroup of these sites, the local voltage and myocardial electrical impedance were recorded both in sinus rhythm and during RV pacing. At the end of the study, the animals were euthanized by an intravenous overdose of KCl and the hearts were explanted.

The study protocol was approved by the Animal Care and Use Committee of our institution and conformed to the *Guide for the Care and Use of Laboratory Animals*, 8th edition (National Research Council, The National Academies Press, Washington, DC, 2010).

Statistical analysis

Data were expressed as mean ± SD. Differences in the study variables were assessed using an analysis of variance with Bonferroni correction for post hoc comparisons. A binary logistic regression model was built to assess the influence of different impedance parameters to distinguish between normal and infarcted tissues. The discriminating power of the models was assessed using the receiver operating characteristic curve (ROC) and the area under the curve (AUC). Optimal cutoffs and accuracies were calculated for each impedance parameter model. The *P* value for the AUC comparison was based on the DeLong method. A *P* value of $<.05$ was considered statistically significant. Statistical analysis was performed using R version 3.2.2 (R Foundation for Statistical Computing, Vienna, Austria) and SPSS version 22.0 (IBM Corp., Armonk, NY).

Results

Two of the 7 (29%) pigs died during acute coronary occlusion due to irreversible ventricular fibrillation. The remaining 5 (71%) animals completed the entire protocol and were included in the final analysis. A total number of 156 sites were explored (27 ± 4 sites per animal). Nineteen (12%)

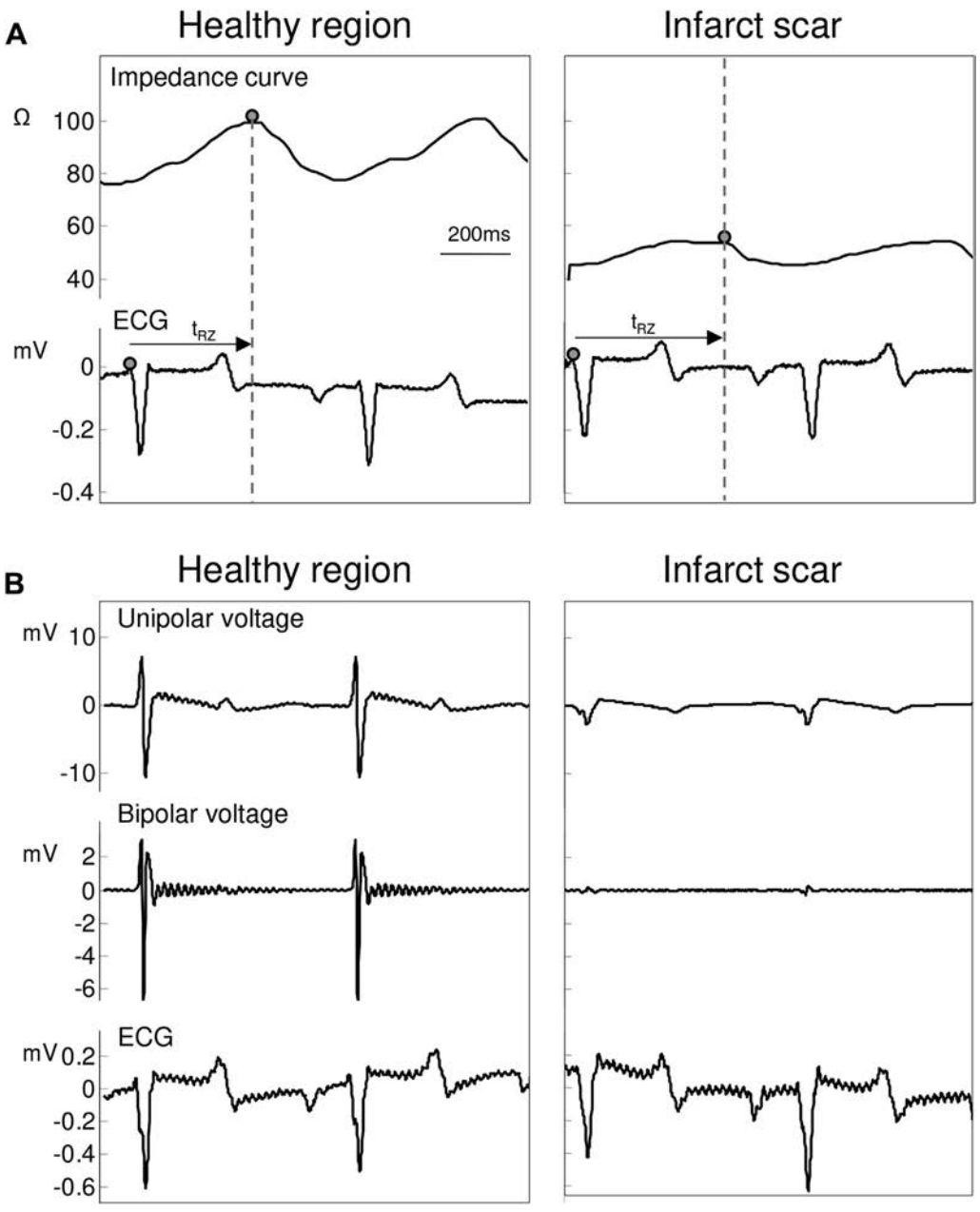

Figure 3 Myocardial impedance and voltage signals in healthy and scar tissues. **A:** Myocardial impedance curve and electrocardiographic (ECG) lead III recorded in healthy (left) and scar (right) regions in an anesthetized swine. The arrows indicate the time interval between the R-wave peak and the maximum of the myocardial impedance curve (t_{RZ}). **B:** Unipolar, bipolar, and ECG (lead III) signals at the site where impedance was measured in healthy (left) and scar (right) regions.

of these samples were excluded according to the categorization criteria; thus, 137 (88%) entered in the final analysis: 50 (36%) were classified as healthy and 87 (64%) as infarct scar.

Myocardial electrical impedance spectroscopy

As shown in Figure 2, the infarct scar showed lower electrical impedance magnitude and less negative phase angle than did healthy tissue (37.4% reduction in impedance magnitude at 1 kHz; $P < .001$ and 21.5% decrease in phase angle at 307 kHz; $P < .001$). The impedance magnitude (Z) decreased gradually at increasing current frequencies in normal tissue (from 75.5 ± 23.0 Ω at 1 kHz to 36.6 ± 9.2 Ω at 1000 kHz), but this change was less marked in scar tissue (from 47.3 ± 10.2 Ω at 1 kHz to 29.2 ± 9.0 Ω at 1000 kHz). Moreover, the phase angle spectrum showed a relaxation at high frequencies more apparent in healthy tissue than in scar tissue. Figure 2 shows that the excitation frequencies that best discriminate between healthy and scar tissues are 1, 41, and 307 kHz for the impedance magnitude and 1, 307, and 1000 kHz for the phase angle. All individuals showed a similar trend of changes in the impedance spectra in healthy and scar regions (Supplemental Figure 1).

Table 1 Values of the AUC-ROC and their optimal classification accuracy for the different myocardial electrical impedance parameters, either alone or in combination, measured at their most distinctive current frequency in 5 pigs with chronic myocardial infarction

Model	AUC-ROC (95% CI)	*P*	Optimal classification accuracy (%)
Impedance magnitude at 41 kHz	0.87 (0.81–0.94)	.001	79.8
Impedance phase angle at 307 kHz	0.78 (0.70–0.87)	.001	68.1
Impedance magnitude + phase angle	0.93 (0.87–0.99)	.001	93.3
Impedance curve (amplitude + peak time) at 41 kHz	0.93 (0.88–0.98)	.01	89.1
Combination of all impedance parameters	0.96 (0.92–1.00)	.001	93.3

AUC-ROC = area under the receiver operating characteristic curve; CI = confidence interval.

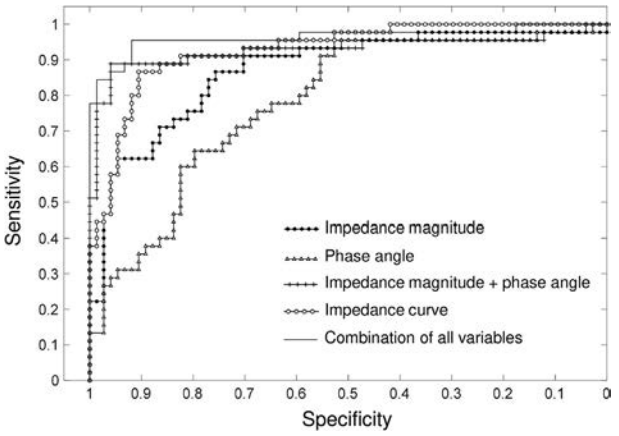

Figure 4 Receiver operating characteristic curves to assess the predictive ability of the different myocardial electrical impedance parameters. The impedance parameters used were (1) the impedance magnitude at 41 kHz (line with black circles), (2) the phase angle at 307 kHz (line with white triangles), (3) the combination of the impedance magnitude at 41 kHz and the phase angle at 307 kHz (line with plus markers), and (4) the combination of the amplitude of the impedance curve and the R wave-impedance peak time at 41 kHz (line with white circles). (5) The combination of all 4 impedance parameters (straight line).

Phasic pattern of myocardial electrical impedance

Myocardial impedance showed a biphasic pattern during the cardiac cycle. Figure 3 illustrates the relationship between the cyclic myocardial impedance changes and the ECG in healthy and scar regions. The amplitude of the phasic changes was lower in scar tissue at all tested current frequencies (13.5 ± 7.9 Ω vs 39.7 ± 15.6 Ω at 1 kHz, 10.3 ± 5.8 Ω vs 27.7 ± 10.7 Ω at 41 kHz, 8.9 ± 5.1 Ω vs 20.6 ± 9.9 Ω at 307 kHz, and 6.3 ± 3.8 Ω vs 11.6 ± 5.1 Ω at 1000 kHz; $P < .001$). The time interval between the R-wave peak of the ECG and the moment of the maximum value of the impedance curve was longer in scar areas than in the healthy myocardium (404 ± 102 ms vs 349 ± 115 ms; $P < .05$). The mean values of all impedance parameters recorded in each animal are presented in Supplemental Table 1.

Predictive ability of myocardial impedance

To assess the predictive ability of myocardial impedance measurement to discriminate between infarct scar and healthy tissue, we calculated the cutoff values and classification accuracy using the ROC curves (Table 1 and Figure 4). Cutoff values were 49.7 Ω for the impedance magnitude, −11.8° for the phase angle, 10 Ω for the amplitude of the impedance curve, and 394.5 ms for the R wave-impedance peak time. The inclusion of the 4 impedance parameters in the ROC model afforded the highest AUC, indicating optimal predictive ability ($P < .01$).

Effects of RV pacing on local voltage and tissue impedance

In 58 of the 137 (42%) explored sites, we analyzed the effects of RV pacing on both the amplitude of local electrograms and the magnitude of myocardial electrical impedance in each recording site. As shown in Figure 5A, RV pacing induced appreciable changes in the amplitude of bipolar and unipolar electrograms but not in the magnitude of myocardial impedance. The variability in these changes is graphically illustrated in Figure 5B, and their interquartile range values are reported in Table 2. Of note, in 12% (7) of the explored sites, the RV pacing entailed a switch on their bipolar threshold voltage classification: 8.6% (5) of sites changed from <1.5 mV in sinus rhythm to ≥1.5 mV during RV pacing and 3.4% (2) of sites from ≥1.5 to <1.5 mV. Likewise, unipolar electrograms followed a similar trend of changes in 10.4% (6) of the explored sites: 5.2% (3) changed from <8.3 mV in sinus rhythm to ≥8.3 mV during RV pacing and 5.2% (3) from ≥8.3 to <8.3 mV.

Discussion

Main findings

This study is the first to analyze the ability to recognize areas of infarct scar using a novel approach based on the endocardial catheter measurement of systolic-diastolic local myocardial electrical impedance. Our data indicate that the measurement of endocardial impedance allow the recognition of infarct scar and, as an advantage over the voltage mapping, the impedance data are not affected by abrupt changes in cardiac activation sequence.

Ability of myocardial impedance to identify infarcted tissue

Earlier experimental studies have demonstrated that the measurement of local myocardial electrical impedance permitted recognition of areas of acute and healed myocardial infarction by using either implanted transmural needle

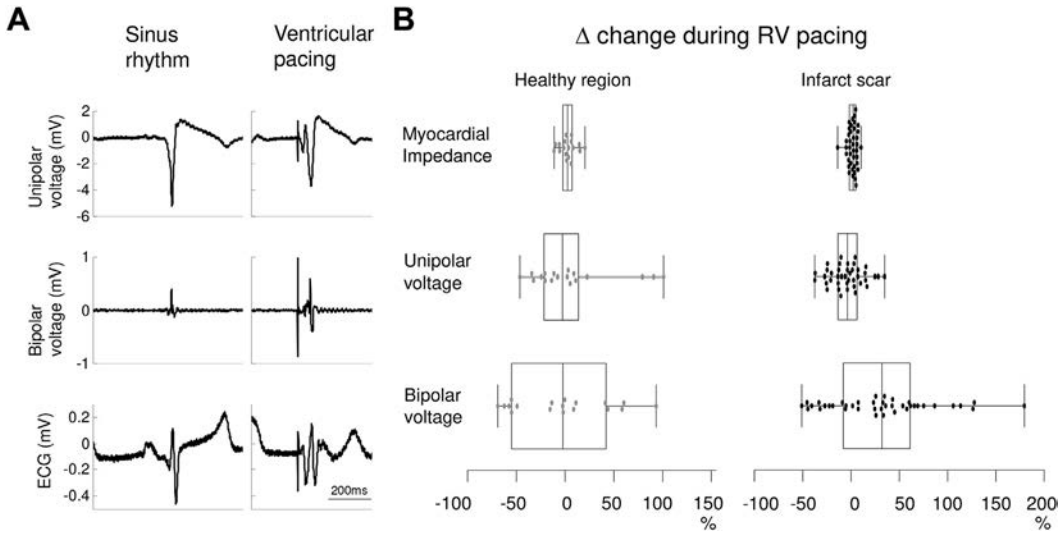

Figure 5 Effects of changes in cardiac activation sequence on local endocardial voltage and tissue electrical impedance. **A:** Unipolar and bipolar electrograms and electrocardiogram (lead III) recorded in sinus rhythm and during right ventricular (RV) pacing. **B:** Ratio of change (in percent) in myocardial impedance and endocardial voltage (unipolar and bipolar) induced by right ventricular pacing in healthy and infarct scar regions. The left side of the box plot represents the 25th percentile, and the right side represents the 75th percentile. The vertical line across the boxes represents the median value. The ends of the whiskers correspond to the lowest and highest values.

electrodes[7–9,15] or contact endocardial electrocatheters.[13,16] Most of these studies were conducted in open-chest models, and this limited the transferability of this technique to clinical practice. Moreover, myocardial impedance measurements could only be obtained at random moments within the cardiac cycle and this did not allow recording of the continuous changes induced by cardiac mechanical activity. More recently, with the use of fast broadband electrical impedance spectroscopy,[11] it has been possible to measure the impedance changes throughout the cardiac cycle using a wide range of current frequencies from 1 to 1000 kHz.[10,17] Using intramural needle electrodes, one of these studies[10] showed that the infarcted regions with greater fibrotic content had the lower mean impedance values and the more depressed systolic-diastolic impedance curve. The present data confirm that compared to the healthy myocardium, the impedance curve of the infarct scar has a reduced amplitude and a delayed peak value. The combined inclusion of the 4 impedance parameters (impedance magnitude, phase angle, amplitude of the impedance curve, and R wave-impedance peak time) into the ROC curve model increased the predictive ability and accuracy to differentiate healthy and infarcted tissues.

Effects of changes in cardiac activation sequence

Studies in patients submitted to catheter ablation of infarct-related ventricular arrhythmias have reported a voltage variability in local unipolar and bipolar electrograms when the intrinsic cardiac rhythm is replaced by ventricular pacing.[4,5] Specifically, these authors found that 8%–18% of the explored sites presented discordant voltage values during ventricular pacing (ie, sites with voltage amplitude <1.5 mV during 1 cardiac activation sequence changed to >1.5 mV during another activation sequence). Our results are consistent with these findings since we have found a similar pattern of voltage discordancy in 12% of the bipolar recording sites during RV pacing. Of note, the present study reveals that contrary to bipolar and unipolar voltage mapping, the measurements of myocardial electrical impedance in normal and infarcted regions were not modified by RV pacing. Thus, implementation of impedance measures in the 3D electroanatomic cardiac navigators would theoretically help assess more accurately the target infarcted areas, especially in the presence of recurrent ventricular arrhythmias during the procedure.

Table 2 Interquartile range values of the changes in local voltage and myocardial impedance induced by right ventricular pacing in 58 endocardial sites in 5 pigs with chronic myocardial infarction

Site	Unipolar voltage	Bipolar voltage	Impedance
Healthy (n = 18)	31.2%	87.2%	7.7%
Scar (n = 40)	18.4%	67.0%	6.4%

Study limitations

This study was designed to proof the concept that the impedance characteristics of the infarct scar can be detected by endocardial catheter mapping in closed-chest models and, secondly, to verify the lack of variability in impedance measures upon abrupt changes in cardiac activation sequence. At this stage, we divided the explored sites in only 2 well-defined categories (healthy or infarcted) taking as criterion standard both the bipolar voltage amplitude and the degree of gadolinium enhancement at each recording site (bipolar amplitude ≥ 1.5 mV and MPI $<40\%$ for healthy and bipolar amplitude <1.5 mV and MPI $>40\%$ for infarcted). Thus, to assess the diagnostic yielding of the impedance technique in nontransmural infarct sites, multisite recordings at the infarct border zone will be required.

Most of the commercial cardiac navigators can measure impedance parameters in order to check the appropriateness of electrode-tissue contact or to control the radiofrequency energy delivery during the ablation procedures. However, in contrast to our method, these systems do not permit continuous recording of the impedance during the cardiac cycle.

The present impedance data are specific for the mapping electrocatheter used in this study (Blazer), but other electrocatheter types can be used, provided a previous ad hoc in vitro impedance calibration will be performed.

Clinical implications

The transferability of our observations to the field of catheter ablation in patients with infarct-related ventricular arrhythmias is founded on (1) the cardiac electrophysiological similarities between humans and swine,[18] (2) the closed-chest approach in our study, (3) the use of electrocatheters and commercial 3D electroanatomic systems routinely used in clinical arrhythmia ablation, and (4) the use of the image merging process of CMR and electroanatomic data. Thus, our study suggests that the implementation of impedance mapping into current cardiac navigators will improve the identification of infarct scar targets.

Conclusion

Endocardial catheter measurement of tissue electrical impedance can identify infarct scar regions and, in contrast to voltage mapping, is not affected by changes in cardiac activation sequence.

Acknowledgments

We thank Francisco Alarcón, MSc, and David Soto-Iglesias, PhD for technical assistance.

Appendix

Supplementary data

Supplementary data associated with this article can be found in the online version at https://doi.org/10.1016/j.hrthm.2017.11.031.

References

1. Wissner E, Stevenson WG, Kuck KH. Catheter ablation of ventricular tachycardia in ischaemic and non-ischaemic cardiomyopathy: where are we today? A clinical review. Eur Heart J 2012;33:1440–1450.
2. Callans DJ, Ren JF, Michele J, Marchlinski FE, Dillon SM. Electroanatomic left ventricular mapping in the porcine model of healed anterior myocardial infarction: correlation with intracardiac echocardiography and pathological analysis. Circulation 1999;100:1744–1750.
3. Marchlinski FE, Callans DJ, Gottlieb CD, Zado E. Linear ablation lesions for control of unmappable ventricular tachycardia in patients with ischemic and nonischemic cardiomyopathy. Circulation 2000;101:1288–1296.
4. Tung R, Josephson ME, Bradfield JS, Shivkumar K. Directional influences of ventricular activation on myocardial scar characterization: voltage mapping with multiple wavefronts during ventricular tachycardia ablation. Circ Arrhythm Electrophysiol 2016;9:e004155.
5. Bruncklorst CB, Delacretaz E, Soejima K, Maisel WH, Friedman PL, Stevenson WG. Impact of changing activation sequence on bipolar electrogram amplitude for voltage mapping of left ventricular infarcts causing ventricular tachycardia. J Interv Card Electrophysiol 2005;12:137–141.
6. Sperelakis N, Hoshiko T. Electrical impedance of cardiac muscle. Circ Res 1961;9:1280–1283.
7. Cinca J, Warren M, Carreño A, Tresànchez M, Armadans L, Gómez P, Soler-Soler J. Changes in myocardial electrical impedance induced by coronary artery occlusion in pigs with and without preconditioning: correlation with local ST-segment potential and ventricular arrhythmias. Circulation 1997;96:3079–3086.
8. Cinca J, Warren M, Rodríguez-Sinovas A, Tresànchez M, Carreño A, Bragós R, Casas O, Domingo A, Soler-Soler J. Passive transmission of ischemic ST segment changes in low electrical resistance myocardial infarct scar in the pig. Cardiovasc Res 1998;40:103–112.
9. Schwartzman D, Chang I, Michele JJ, Mirotznik MS, Foster KR. Electrical impedance properties of normal and chronically infarcted left ventricular myocardium. J Interv Card Electrophysiol 1999;3:213–224.
10. Amorós-Figueras G, Jorge E, García-Sánchez T, Bragós R, Rosell-Ferrer J, Cinca J. Recognition of fibrotic infarct density by the pattern of local systolic-diastolic myocardial electrical impedance. Front Physiol 2016;7:389.
11. Sanchez B, Schoukens J, Bragos R, Vandersteen G. Novel estimation of the electrical bioimpedance using the local polynomial method: application to in vivo real-time myocardium tissue impedance characterization during the cardiac cycle. IEEE Trans Biomed Eng 2011;58:3376–3385.
12. Fedorov A, Beichel R, Kalpathy-Cramer J, et al. 3D Slicer as an image computing platform for the Quantitative Imaging Network. Magn Reson Imaging 2012;30:1323–1341.
13. Warren M, Bragós R, Casas O, Rodríguez-Sinovas A, Rosell J, Anivarro I, Cinca J. Percutaneous electrocatheter technique for on-line detection of healed transmural myocardial infarction. Pacing Clin Electrophysiol 2000;23:1283–1287.
14. Andreu D, Berruezo A, Ortiz-Pérez JT, Silva E, Mont L, Borràs R, De Caralt TM, Perea RJ, Fernández-Armenta J, Zeljko H, Brugada J. Integration of 3D electroanatomic maps and magnetic resonance scar characterization into the navigation system to guide ventricular tachycardia ablation. Circ Arrhythm Electrophysiol 2011;4:674–683.
15. Fallert MA, Mirotznik MS, Downing SW, Savage EB, Foster KR, Josephson ME, Bogen DK. Myocardial electrical impedance mapping of ischemic sheep hearts and healing aneurysms. Circulation 1993;87:199–207.
16. Wolf T, Gepstein L, Hayam G, Zaretzky A, Shofty R, Kirshenbaum D, Uretzky G, Oron U, Ben-haim SA. Three-dimensional endocardial impedance mapping: a new approach for myocardial infarction assessment. Am J Physiol Heart Circ Physiol 2001;280:H179–H188.
17. Jorge E, Amorós-Figueras G, García-Sánchez T, Bragós R, Rosell-Ferrer J, Cinca J. Early detection of acute transmural myocardial ischemia by the phasic systolic- diastolic changes of local tissue electrical impedance. Am J Physiol Heart Circ Physiol 2016;310:H436–H443.
18. Cinca J, Janse MJ, Moréna H, Candell J, Valle V, Durrer D. Mechanism and time course of the early electrical changes during acute coronary artery occlusion: an attempt to correlate the early ECG changes in man to the cellular electrophysiology in the pig. Chest 1980;77:499–505.

Discusión

El objetivo principal de esta Tesis Doctoral ha sido desarrollar una nueva técnica para la detección y caracterización de la cicatriz de infarto de miocardio basada en medidas de bioimpedancia, en un modelo experimental. Para ello, hemos dividido nuestro trabajo en tres fases. En la primera, hemos caracterizado la impedancia local del miocardio sano e isquémico a lo largo de todo el ciclo cardíaco describiendo su relación temporal con el ECG, la presión del ventrículo izquierdo y el flujo aórtico en un modelo porcino. En la segunda fase hemos analizado la capacidad de esta técnica para reconocer el grado de fibrosis en una cicatriz post-infarto. Las medidas en estas dos fases se realizaron mediante agujas insertadas en el espesor de la pared ventricular en cerdos anestesiados y a tórax abierto. Aunque la medida intramiocárdica es altamente invasiva, es el método más apropiado para una caracterización precisa de la impedancia local. En la tercera parte hemos evaluado la capacidad de la bioimpedancia en reconocer el tejido cicatricial en cerdos anestesiados y a tórax cerrado utilizando un electrocatéter intracavitario y un sistema de navegación cardíaco idéntico al usado en la clínica durante la ablación eléctrica de arritmias. Así mismo, hemos comprobado la estabilidad de la medida frente a cambios en la secuencia de activación cardíaca. Los resultados muestran que es posible detectar la cicatriz de infarto midiendo los cambios cíclicos de la impedancia local a través de un electrocatéter convencional en un modelo a tórax cerrado.

Nuestro estudio aporta información traslacional original que sienta las bases para desarrollar una nueva técnica capaz de detectar y caracterizar la cicatriz post-infarto.

Nuestras aportaciones se pueden agrupar en dos bloques: unas centradas en la medida experimental de la impedancia miocárdica, pertenecientes al campo de la ingeniería biomédica, y otras centradas en la aplicación clínica de estas medidas, pertenecientes al campo de la medicina cardiovascular.

1. Aportaciones al campo de la ingeniería biomédica

La medida experimental de la impedancia eléctrica del miocardio es una tarea compleja que presenta varios retos desde el punto de vista de la ingeniería biomédica. El primero, y más evidente, es que la inyección de corriente necesaria para realizar la medida no dañe el corazón ni altere su normal funcionamiento. Así, la corriente debe tener unos parámetros de seguridad estrictos, que eviten la inducción de una arritmia, un reflejo neural o daño estructural. Al mismo tiempo, la corriente debe tener una amplitud, frecuencia y duración de suficiente magnitud que garantice una buena adquisición de la señal, con una amplitud superior al ruido existente. Para superar este reto hemos usado un nuevo sistema de registro de la bioimpedancia basado en excitaciones multiseno con un factor de cresta bajo. El factor de cresta de una señal muestra la relación entre el valor de sus picos máximos y su media cuadrática y es de interés que sea bajo para que la fuente de corriente pueda alcanzar la potencia requerida. Así pues, nuestro sistema utiliza corrientes de 1 miliamperio entre las frecuencias de 1 y 1000 kHz, con una resolución temporal muy elevada (58). De esta forma hemos obtenido registros estables y reproducibles.

El segundo reto al que nos enfrentamos es la propia obtención de la medida experimental de la impedancia del miocardio en el corazón latiendo. Esta es una tarea compleja porque debe tener en cuenta el movimiento constante del corazón y su variación cíclica de volumen. Para realizar la medida a tórax abierto y con el corazón latiendo hicimos un tratamiento previo de los electrodos mediante la técnica de sputtering que permite maximizar su superficie de contacto y aumentar su rugosidad. La técnica de sputtering es un proceso físico en el que se produce la

vaporización de los átomos de un material sólido mediante el bombardeo de éste por iones energéticos. En los registros a tórax cerrado verificamos la posición del catéter a través del fluoroscopio y del navegador cardíaco.

El tercer reto consiste en el análisis y la interpretación de los registros obtenidos. Para poder caracterizar de forma detallada los cambios de la impedancia eléctrica durante el ciclo cardíaco realizamos un registro simultaneo con otras señales fisiológicas. Con esta información hemos realizado las siguientes aportaciones.

1.1. Interrelación entre la medida de la impedancia eléctrica del miocardio y la actividad mecánica del corazón

En el pasado, las medidas de la impedancia eléctrica del miocardio *in vivo* no permitían detectar las variaciones de la misma durante las diferentes fases del ciclo cardíaco debido a la baja frecuencia de muestreo de la señal (19,39). En este trabajo hemos utilizado un nuevo sistema de registro rápido del espectro de impedancia eléctrica que, a diferencia de los sistemas anteriores, es capaz de generar hasta 1000 medidas por segundo (9). Gracias a este avance, hemos podido caracterizar por primera vez sus variaciones a lo largo de todo el ciclo cardíaco en el miocardio sano, isquémico y cicatricial. Concretamente, este trabajo muestra que su valor medio en el miocardio sano tiene una variación del 9% entre la sístole y la diástole que sería debida a los cambios geométricos de la estructura local del tejido registrado. Estudios previos han reportado variaciones similares del 10% para la impedancia registrada a 50 kHz (8,31) y del 8% para la registrada entre 5 y 60 kHz (20). Sin embargo, el mecanismo de la relación entre los cambios geométricos del miocardio durante la sístole y la diástole y la magnitud de la impedancia está sujeto

a controversia. Steendijk et al. (20) describieron un incremento de la resistividad longitudinal durante la sístole y lo atribuyeron a que en esta fase del ciclo cardíaco las fibras se acortan y engruesan. Por el contrario, Sasaki et al. (31) describieron un descenso en la resistividad durante la sístole y lo atribuyeron también al aumento de grosor de las fibras. Además, ambos estudios postularon que el aumento de la resistividad podía ser debido a la disminución del volumen de sangre intracardiaca durante la sístole, pero solo el estudio de Steendijk et al. evidenció este efecto.

La diferencia en los hallazgos de estos estudios podría estar en relación con el diseño de los electrodos, ya que en el estudio de Steendijk se utilizaron electrodos tetrapolares de contacto epicárdico mientras que en el estudio de Sasaki et al. se utilizaron electrodos bipolares insertados en el espesor del miocardio. Además, dado que en el trabajo de Sasaki et al. se medían simultáneamente la impedancia y los cambios de la motilidad miocárdica local con cristales ultrasónicos, no se puede excluir un efecto de estos materiales en las medidas experimentales.

Los resultados de nuestro estudio sugieren que, a parte del valor medio, la morfología de la curva de la resistividad refleja también los cambios dinámicos del ventrículo durante el ciclo cardíaco. Esta afirmación está fundamentada en que:

1) Existe una gran similitud entre la morfología de esta curva y la morfología de la curva de deformación mecánica local durante los primeros minutos de isquemia medido con cristales ultrasónicos (59), 2) Durante la isquemia aguda, las curvas de la relación presión del VI-deformación local del VI (60) y las curvas de presión del VI-resistividad del VI sufren una reducción similar y significativa de sus áreas, 3) En el tejido miocárdico necrótico se observa un aplanamiento de la curva de resistividad en paralelo con una depresión significativa de la actividad mecánica local (61) y 4) La amplitud de esta curva es constante entre 1 y 1000 kHz ya que no está

influenciada por las resistencias intra- y extracelulares, a diferencia su valor medio que decrece con la frecuencia.

1.2. Rendimiento de los parámetros de impedancia en la caracterización del tejido miocárdico

El valor medio de la resistencia y el ángulo de fase son los componentes de la impedancia que tradicionalmente se han usado para caracterizar el tejido miocárdico sano o afectado de alguna patología (6,18,25,39). En este trabajo hemos podido realizar además el análisis de la curva de la impedancia durante todo el ciclo cardíaco y así obtener dos nuevos parámetros para caracterizar el estado del miocardio: la morfología de la curva de resistividad y el retraso temporal del pico máximo de esta curva con respecto de la onda R del ECG.

Amplitud y momento temporal de la curva de impedancia

Hasta la fecha, el análisis de la variación cíclica de la impedancia local del miocardio se había realizado en un reducido rango de frecuencias (5-60 kHz) y se centraba en describir que su valor medio aumentaba en la sístole y disminuía en la diástole (20,31). Además, aquellos estudios se habían llevado a cabo en el miocardio sano e isquémico de perros anestesiados, limitando su traslación a la clínica ya que los perros, a diferencia de los humanos, poseen un sistema de arterias colaterales muy desarrollado que les da una mayor protección a la isquemia aguda (62). En este trabajo hemos realizado un análisis detallado de la curva de impedancia en un modelo porcino de isquemia aguda y en otro de infarto crónico. Todos los análisis de la curva se han efectuado de forma semiautomática, a través de algoritmos en Matlab que posteriormente se han verificado de forma manual por

varios investigadores para minimizar la subjetividad en el cálculo de los diferentes parámetros de la impedancia. Estos parámetros son: 1) Promedio de la amplitud (valor máximo-valor mínimo) durante tres ciclos cardíacos, a las frecuencias entre 1 y 1000 kHz, 2) Valor de la magnitud en tres instantes específicos del ciclo cardíaco (pre-sístole, eyección y relajación) definidos de forma muy precisa a través del ECG y de la señal de flujo aórtico, 3) Intervalo de tiempo entre el pico máximo de la curva y el pico de la onda R del ECG en el tejido miocárdico sano y cicatricial.

La inclusión combinada de estos nuevos parámetros (amplitud y retraso de la curva) junto con los parámetros clásicos (magnitud y ángulo de fase) en un modelo lineal general incrementó de forma significativa la capacidad predictiva del modelo en diferenciar el tejido miocárdico sano del tejido cicatricial. Nuestros resultados ponen de manifiesto que la medida continua de la impedancia durante el ciclo cardíaco mejora la precisión de la medida clásica en la identificación de las alteraciones estructurales del corazón.

Ángulo de fase

Para caracterizar de forma completa la impedancia de un tejido biológico es necesario registrar su resistencia y reactancia. Solo conociendo ambas magnitudes es posible calcular el ángulo de fase, que tiene en cuenta las pérdidas de corriente por el almacenamiento de carga en las membranas celulares y que ha demostrado ser útil para evaluar el estado de integridad estructural del miocardio (21). Sin embargo, una gran parte de los estudios en este campo solo reportan los valores de resistencia o resistividad (18,20,29,31,42,63). En este trabajo hemos registrado el ángulo de fase local del miocardio durante el ciclo cardíaco entre 1 y 1000 kHz. Los valores hallados están en concordancia con estudios previos que muestran que el

ángulo de fase del miocardio: 1) se reduce aproximadamente unos 3º a bajas frecuencias durante las primeras fases de la isquemia aguda (6,30,64), y 2) disminuye su relajación a altas frecuencias y sus valores se hacen más positivos en la cicatriz densa post-infarto (7,19). De forma novedosa hemos demostrado que el ángulo de fase permite detectar las regiones donde la cicatriz post-infarto es heterogénea, ya que existe una buena correlación lineal entre el grado local de fibrosis y su valor absoluto.

Selección de las frecuencias más discriminatorias

La impedancia eléctrica de los tejidos biológicos depende de la frecuencia de la corriente aplicada. Debido a que los medios intra- y extracelulares se comportan eléctricamente como medios conductores y las membranas celulares como dieléctricos, las corrientes de baja frecuencia fluirán principalmente a través del medio extracelular y las de alta frecuencia a través del medio intra- y extracelular (30). Gracias a estas circunstancias, hay algunas frecuencias de corriente que ofrecen una mayor sensibilidad para detectar los cambios en las propiedades estructurales del miocardio sometido a isquemia aguda o crónica (23). En esta tesis hemos hallado que las frecuencias de corriente que presentan una sensibilidad mayor para detectar de forma temprana la isquemia miocárdica son 1 kHz para la resistividad y 307 kHz para el ángulo de fase. Estos resultados concuerdan con estudios previos y los amplían mediante el uso de un mayor número de frecuencias intermedias (en total 26 entre 1 y 1000 kHz) el registro de los valores máximos y mínimos del espectro de la resistividad del miocardio durante el ciclo cardíaco (23,64). Las frecuencias de corriente que diferencian mejor el tejido sano del tejido cicatricial son 1 kHz para la resistividad, si realizamos el registro mediante agujas

insertadas en el miocardio, y 41 kHz si lo hacemos a través de un catéter endocavitario. Para el ángulo de fase la frecuencia más sensible es la de 307 kHz, independientemente del método de registro. Ambos resultados concuerdan con la literatura y muestran de forma novedosa que los valores de la magnitud y fase entre las frecuencias de 1 y 1000 kHz tienen una correlación con el porcentaje de fibrosis evaluado por histología (7,19,23). Además, hemos observado que tanto la amplitud como el retraso de la curva no varían con la frecuencia de corriente.

1.3. Configuración de los electrodos para medir la impedancia del miocardio.

El registro de la impedancia eléctrica está influenciado por la configuración de los electrodos de medida (12). Para realizar las medidas a tórax cerrado mediante un electrocatéter se inyectaron corrientes alternas a través del electrodo distal del electrocatéter y un electrodo de referencia localizado en la región precordial. El voltaje inducido se midió entre el mismo electrodo del catéter distal y un segundo electrodo de referencia ubicado en la región precordial lateral izquierda. Escogimos esta configuración de electrodos para reducir el efecto de la anatomía del tórax y para atenuar el efecto de los electrodos en contacto con la piel. Además, para mitigar el efecto del diseño del electrocatéter (tamaño del electrodo, punta irrigada vs. punta no irrigada), se midió la resistencia intrínseca del electrocatéter antes del estudio y su valor se sustrajo de las medidas experimentales.

2. Aportaciones al campo de la medicina cardiovascular

Los grandes avances en la Física, Ingeniería y Biología siempre han ido acompañados de grandes avances en la Medicina. Las primeras investigaciones aplicando la medida de la impedancia a la cardiología experimental se remontan a finales del siglo XIX, cuando George Neil Stewart usó la medida de la conductividad de la sangre para determinar el gasto cardíaco (65). Desde entonces, el uso de la impedancia como detector de procesos biológicos funcionales y estructurales ha ido en aumento. Actualmente el registro de la impedancia eléctrica se emplea tanto en el campo de cardiología clínica como la experimental y en aspectos tan diversos como el cálculo del volumen instantáneo de sangre del ventrículo (66), la caracterización de la lesión por radiofrecuencia durante la ablación eléctrica de arritmias (67), la detección del rechazo agudo en el trasplante de corazón (25) o la monitorización del grado de regeneración local del miocardio infartado después de ser tratado con células madre (51). Además, la medida de la impedancia se utiliza en otras disciplinas de la medicina como por ejemplo para la monitorización de la actividad respiratoria, para el cálculo de la masa muscular corporal en geriatría, o para la detección de cáncer de mama, entre muchos otros (12).

La investigación preclínica en esta Tesis Doctoral se ha centrado en desarrollar un sistema para la detección y caracterización de la cicatriz de infarto basada en medidas de espectroscopia de impedancia a través de un catéter conectado a un sistema de navegación cardíaca.

2.1. Detección de la isquemia miocárdica aguda

La isquemia miocárdica aguda ejerce dos efectos sobre la impedancia local del tejido. El primero se ha confirmado en el presente estudio y consiste en un aumento de la resistividad y un descenso en el ángulo de fase (19,21,39). El segundo efecto es un cambio en la morfología de la curva de resistividad a partir de los primeros 5 minutos de isquemia caracterizado por una elevación sostenida de la resistividad que se mantiene desde la apertura al cierre de la válvula aórtica. Este efecto no se había descrito previamente y es interesante señalar que comparte una estrecha relación temporal con el abombamiento sistólico mecánico local (*bulging*) que se desarrolla durante los primeros minutos de interrupción del flujo coronario en la región isquémica en el mismo modelo animal (59).

En este estudio hemos reportado por primera vez la curva de presión-impedancia. Esta curva detalla la relación temporal entre la resistividad local del tejido miocárdico y la presión global del ventrículo izquierdo durante el ciclo cardíaco. Otros autores han estudiado la relación entre la presión del ventrículo izquierdo y la deformación local de segmentos del miocardio sano e isquémico mediante el análisis de la curva presión-deformación local (60,68). En estos estudios, las regiones isquémicas con motilidad deprimida presentaron un área bajo la curva de presión-deformación local prácticamente inexistente, que refleja el trabajo nulo que realizan estos segmentos disquinéticos. Los resultados de nuestro estudio muestran que, poco después de la oclusión coronaria, el área bajo la curva de presión-impedancia se reduce drásticamente en comparación con el área bajo la curva de las regiones no isquémicas. Nuestros hallazgos sugieren que la magnitud del área bajo la curva de presión-impedancia permitiría diferenciar los segmentos que generan fuerza activa (tejido sano) de aquellos segmentos disquinéticos isquémicos que son

mecánicamente pasivos. De hecho, las regiones miocárdicas con contracción celular (regiones activas) contribuyen a los cambios de presión, mientras que las regiones isquémicas con disquinesia local (regiones pasivas) no contribuyen a la generación de presión y, en cambio, sufren una deformación paradójica como consecuencia de los cambios de la presión intraventricular.

2.2. Reconocimiento del infarto de miocardio cicatricial

La cicatriz de infarto de miocardio presenta una disminución muy marcada de la resistividad y un ángulo de fase cercano a cero. Estos parámetros reflejan la pérdida de miocitos y la presencia de colágeno intersticial (19,49,50). Nuestro trabajo muestra de forma novedosa que existe una correlación lineal entre el contenido de fibrosis y la impedancia local del miocardio punto a punto, y que además es posible evaluar el estado funcional del tejido miocárdico mediante la amplitud de los cambios cíclicos de la resistividad. Estos resultados representan la prueba de concepto que la medida de la resistividad y el ángulo de fase del miocardio durante el ciclo cardíaco son capaces de identificar el grado de fibrosis y, por tanto, determinar la extensión de tejido cicatricial heterogéneo y necrótico. La mejora en la caracterización de la cicatriz de infarto supondría un mejor guiado de la ablación eléctrica de las arritmias ventriculares en pacientes con infarto de miocardio. Teóricamente, la infiltración fibrótica de origen no isquémico (enfermedades infiltrativas, miocarditis, hipertensión) también podría detectarse mediante el registro de la bioimpedancia.

La detección de la cicatriz de infarto a través del registro de la resistividad del miocardio es posible, tanto externamente insertando un electrodo de agujas en la pared del ventrículo (19,48–50,63), como internamente desde el endocardio a través

de un electrocatéter intracavitario (7,8). Sin embargo, en la mayoría de trabajos publicados la impedancia se estudió en modelos animales a tórax abierto, reduciendo su aplicabilidad clínica. En los escasos estudios en que se midió la impedancia desde el endocardio en un modelo animal a tórax cerrado, esta no se registró de forma continua durante el ciclo cardiaco. Así, la aportación de nuestro trabajo consiste en el registro preciso de la impedancia durante todo el ciclo cardíaco, a tórax cerrado, usando un electrocatéter intracavitario conectado a un sistema de navegación cardíaco igual al utilizado en la clínica.

2.3. Estabilidad de la medida de impedancia frente los cambios en el patrón de activación

El éxito de la ablación eléctrica de las arritmias ventriculares en pacientes que han sufrido un infarto depende en gran parte de la identificación precisa de la cicatriz durante el procedimiento clínico. Esta identificación se realiza mediante un sistema de navegación cardíaco que utiliza la amplitud del voltaje de los electrogramas locales como criterio de referencia. Así, el tejido miocárdico se clasifica como sano si los electrogramas bipolares tienen un voltaje igual o superior a 1,5 mV, como cicatriz heterogénea si el voltaje está comprendido entre 0,5 y 1,5 mV, y como cicatriz densa si es inferior a 0,5 mV (69–71). Una limitación de este método es que la amplitud de los electrogramas locales puede variar si el paciente sufre un cambio súbito en el patrón de activación cardíaco, alterando así la localización y caracterización del tejido cicatricial. Estudios recientes muestran que la inducción de un cambio en el frente de activación cardíaco conlleva que entre un 8% y un 18% de los electrogramas de voltaje registrados presenten cambios en su amplitud (de >1,5 mV durante una secuencia de activación a ≤1,5 mV durante otra secuencia) y por tanto

se modifique la clasificación entre regiones sanas o cicatriciales (5,72). Nuestro estudio muestra por primera vez que, a diferencia del mapeo de voltaje, la impedancia eléctrica no se ve alterada por cambios en el frente de activación cardíaco ya que es una propiedad pasiva del corazón. Por tanto, la medida conjunta de la impedancia y el voltaje permitiría reconocer de forma más rápida y robusta el estado del tejido miocárdico explorado.

2.4. Transferencia a la clínica

Este trabajo sugiere que la implementación conjunta de la medida continua del voltaje y la impedancia eléctrica en los sistemas de navegación electroanatómicos mejorará la caracterización de la cicatriz post-infarto. La extrapolación de estos hallazgos al tratamiento clínico de las arritmias ventriculares post-infarto por ablación eléctrica se basa en: 1) las semejanzas en las propiedades electrofisiológicas entre los corazones de la especie humana y porcina (73), 2) el haber usado un modelo animal a tórax cerrado, 3) el haber empleado electrocatéteres y sistemas de navegación cardíacos idénticos a los utilizados en la clínica para la ablación de arritmias ventriculares.

Conclusiones

Las conclusiones principales de este trabajo son:

1. La impedancia eléctrica local del miocardio tiene una variación cíclica ligada a la actividad mecánica del corazón que permite detectar de forma temprana la isquemia aguda y el contenido de fibrosis del miocardio infartado.
2. La medida intracavitaria de la impedancia local del miocardio permite reconocer la cicatriz de infarto y no se ve afectada por los cambios en el patrón de activación. Es, por tanto, una nueva herramienta preclínica para la detección y caracterización de la cicatriz de infarto de miocardio.

Futuras líneas de trabajo

Los resultados de este trabajo plantean dos futuras líneas de investigación. La primera consistiría en la realización de un ensayo clínico en pacientes que han sufrido un infarto para evaluar los beneficios del mapeo de impedancia en la caracterización de la cicatriz de infarto. El objetivo final de este proyecto consistirá en implementar la tecnología de la impedancia a los navegadores cardíacos.

La segunda línea de investigación contemplaría la posibilidad de que la bioimpedancia pueda detectar la fibrosis auricular en un modelo de infarto auricular. En la actualidad la detección de fibrosis auricular no es posible con las técnicas estándar de cardio-resonancia magnética y por tanto esta nueva línea de investigación tendría aplicación clínica en la ablación de las arritmias auriculares.

Bibliografía

1. Henkel DM, Witt BJ, Gersh BJ, Jacobsen SJ, Weston SA, Meverden RA, et al. Ventricular arrhythmias after acute myocardial infarction: A 20-year community study. Am Heart J. 2006;151(4):806–12.

2. Al-Khatib SM, Yancy CW, Solis P, Becker L, Benjamin EJ, Carrillo RG, et al. 2016 AHA/ACC clinical performance and quality measures for prevention of sudden cardiac death: A report of the American College of Cardiology/American Heart Association Task Force on performance measures. Vol. 10, Circulation: Cardiovascular Quality and Outcomes. 2017.

3. Priori SG, Blomström-Lundqvist C, Mazzanti A, Blom N, Borggrefe M, Camm J, et al. 2015 ESC Guidelines for the management of patients with ventricular arrhythmias and the prevention of sudden cardiac death. Eur Heart J. 2015;36(41):2793–867.

4. Marchlinski FE, Callans DJ, Gottlieb CD, Zado E. Linear Ablation Lesions for Control of Unmappable Ventricular Tachycardia in Patients With Ischemic and Nonischemic Cardiomyopathy. Circulation. 2000;101(11):1288–96.

5. Tung R, Josephson ME, Bradfield JS, Shivkumar K. Directional Influences of Ventricular Activation on Myocardial Scar Characterization: Voltage Mapping with Multiple Wavefronts during Ventricular Tachycardia Ablation. Circ Arrhythm Electrophysiol. 2016;9(8):e004155.

6. Gersing E. Impedance spectroscopy on living tissue for determination of the state of organs. Bioelectrochemistry Bioenerg. 1998;45(2):145–9.

7. Warren M, Bragós R, Casas O, Rodríguez-Sinovas A, Rosell J, Anivarro I, et al. Percutaneous electrocatheter technique for on-line detection of healed transmural myocardial infarction. PACE. 2000;23:1283–7.

8. Wolf T, Gepstein L, Hayam G, Zaretzky A, Shofty R, Kirshenbaum D, et al. Three-dimensional endocardial impedance mapping : a new approach for myocardial infarction assessment. Am J Physiol Heart Circ Physiol. 2001;280:H179–88.

9. Sanchez B, Schoukens J, Bragos R, Vandersteen G. Novel estimation of the electrical bioimpedance using the local polynomial method. Application to in vivo real-time myocardium tissue impedance characterization during the cardiac cycle. IEEE Trans Biomed Eng. 2011;58:3376–85.

10. Grimnes S, Martinsen ØG. Bioimpedance and bioelectricity basics. Academic P. 2008.

11. Ivorra A. Bioimpedance monitoring for physicians: an overview. Cent Nac Microelectrònica. 2003;

12. Morucci J-P, Valentinuzzi ME, Rigaud B, Felice CJ, Chauveau N, Marsili P-M. Bioelectrical impedance techniques in medicine. Part II: Monitoring of physiological events by impedance. Crit Rev Biomed Eng. 1996;24(4–6):353–466.

13. Foster KR, Schwan HP. Dielectric properties of tissues and biological materials: a critical review. Crit Rev Biomed Eng. 1989;17(1):25–104.

14. Cole KS, Cole RH. Dispersion and Absorption in Dielectrics I. Alternating Current Characteristics. J Chem Phys. American Institute of Physics; 1941;9(4):341–51.

15. Webster JG, Clark JW, Neuman MR, Olson WH, Peura RA, Primiano FP, et al. Medical instrumentation: Application and design. Control Eng Pract. 2010;296.

16. Ivorra A. Contributions to the measurement of electrical impedance for living tissue ischemia injury monitoring. Universitat Politècnica de Catalunya; 2005.

17. Geddes LA, Foster KS, Reilly J, Voorhees WD, Bourland JD, Ragheb T, et al. The Rectification Properties of an Electrode-Electrolyte Interface Operated at High Sinusoidal Current Density. IEEE Trans Biomed Eng. 1987;(9):669–72.

18. Ellenby MI, Small KW, Wells RM, Hoyt DJ, Lowe JE. On-line detection of reversible myocardial ischemic injury by measurement of myocardial electrical impedance. Ann Thorac Surg. The Society of Thoracic Surgeons; 1987;44(6):587–97.

19. Fallert MA, Mirotznik MS, Downing SW, Savage EB, Foster KR, Josephson ME, et al. Myocardial electrical impedance mapping of ischemic sheep hearts and healing aneurysms. Circulation. 1993;87(I):199–207.

20. Steendijk P, Vandervelde ET, Baan J. Dependence of Anisotropic Myocardial Electrical-Resistivity on Cardiac Phase and Excitation-Frequency. Basic Res Cardiol. 1994;89:411–26.

21. Cinca J, Warren M, Carreño A, Tresànchez M, Armadans L, Gómez P, et al. Changes in myocardial electrical impedance induced by coronary artery occlusion in pigs with and without preconditioning. Circulation. 1997;96(9):3079–86.

22. Padilla F, Garcia-Dorado D, Rodríguez-Sinovas A, Ruiz-Meana M, Inserte J, Soler-Soler J. Protection afforded by ischemic preconditioning is not mediated by effects on cell-to-cell electrical coupling during myocardial ischemia-reperfusion. Am J Physiol Heart Circ Physiol. 2003;285:H1909–16.

23. Salazar Y, Bragos R, Casas O, Cinca J, Rosell J. Transmural versus nontransmural in situ electrical impedance spectrum for healthy, ischemic, and healed myocardium. IEEE Trans Biomed Eng. 2004;51(8):1421–7.

24. Salazar Y. Caracterización de tejidos cardíacos mediante métodos mínimamente invasivos y no invasivos basados en espectroscopia de impedancia eléctrica. Universitat Politècnica de Catalunya; 2004.

25. Cinca J, Ramos J, Garcia MA, Bragos R, Bayés-Genís A, Salazar Y, et al. Changes in myocardial electrical impedance in human heart graft rejection. Eur J Heart Fail. 2008;10:594–600.

26. Dzwonczyk R, Del Rio CL, Sai-Sudhakar C, Sirak JH, Michler RE, Sun B, et al. Vacuum-assisted apical suction devices induce passive electrical changes consistent with myocardial ischemia during off-pump coronary artery bypass graft surgery. Eur J Cardio-thoracic Surg. 2006;30(6):873–6.

27. Mellert F, Winkler K, Schneider C, Dudykevych T, Welz A, Osypka M, et al. Detection of (Reversible) myocardial ischemic injury by means of electrical bioimpedance. IEEE Trans Biomed Eng. 2011;58(6):1511–8.

28. Pallás-Areny R, Webster JG. AC Instrumentation Amplifier for Bioimpedance Measurements. IEEE Trans Biomed Eng. 1993;40(8):830–3.

29. Sperelakis N, Hoshiko T. Electrical impedance of cardiac muscle. Circ Res. 1961;9:1280–3.

30. Gebhard MM, Gersing E, Brockhoff CJ, Schnabel P a, Bretschneider HJ. Impedance spectroscopy: a method for surveillance of ischemia tolerance of the heart. Thorac Cardiovasc Surg. 1987;35(1):26–32.

31. Sasaki E, Conger JL, Kadipasaoglu K a, Pehlivanoglu S, Frazier OH. Simultaneous evaluation of cardiac wall motion and myocardial ischemic injury by measurement of electrical impedance. Vol. 40, ASAIO journal. 1994. p. M826-9.

32. González-Vílchez F, Segovia Cubero J, Almenar L, Crespo-Leiro MG, Arizón JM, Sousa I, et al. Registro Español de Trasplante Cardiaco. XXVII Informe Oficial de la Sección de Insuficiencia Cardiaca y Trasplante Cardiaco de la Sociedad Española de Cardiología (1984-2015). Rev Española Cardiol. 2016;69(11):1071–82.

33. From AM, Maleszewski JJ, Rihal CS. Current Status of Endomyocardial Biopsy. Mayo Clin Proc. 2011;86(11):1095–102.

34. Miller CA, Fildes JE, Ray SG, Doran H, Yonan N, Williams SG, et al. Non-invasive approaches for the diagnosis of acute cardiac allograft rejection. Heart. 2013;99(7):445–53.

35. Tarazón E, Ortega A, Gil-Cayuela C, Sánchez-Lacuesta E, Marín P, Lago F, et al. SERCA2a: A potential non-invasive biomarker of cardiac allograft rejection. J Hear Lung Transplant. 2017;36(12):1322–8.

36. Grauhan O, Müller J, Knosalla C, Cohnert T, Siniawski H, Volk HD, et al. Electric myocardial impedance registration in humoral rejection after heart transplantation. J Hear lung Transplant. 1996;15(1):136–43.

37. Pfitzmann R, Muáller J, Grauhan O, Hetzer R. Intramyocardial impedance measurements for diagnosis of acute cardiac allograft rejection. Ann Thorac Surg. 2000;70(2):527–32.

38. Fleischhauer J, Lehmann L, Kléber AG. Electrical Resistances of Interstitial and Microvascular Space as Determinants of the Extracellular Electrical Field and Velocity of Propagation in Ventricular Myocardium. Circulation. 1995;92(3).

39. van Oosterom A, de Boer RW, van Dam RT. Intramural resistivity of cardiac tissue. Med Biol Eng Comput. 1979;17(3):337–43.

40. Kléber AG, Riegger CB, Janse MJ. Electrical uncoupling and increase of extracellular resistance after induction of ischemia in isolated, arterially perfused rabbit papillary muscle. Circ Res. 1987;61(2):271–9.

41. Rodriguez-Sinovas A, García-Dorado D, Pina P, Ruiz-Meana M, Soler-Soler J. Effect of sarcolemmal rupture on myocardial electrical impedance during oxygen deprivation. Am J Physiol Heart Circ Physiol. 2005;288(3):H1396-403.

42. Del Rio CL, McConnell PI, Clymer BD, Dzwonczyk R, Michler RE, Billman GE, et al. Early time course of myocardial electrical impedance during acute coronary artery occlusion in pigs, dogs, and humans. J Appl Physiol. 2005;99(4):1576–81.

43. Ishikawa M, Hirose H, Sasaki E, Mori Y, Murakawa S, Fuwa S, et al. Detection of myocardial ischemic injury during simple cold storage by measurement of myocardial electrical impedance. J Cardiovasc Surg (Torino). 1996;37(3):261–7.

44. Noguera N, Gómez R, Villa R, Ivorra A, Aguiló J, Luis J, et al. Aplicación y evaluación de un sistema para la monitorización de la preservación durante el transplante cardiaco. In: XX Congreso Anual de la Sociedad Española de Ingeniería Biomédica. 2011. p. 365–8.

45. Dzwonczyk R, Del Rio C, Brown DA, Michler RE, Wolf RK, Howie MB. Myocardial electrical impedance responds to ischemia and reperfusion in humans. IEEE Trans Biomed Eng. 2004;51(12):2206–9.

46. Dzwonczyk R, Del Rio CL, Sun B, Howie MB. Myocardial electrical impedance correlates with ischemic ECG ST-segment changes in humans. Annu Int Conf IEEE Eng Med Biol - Proc. 2006;2568–9.

47. Talman V, Ruskoaho H. Cardiac fibrosis in myocardial infarction—from repair and remodeling to regeneration. Cell Tissue Res. Cell and Tissue Research; 2016;365(3):563–81.

48. Del Rio CL, McConnell PI, Kukielka M, Dzwonczyk R, Clymer BD, Howie MB, et al. Electrotonic remodeling following myocardial infarction in dogs susceptible and resistant to sudden cardiac death. J Appl Physiol. 2008;104(2):386–93.

49. Schwartzman D, Chang I, Michele JJ, Mirotznik MS, Foster KR. Electrical impedance properties of normal and chronically infarcted left ventricular myocardium. J Interv Card Electrophysiol. 1999;3:213–24.

50. Cinca J, Warren M, Rodríguez-Sinovas A, Tresànchez M, Carreño A, Bragós R, et al. Passive transmission of ischemic ST segment changes in low electrical resistance myocardial infarct scar in the pig. Cardiovasc Res. 1998;40(1):103–12.

51. Gálvez-Montón C, Bragós R, Soler-Botija C, Díaz-Güemes I, Prat-Vidal C, Crisóstomo V, et al. Noninvasive Assessment of an Engineered Bioactive Graft in Myocardial Infarction: Impact on Cardiac Function and Scar Healing. Stem Cells Transl Med. 2017;6:647–55.

52. Jugdutt BI, Amy RWM. Healing after myocardial infarction in the dog: Changes in infarct hydroxyproline and topography. J Am Coll Cardiol. American College of Cardiology Foundation; 1986;7(1):91–102.

53. González-Juanatey JR, Cea-Calvo L, Bertomeu V, Aznar J. Criterios electrocardiográficos de hipertrofia ventricular izquierda y perfil de riesgo cardiovascular en hipertensos. Estudio VIIDA. Rev Española Cardiol. 2007;60(2):148–56.

54. Bacharova L. Left ventricular hypertrophy: Disagreements between increased left ventricular mass and ECG-LVH criteria: The effect of impaired electrical properties of myocardium. J Electrocardiol. Elsevier Inc.; 2014;47(5):625–9.

55. Winterton SJ, Turner MA, O'gorman DJ, Flores NA, Sheridan DJ. Hypertrophy causes delayed conduction in human and Guinea pig myocardium: Accentuation during ischaemic perfusion. Cardiovasc Res. 1994;28(1):47–54.

56. Cooklin M, Wallis WR, Sheridan DJ, Fry CH. Changes in cell-to-cell electrical coupling associated with left ventricular hypertrophy. Circ Res. 1997;80(6):765–71.

57. Cooklin M, Wallis WR, Sheridan DJ, Fry CH. Conduction velocity and gap junction resistance in hypertrophied, hypoxic guinea-pig left ventricular myocardium. Exp Physiol. 1998;83(6):763–70.

58. Sanchez B, Vandersteen G, Bragos R, Schoukens J. Optimal multisine excitation design for broadband electrical impedance spectroscopy. Meas Sci Technol. 2011;22(11).

59. Cinca J, Carreño A, Mont L, Blanch P, Soler-Soler J. Neurally mediated negative inotropic effect impairs myocardial function during cholinergic coronary vasoconstriction in pigs. Circulation. 1996;94(Lv):1101–8.

60. Lyseggen E, Skulstad H, Helle-Valle T, Vartdal T, Urheim S, Rabben SI, et al. Myocardial strain analysis in acute coronary occlusion: A tool to assess myocardial viability and reperfusion. Circulation. 2005;112(25):3901–10.

61. Helle-Valle T, Remme EW, Lyseggen E, Pettersen E, Vartdal T, Opdahl A, et al. Clinical assessment of left ventricular rotation and strain: a novel approach for quantification of function in infarcted myocardium and its border zones. Am J Physiol Heart Circ Physiol. 2009;297(1):H257-67.

62. Maxwell M, Hearse D, Yellon D. Species Variation in the Coronary Collateral Circulation During Regional Myocardial-Ischemia - a Critical Determinant of the Rate of Evolution and Extent of Myocardial-Infarction. Cardiovasc Res. 1987;21:737–46.

63. Farraha M, Nguyen DT, Barry MA, Lu J, Mcewan AL, Pouliopoulos J. Investigating the utility of in vivo bio-impedance spectroscopy for the assessment of post-ischemic myocardial tissue. Conf Proc IEEE Eng Biol Soc. 2014;2014:1111–4.

64. Casas O, Bragós R, Riu P, Rosell J, Tresànchez M, Warren M, et al. In vivo and in situ ischemic tissue characterization using electrical impedance spectroscopy. Ann N Y Acad Sci. 1999;873:51–8.

65. Stewart GN. Researches on the Circulation Time and on the Influences which affect it. J Physiol. 1897;22(3):159–83.

66. Baan J, van der Velde ET, de Bruin HG, Smeenk GJ, Koops J, van Dijk AD, et al. Continuous measurement of left ventricular volume in animals and humans by conductance catheter. Circulation. 1984;70(5):812–23.

67. Knecht S, Reichlin T, Pavlovic N, Schaer B, Osswald S, Sticherling C, et al. Contact force and impedance decrease during ablation depends on catheter location and orientation : insights from pulmonary vein isolation using a contact force-sensing catheter. J Interv Card Electrophysiol. 2015;297–306.

68. Tyberg J V, Forrester JS, Wyatt HL, Goldner SJ, Parmley WW, Swan HJC. An Analysis of Segmental Ischemic Dysfunction Utilizing the Pressure-Length Loop. Circulation. 1974;49:748–54.

69. With C, Echocardiography I, Callans DJ, Ren J, Michele J, Marchlinski FE, et al. Electroanatomic Left Ventricular Mapping in the Porcine Model of Healed Anterior Myocardial Infarction. 1999;1744–51.

70. Marchlinski FE, Callans DJ, Gottlieb CD, Zado E. Linear Ablation Lesions for Control of Unmappable Ventricular Tachycardia in Patients With Ischemic and Nonischemic Cardiomyopathy. 2000;1288–97.

71. Wissner E, Stevenson WG, Kuck KH. Catheter ablation of ventricular tachycardia in ischaemic and non-ischaemic cardiomyopathy: Where are we today? A clinical review. Eur Heart J. 2012;33(12):1440–50.

72. Brunckhorst CB, Delacretaz E, Soejima K, Maisel WH, Friedman PL, Stevenson WG. Impact of changing activation sequence on bipolar electrogram amplitude for voltage mapping of left ventricular infarcts causing ventricular tachycardia. J Interv Card Electrophysiol. 2005;12(2):137–41.

73. Cinca J, Janse MJ, Moréna H, Candell J, Valle V, Durrer D. Mechanism and Time Course of the Early Electrical Changes During Acute Coronary Artery Occlusion. Chest. 1980;77(4):499–505.